NASA TECHNICAL MEMORANDUM

NASA TM X-53587

March 9, 1967

NASA TM X-53587

STATIC AERODYNAMIC CHARACTERISTICS OF THE ABORTED APOLLO-SATURN V VEHICLE

By Robert M. Glasgow
Aero-Astrodynamics Laboratory

NASA

George C. Marshall
Space Flight Center,
Huntsville, Alabama

TECHNICAL MEMORANDUM X-53587

STATIC AERODYNAMIC CHARACTERISTICS OF THE ABORTED APOLLO-SATURN V VEHICLE

by

Robert M. Glasgow*

George C. Marshall Space Flight Center

Huntsville, Alabama

ABSTRACT

Presented are the static aerodynamic characteristics of the aborted Apollo-Saturn V vehicle. The data are based primarily on wind tunnel tests of scale models. Total normal and axial force characteristics with local normal, local axial, and local pressure force distributions necessary for performance, control, and basic structural analyses of the vehicle are presented. All results are presented for various Mach numbers between 0 and 3.0 and vehicle angle-of-attack variations between 0 and 16 degrees.

---

* Mr. Glasgow is associated with Northrop Space Laboratories, Huntsville, Alabama.

NASA - GEORGE C. MARSHALL SPACE FLIGHT CENTER

Technical Memorandum X-53587

March 9, 1967

STATIC AERODYNAMIC CHARACTERISTICS OF THE ABORTED APOLLO-SATURN V VEHICLE

by

Robert M. Glasgow *

This analysis was performed by Northrop Space Laboratories, Huntsville, Alabama, while under contract to the Aero-Astrodynamics Laboratory, George C. Marshall Space Flight Center (NAS8-20082). The work was carried out in response to the requirement of Appendix B-1, Schedule Order No. 56. The NASA Technical Coordinator was Mr. B. G. Dunn of the Aerodynamic Design Branch.

*Northrop Space Laboratories

AERODYNAMIC DESIGN BRANCH
AEROPHYSICS DIVISION
AERO-ASTRODYNAMICS LABORATORY
RESEARCH AND DEVELOPMENT OPERATIONS

TABLE OF CONTENTS

DEFINITION OF SYMBOLS

Symbol	Definition
α	angle of attack (degrees)
A_{REF}	reference area $\frac{\pi D_{REF}^2}{4}$ (in^2)
C_{A_B}	base axial force coefficient, $\frac{F_{A_B}}{q_\infty A_{REF}}$
C_{A_T}	total axial force coefficient, $\frac{F_{A_T}}{q_\infty A_{REF}}$
$C_{A_{F+S}}$	fin and shroud axial force coefficient
$C_{A_{NOSE}}$	blunt aborted nose axial force coefficient
C_N	normal force coefficient, $\frac{N}{q_\infty A_{REF}}$
C_{N_α}	normal force coefficient gradient, ($\alpha < 2°$)
$C_{N_{\alpha_{F+S}}}$	fin plus shroud normal force coefficient gradient
$C_{P_{INT}}$	aborted nose internal pressure coefficient
C_{m_g}	pitching moment coefficient about station 100
CP/D	center of pressure, from station 100 (calibers)
D_{REF}	reference diameter, 396 inches (in)
$\frac{dC_A}{d(X/D)}$	local axial force coefficient, $\alpha = 0°$

DEFINITION OF SYMBOLS (Continued)

Symbol	Definition
$\frac{dC_N}{d(X/D)}$	local normal force coefficient
$\frac{dC_{N_\alpha}}{d(X/D)}$	local normal force coefficient gradient, ($\alpha < 2°$)
F_{A_B}	vehicle base axial force (lbf)
F_{A_T}	vehicle total axial force (lbf)
γ	specific heat ratio
M_∞	free stream Mach number
N	normal force (lbf)
P_L	local static pressure (lbf/in^2)
P_∞	free stream static pressure (lbf/in^2)
q_∞	free stream dynamic pressure, $\gamma/2\ P_\infty\ M_\infty^2$ (lbf/in^2)
X/D	distance from vehicle station 100 (calibers)
t	time

TECHNICAL MEMORANDUM X-53587

STATIC AERODYNAMIC CHARACTERISTICS OF THE ABORTED APOLLO-SATURN V VEHICLE

SUMMARY

Presented are the static aerodynamic characteristics of the aborted Apollo-Saturn V vehicle. The data are based primarily on wind tunnel tests of scale models. Total normal and axial force characteristics with local normal, local axial, and local pressure force distributions necessary for performance, control, and basic structural analyses of the vehicle are presented. All results are presented for various Mach numbers between 0 and 3.0 and vehicle angle-of-attack variations between 0 and 16 degrees.

I. INTRODUCTION

The purpose of this report is to supply an adequate and compatible definition of the aerodynamic characteristics of the aborted Apollo-Saturn V vehicle for support of structural, control, and performance analyses. The data are also applicable for support of range safety analyses and abort studies.

The Apollo-Saturn V launch vehicle consists of the S-IC first stage, S-II second stage, S-IVB third stage, IU (instrument unit), and the Apollo spacecraft. The Apollo spacecraft consists of the lunar excursion module adapter (LEM), service module (SM), command module (CM), and the lunar escape system (LES). The vehicle propulsion systems are five F-1 engines developing 7,500,000 pounds of thrust at sea level (S-IC), five J-2 engines developing 1,000,000 pounds of thrust at a vacuum (S-II), one J-2 engine developing 200,000 pounds of thrust at a vacuum (S-IVB), and one service module engine developing 21,500 pounds of thrust at a vacuum.

The aerodynamic characteristics presented in this report are for the aborted Saturn V configuration of figure 1 only. If a malfunction should occur, there are two ways to accomplish command module abort depending on time from launch. If command module abort is necessary during first-stage flight or before approximately 20 seconds into second-stage flight, the vehicle launch escape system will be employed.

However, after approximately 20 seconds into second-stage flight, the launch escape system will be jettisoned and the spacecraft service module propulsion system will be employed to eject the command module. It is important to note that the data presented in this report would not be applicable to an aborted Saturn V where the service module is used to eject the command module. This would yield a different configuration from the one considered in figure 1 and would thus change the aerodynamic characteristics.

The abort data are necessary because, if a malfunction occurs before approximately 45 seconds, an attempt will be made to fly the aborted vehicle a safe distance from the launch area before destruct to prevent debris from impacting in the launch area. The abort data are of great importance and must be used in preparation for such a malfunction.

Geometry of the Saturn V, S-IC stage, base area is presented in figure 2. Geometry of the engine shroud and fin is presented in figure 3, and a typical Apollo-Saturn V trajectory is presented in figure 4.

The author wishes to acknowledge the suggestions and interest of Mr. B. G. Dunn of the Aerodynamic Design Branch, Aero-Astrodynamics Laboratory, George C. Marshall Space Flight Center in support of this report.

II. STATIC STABILITY CHARACTERISTICS

The static stability characteristics of the aborted Apollo-Saturn V vehicle are defined primarily from test data over a 0.333 percent scale model in the AEDC 1-foot transonic wind tunnel and the BRL supersonic wind tunnel No. 1. These data are presented in references 1, 2, and 3. The test model contained a 50' larger LEM adapter frustum angle; however, previous comparisons between these data established no large differences [4]. Therefore, the data from the larger frustum tests are considered an acceptable basis for the vehicle aerodynamic stability criteria.

The vehicle normal force coefficient gradient and center of pressure at zero degree angle of attack are presented as a function of Mach number in figure 5. The vehicle normal force coefficients as a function of angle of attack (0° to 16°) and Mach number (0 to 2.75) are carpet-plotted in figure 6. The corresponding values of the center of pressure are presented in figure 7. The data of figures 5 through 7 do not include effects of external protuberances except for the S-IC engine shrouds and fins. These effects are expected to be small and should be within the estimated accuracies discussed in Section VII.

III. AXIAL FORCE CHARACTERISTICS

The total vehicle axial force coefficients for zero degree angle of attack as a function of Mach number are presented in figure 8. The power-on and power-off variations are presented as required for consideration in vehicle range safety analyses. The power-off axial force coefficient variations are established from reference 1. The power-on axial force variations are established by summing the forebody axial force from reference 1, the base axial force from reference 4, and lift-off base axial force from reference 5.

The base axial force consists of two components as given below:

$$F_{A_B} = C_{A_B}\, q_\infty\, A_{REF} + \left[\frac{12{,}698 \text{ lbf}}{1 + \frac{0.55}{1 + t^2}\,(\sinh t)^{2.3}}\right]_{t \leq 4 \text{ seconds}}.$$

The first term applies at all times, but the second term applies only during the first four seconds of flight. The second term is an empirical formula developed for the example trajectory in figure 4. This empirical formula is the lift-off base axial force caused by an engine pumping effect that reduces the base pressure. After the vehicle clears the launch platform (approximately 4 seconds) the empirical term becomes zero. The total vehicle axial force for the first four seconds is given by

$$F_{A_T} = C_{A_T}\, q_\infty\, A_{REF} + \left[\frac{12{,}698 \text{ lbf}}{1 + \frac{0.55}{1 + t^2}\,(\sinh t)^{2.3}}\right]_{t \leq 4 \text{ seconds}}$$

where the C_{A_B} coefficient is included in the C_{A_T} coefficient. After four seconds the total vehicle axial force is given by

$$F_{A_T} = C_{A_T}\, q_\infty\, A_{REF}.$$

IV. LOCAL NORMAL FORCE COEFFICIENT DISTRIBUTIONS

The distributions of local normal force coefficient gradient through $\alpha = 0°$ and for Mach numbers ranging from 0.50 to 2.75 are presented in figures 9 through 17. The normal force coefficient distributions at angles of attack of 6°, 8°, 10°, 12°, 14°, and 16° and for Mach numbers ranging from 0.50 through 2.75 are presented in figures 18 through 71. These distributions were obtained from a combination of data from references 6, 7, and 8. The normal force gradient is obtained from

$$C_{N_\alpha} = \int \frac{dC_{N_\alpha}}{d(X/D)}\, d(X/D) + C_{N_{\alpha_{F+S}}}$$

and this yields the values presented in figure 5. The normal force is obtained from

$$C_N = \int \frac{dC_N}{d(X/D)}\, d(X/D) + C_{N_{F+S}}.$$

This yields the values presented on the carpet-plotted data in figure 6. The CP/D data presented in figure 7 were obtained from dividing the C_N from the above equation into C_{m_g} values from references 2 and 3.

The local normal force coefficient distributions contain concentrated loads for the contributions due to the engine shroud and fin combinations. These loads are appropriate for total vehicle structural analyses, but not for individual component design. Interference and carry-over effects are included in the fin-shroud loads; therefore, they are not appropriate for defining the structural requirements of the components.

V. LOCAL AXIAL FORCE COEFFICIENT DISTRIBUTIONS

The local axial force coefficients distributions for zero degree angle of attack and Mach numbers ranging from 0.50 through 2.75 are presented in figures 72 through 80. The axial force distributions are developed by combining forebody data forward of the S-IVB stage from reference 7 with data over the remainder of the vehicle from reference 6. The axial force coefficients of the aborted nose, fins and shrouds, and base are presented as concentrated loads because these data are not easily adapted to a distributed presentation. The aborted nose axial force coefficient data, obtained from reference 7, must be corrected to the proper reference diameter. The fin, shroud, and base axial force coefficients are obtained from reference 4. The total axial force coefficient is given by

$$C_{A_T} = \int \frac{dC_A}{d(X/D)} d(X/D) + C_{A_{NOSE}} + C_{A_{F+S}} + C_{A_{BASE}}.$$

This yields the total values presented in figure 8.

Static stability wind tunnel tests have established that the vehicle axial force decreases approximately 5 percent from $\alpha = 0°$ to $\alpha = 10°$ [4]. The zero degree angle-of-attack data are conservative for vehicle analyses at small angles of attack; therefore, for vehicle design, the data presented are suitable for angles of attack less than approximately 10°.

VI. LOCAL PRESSURE COEFFICIENT DISTRIBUTIONS

The local pressure coefficient distributions for $\alpha = 0°$ and Mach numbers ranging from 0.60 through 2.75 are presented in figures 81 through 91. The local pressure coefficients are obtained by combining data from references 6, 7, and 8. The fins, shrouds, and surrounding region are undefined because it is not possible to present the three-dimensional aspects induced on the data at zero degree angle of attack. The pressure distributions over the fins and shrouds are established in references 9 and 10.

The internal pressure coefficient as a function of Mach number is presented in figure 92. After the command module is ejected, the spacecraft intercompartment is subjected to flight stagnation pressures. A combination of this internal pressure with the external pressure in figures 81 through 91 yields much larger burst loads over the compartment walls than would occur during nominal flight.

VII. DISCUSSION OF RESULTS

This report contains an engineering estimate of the Apollo-Saturn V aborted vehicle aerodynamics based on available data for this configuration and similar configurations. The experimental and analytical work conducted for the Apollo-Saturn V aborted vehicle has been much less than for the total vehicle of reference 6. Establishment of design aerodynamics for the aborted vehicle has, for this reason been handicapped. Also, blunt-body aerodynamic data are not as accurate as those presented in reference 6 because the increased bow shock wave strength and angle reduce the probability of obtaining precise experimental data. The set of enclosed data is, however, considered to be consistent and entirely adequate in terms of accuracy for the conditions expected: a short-term unmanned flight before intentional destruction.

To perform space launch vehicle control and performance analyses, the various input criteria must be varied to include the potential deviations from the nominal values. The normal and axial force data presented in this report are considered nominal values suitable for support of vehicle control and performance analyses when given accuracy levels are considered. The approximate accuracy of the enclosed data has been estimated to be as follows:

normal force coefficient, ±10 percent;

center of pressure, ±0.4 calibers; and

axial force coefficient, ±15 percent.

These variations are to be used only with the enclosed abort aerodynamics, and are not intended for application with other vehicle aerodynamics.

The purpose of this report is to supply an adequate and compatible definition of the aborted vehicle aerodynamic characteristics for support of structural, control, and performance analyses. This report does not present a detailed analysis, but includes only a brief description and analyses of the various components of data. Detailed aerodynamic analyses can be obtained from the references.

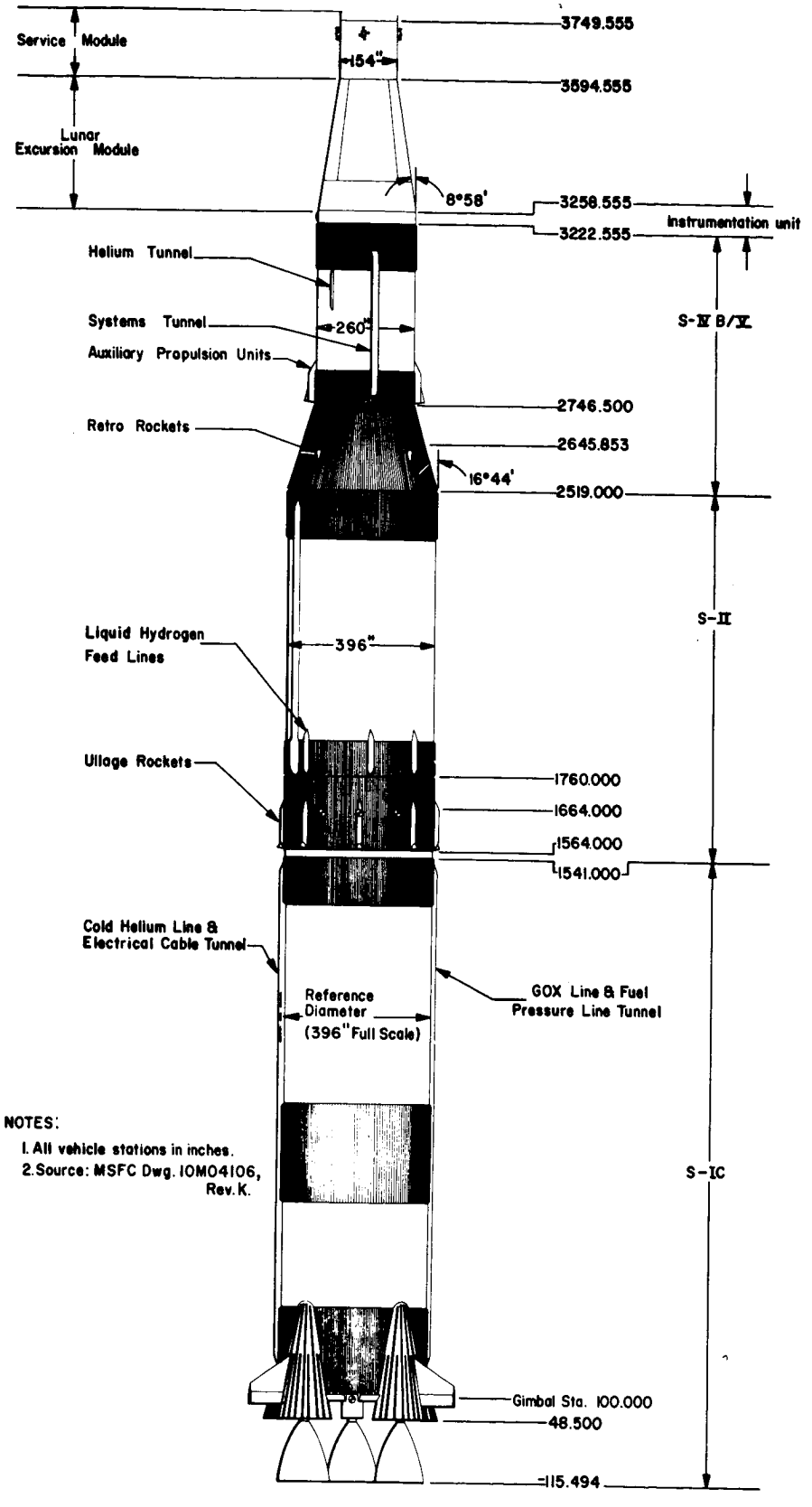

FIGURE 1 GEOMETRY OF THE ABORTED-SATURN V FLIGHT VEHICLE

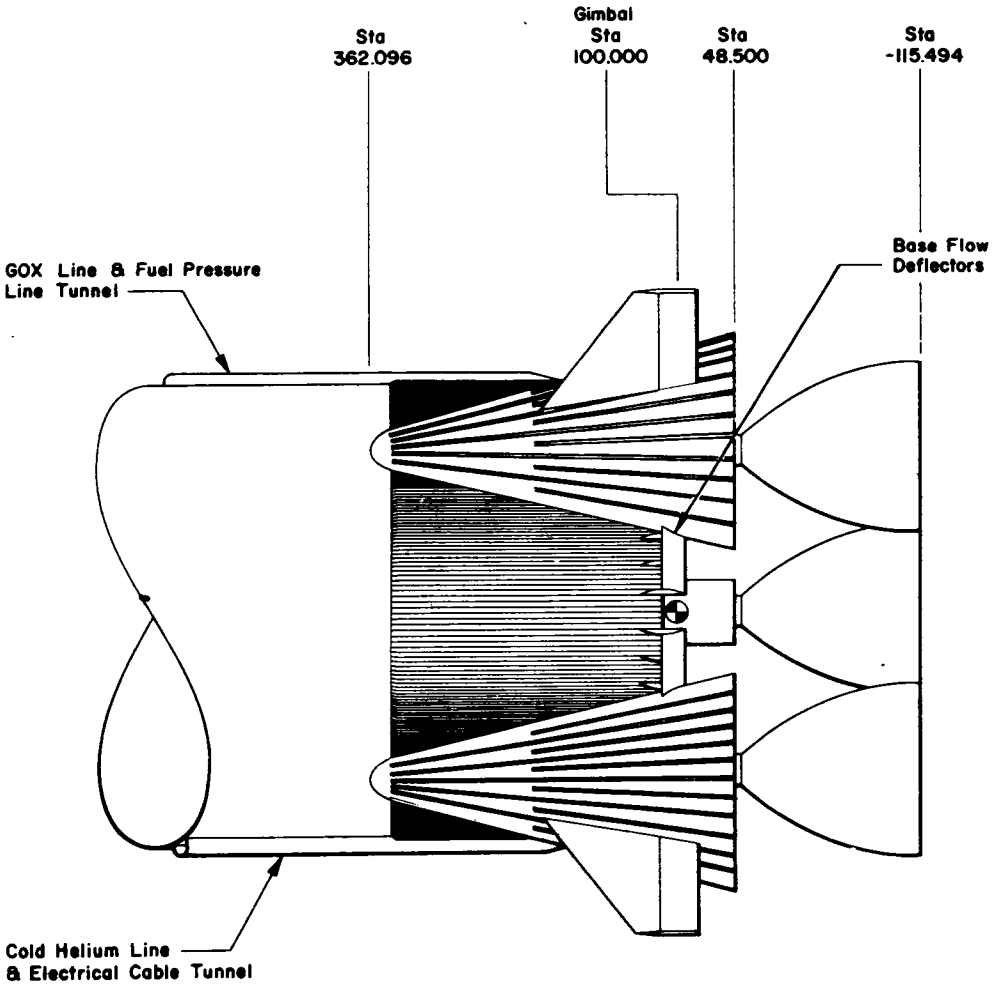

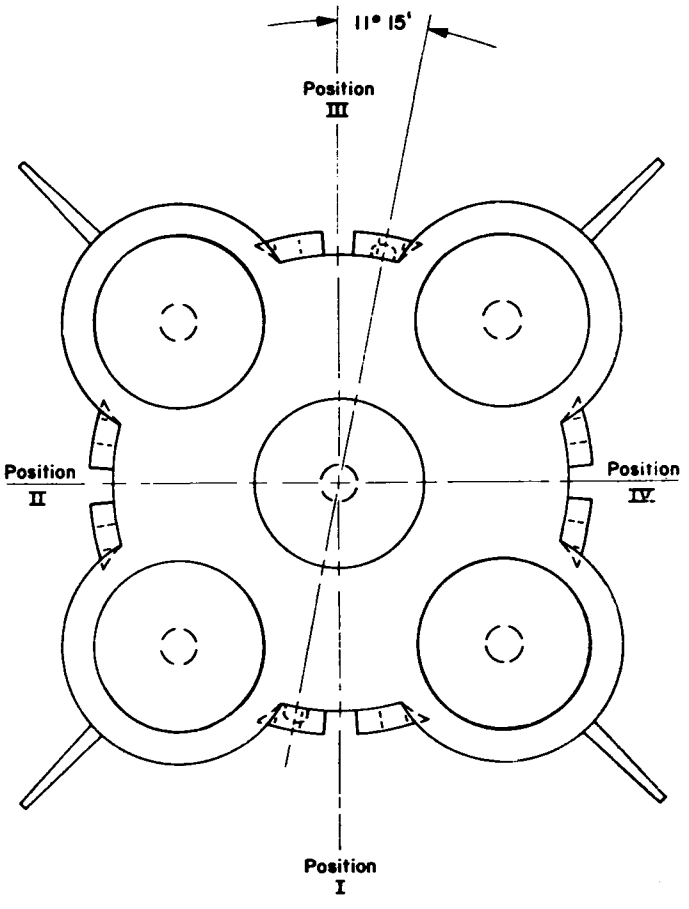

1. All vehicle stations in inches.

FIGURE 2 GEOMETRY OF THE SATURN V, S-IC STAGE, BASE AREA

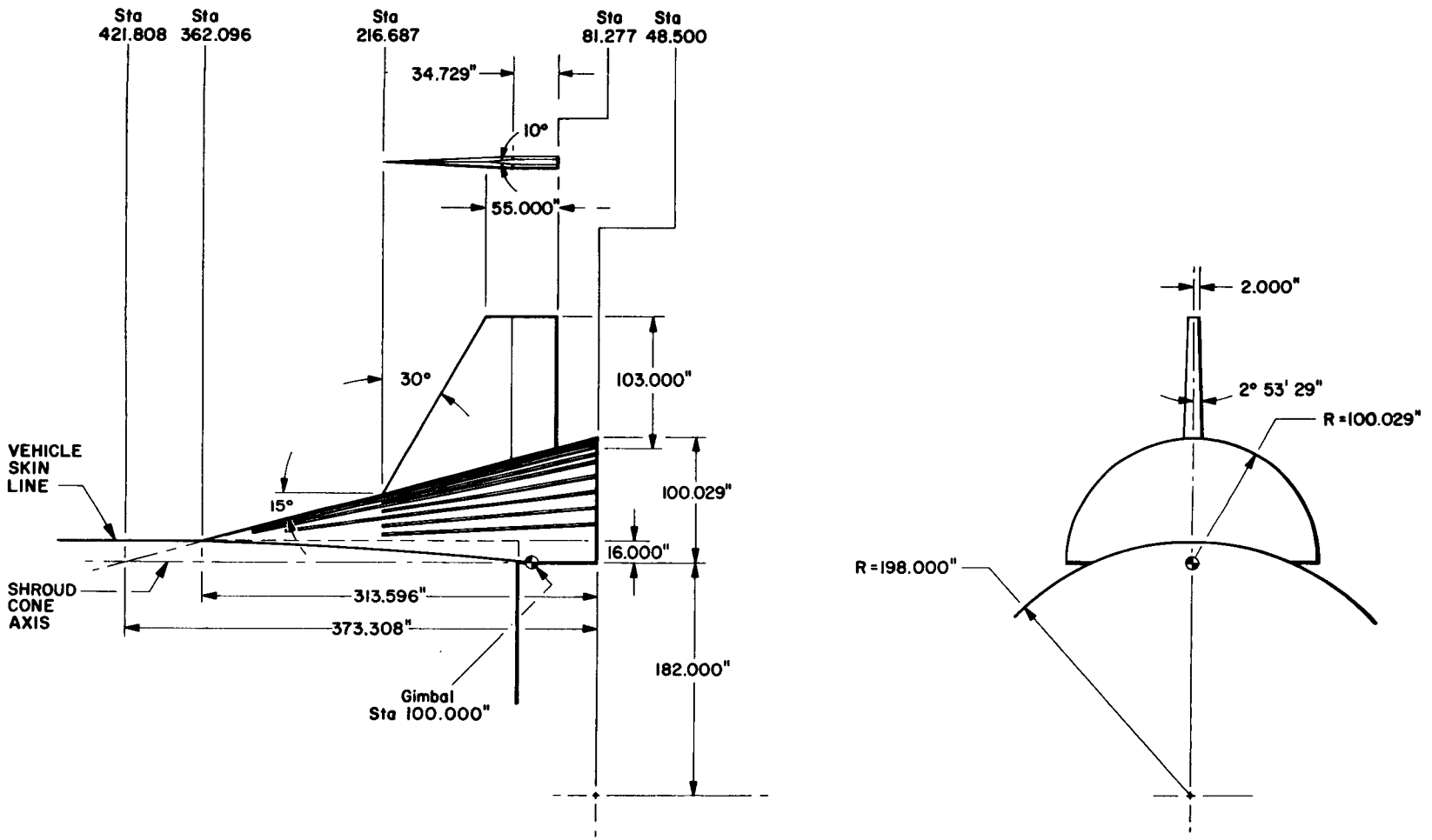

NOTES:
1. All vehicle stations in inches.

FIGURE 3 GEOMETRY OF THE SATURN V, S-IC STAGE ENGINE SHROUD AND FIN

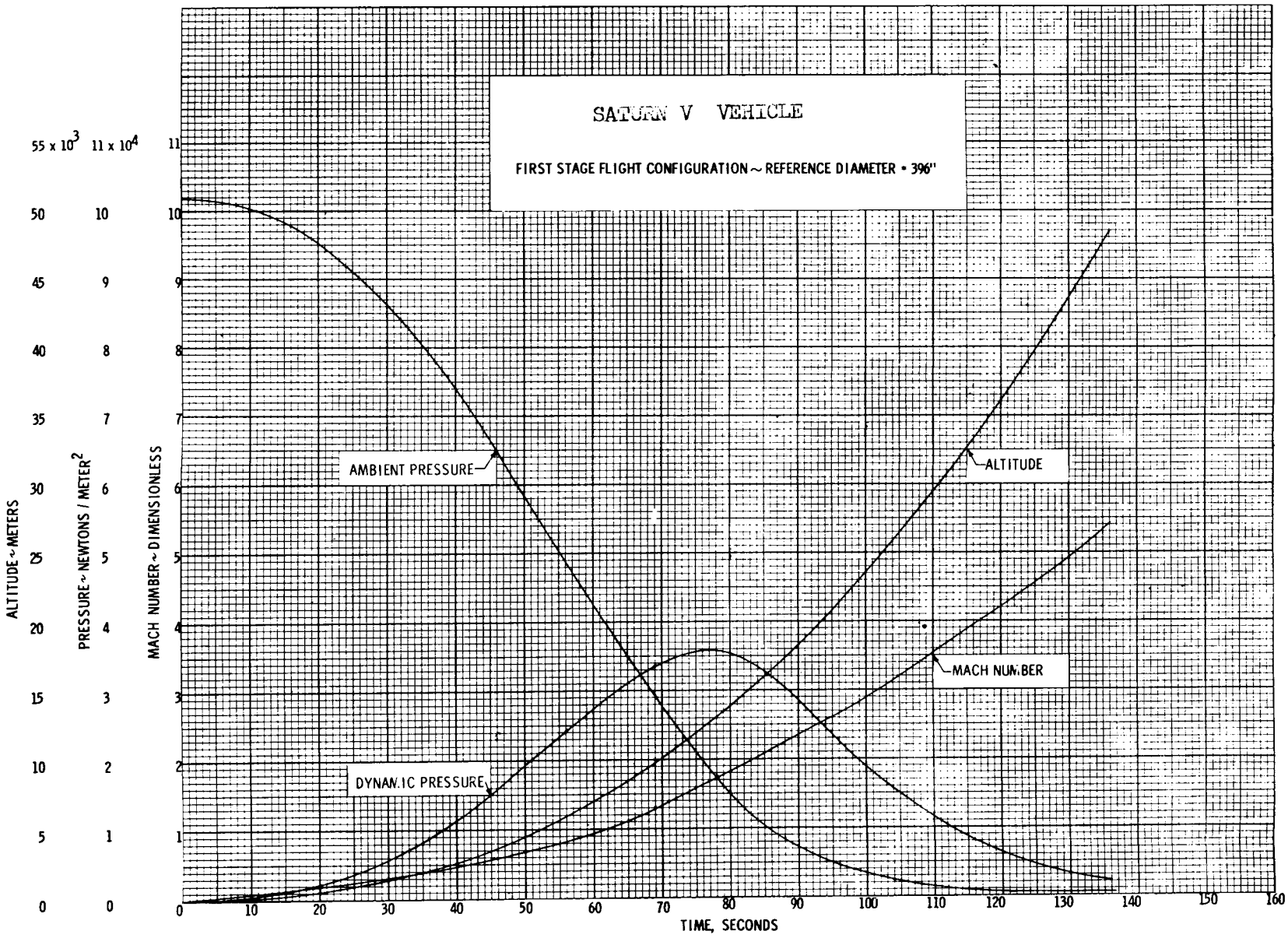

FIGURE 4 DEFINITION OF TYPICAL APOLLO-SATURN V TRAJECTORY DATA

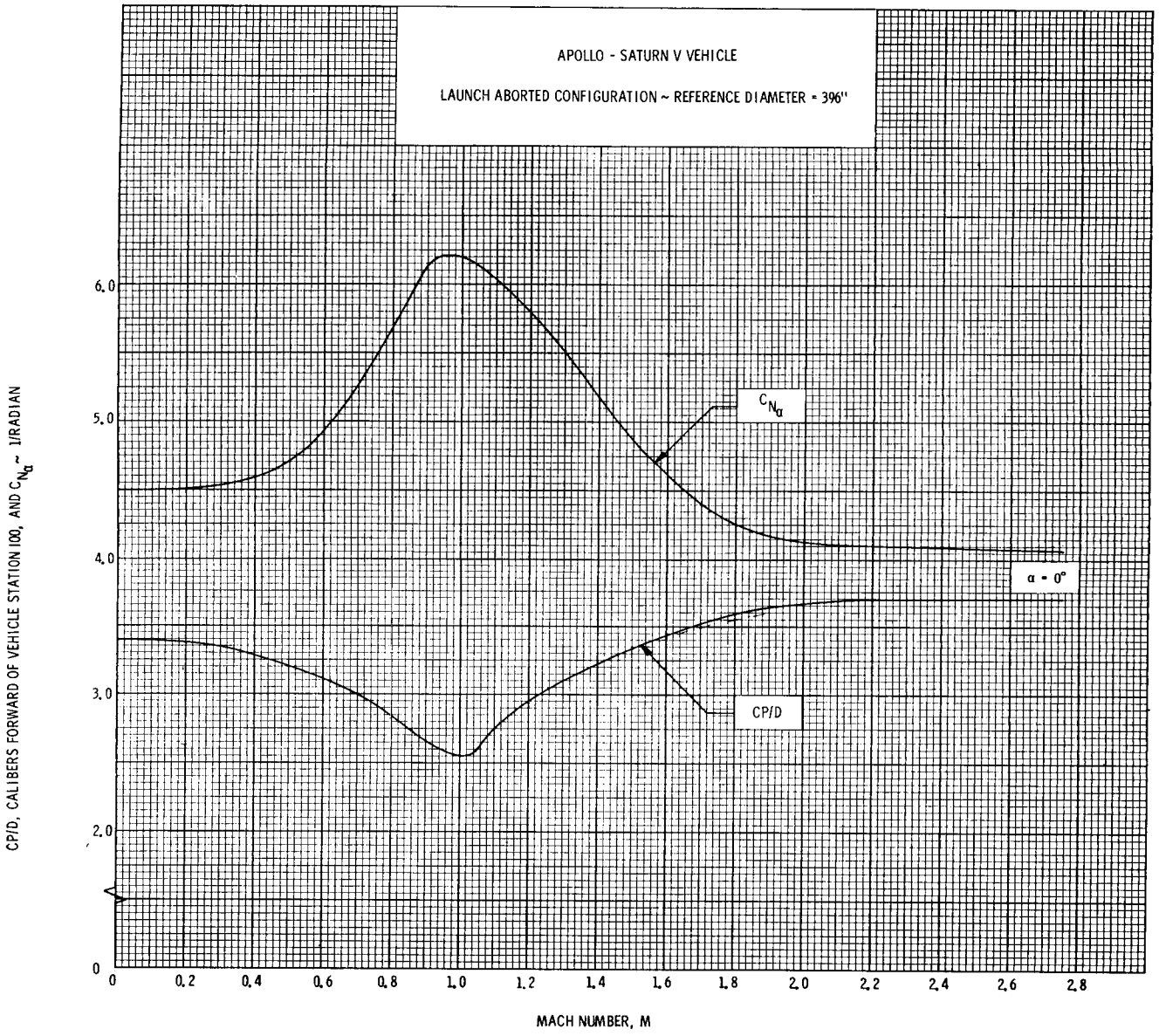

FIGURE 5 VARIATION OF NORMAL FORCE COEFFICIENT GRADIENT AND CENTER OF PRESSURE WITH MACH NUMBER

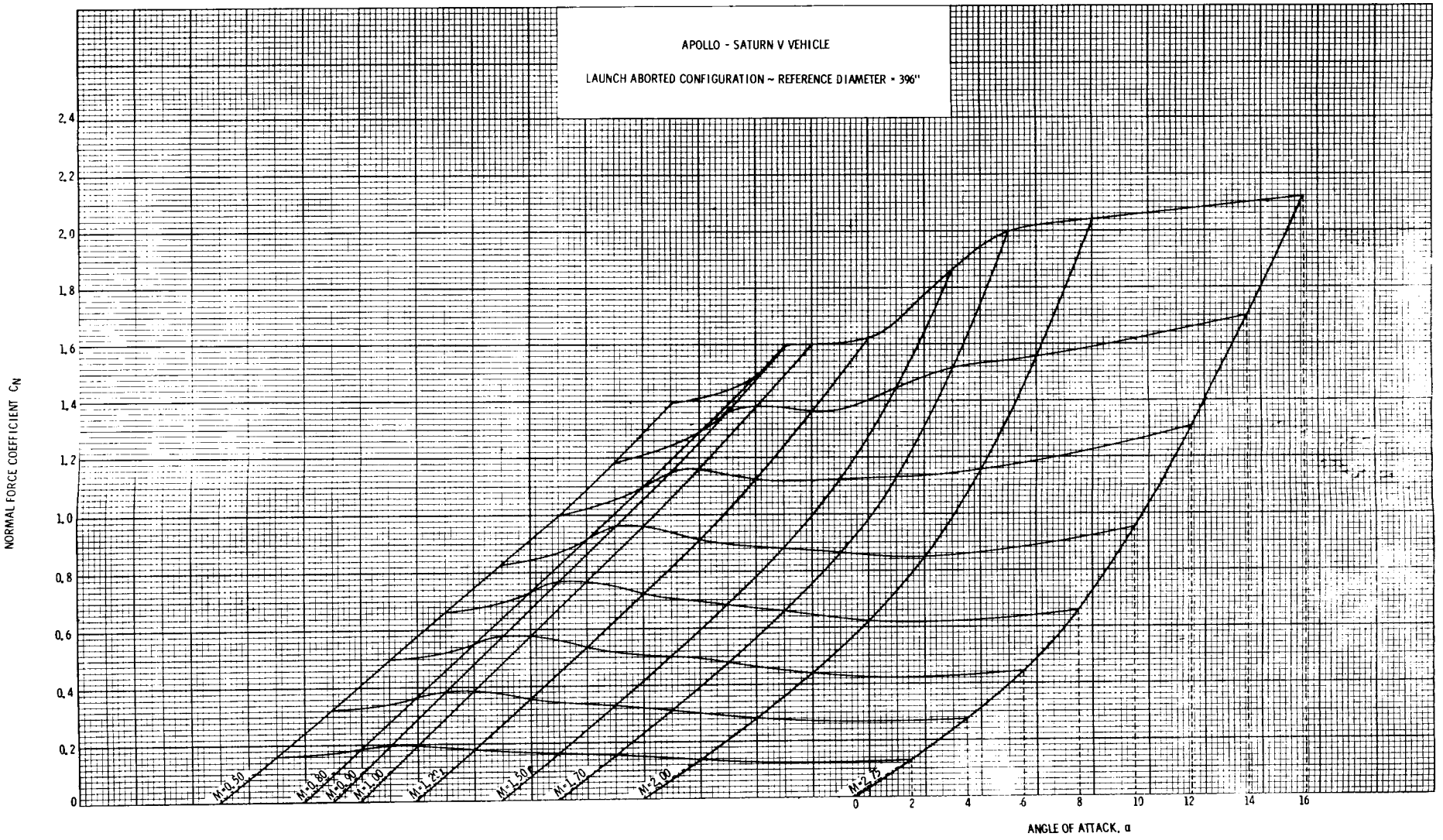

FIGURE 6 VARIATION OF NORMAL FORCE COEFFICIENT AT ANGLES OF ATTACK AND MACH NUMBERS

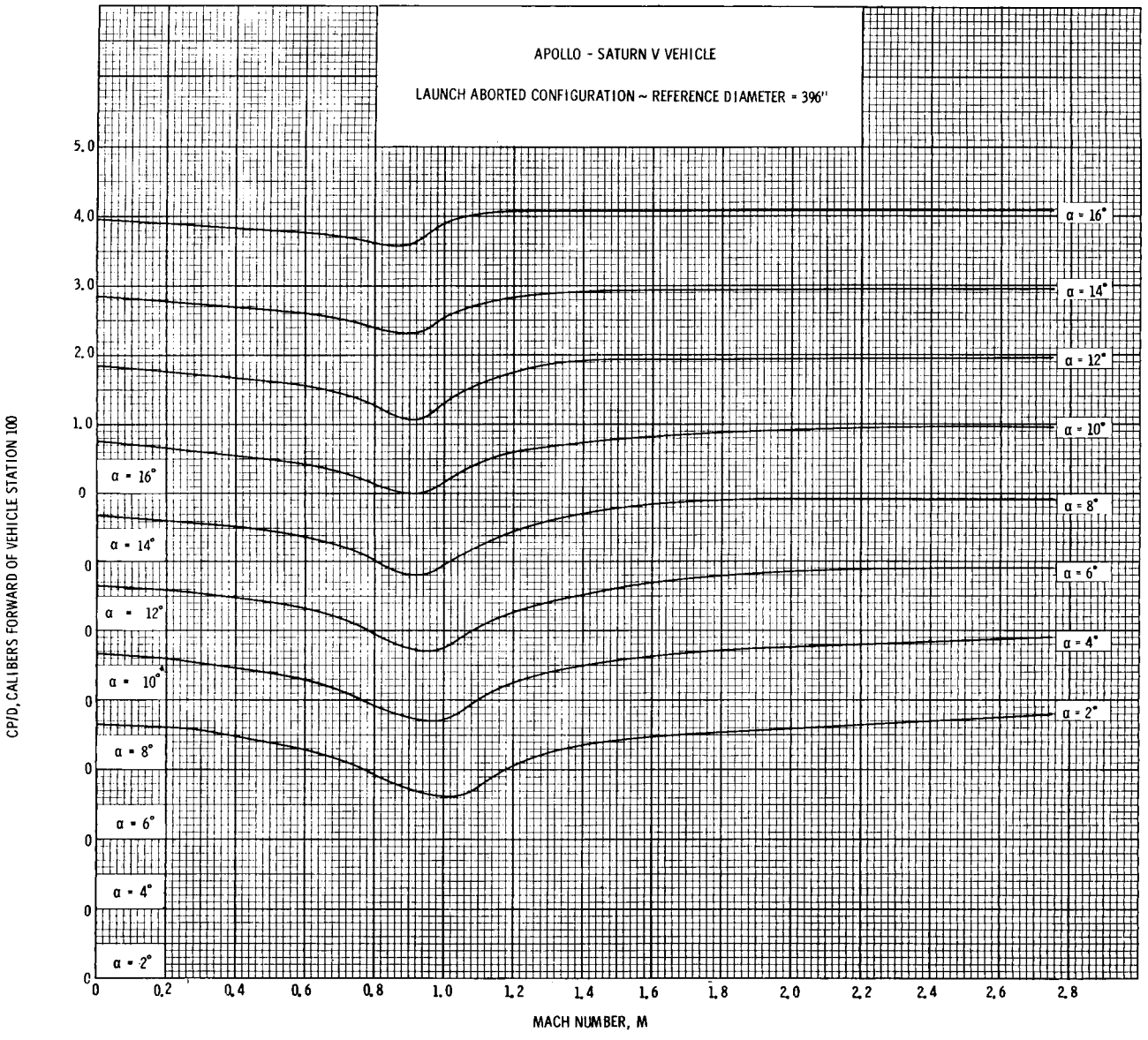

FIGURE 7 VARIATION OF CENTER OF PRESSURE WITH MACH NUMBER AT ANGLES OF ATTACK FOR $2^\circ \leq \alpha \leq 16^\circ$

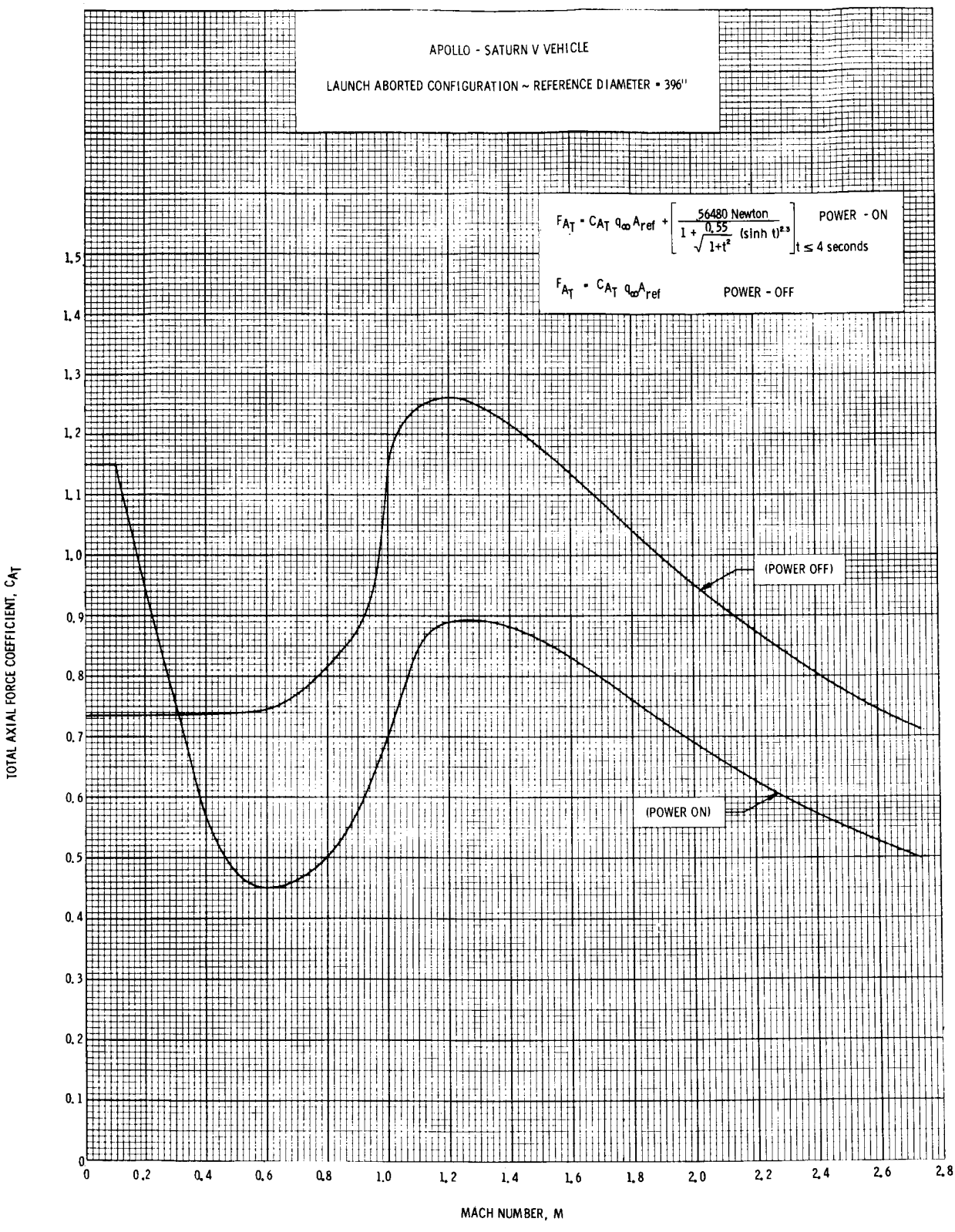

FIGURE 8 VARIATION OF AXIAL FORCE COEFFICIENT WITH MACH NUMBER AT $\alpha = 0$

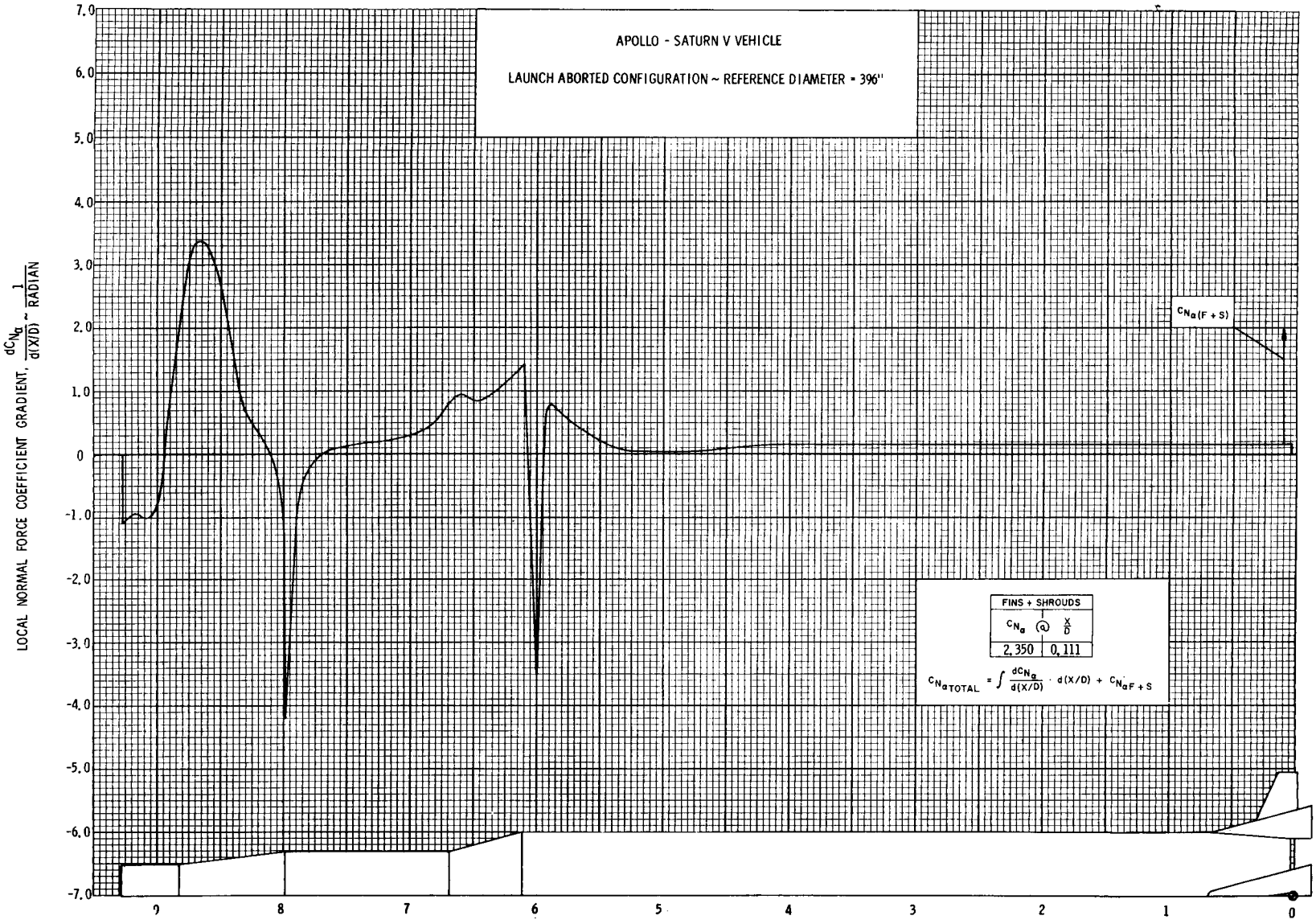

FIGURE 9 DISTRIBUTION OF LOCAL NORMAL FORCE COEFFICIENT GRADIENT, M = 0.50

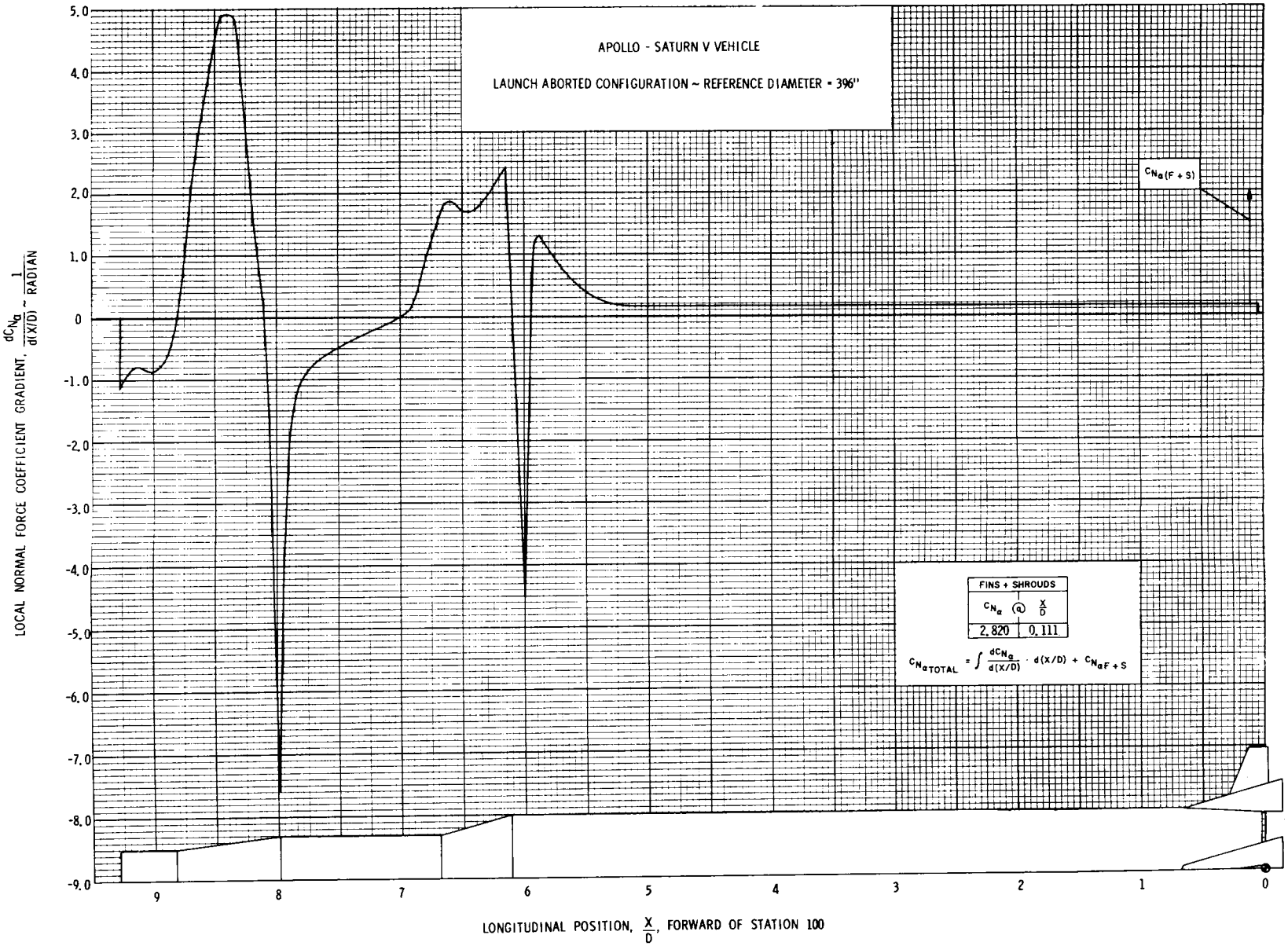

FIGURE 10 DISTRIBUTION OF LOCAL NORMAL FORCE COEFFICIENT GRADIENT, M = 0.80

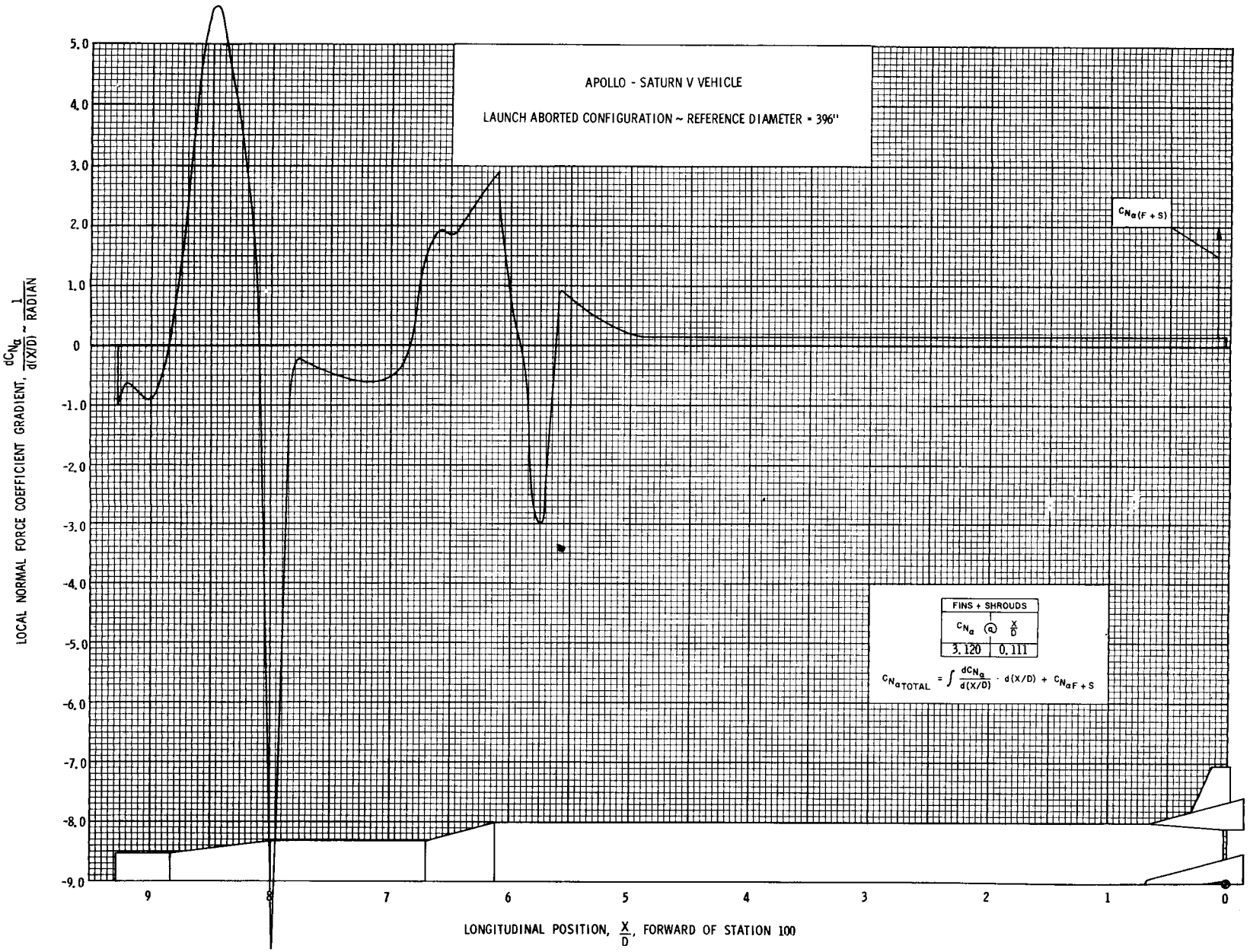

FIGURE 11 DISTRIBUTION OF LOCAL NORMAL FORCE COEFFICIENT GRADIENT, M = 0.90

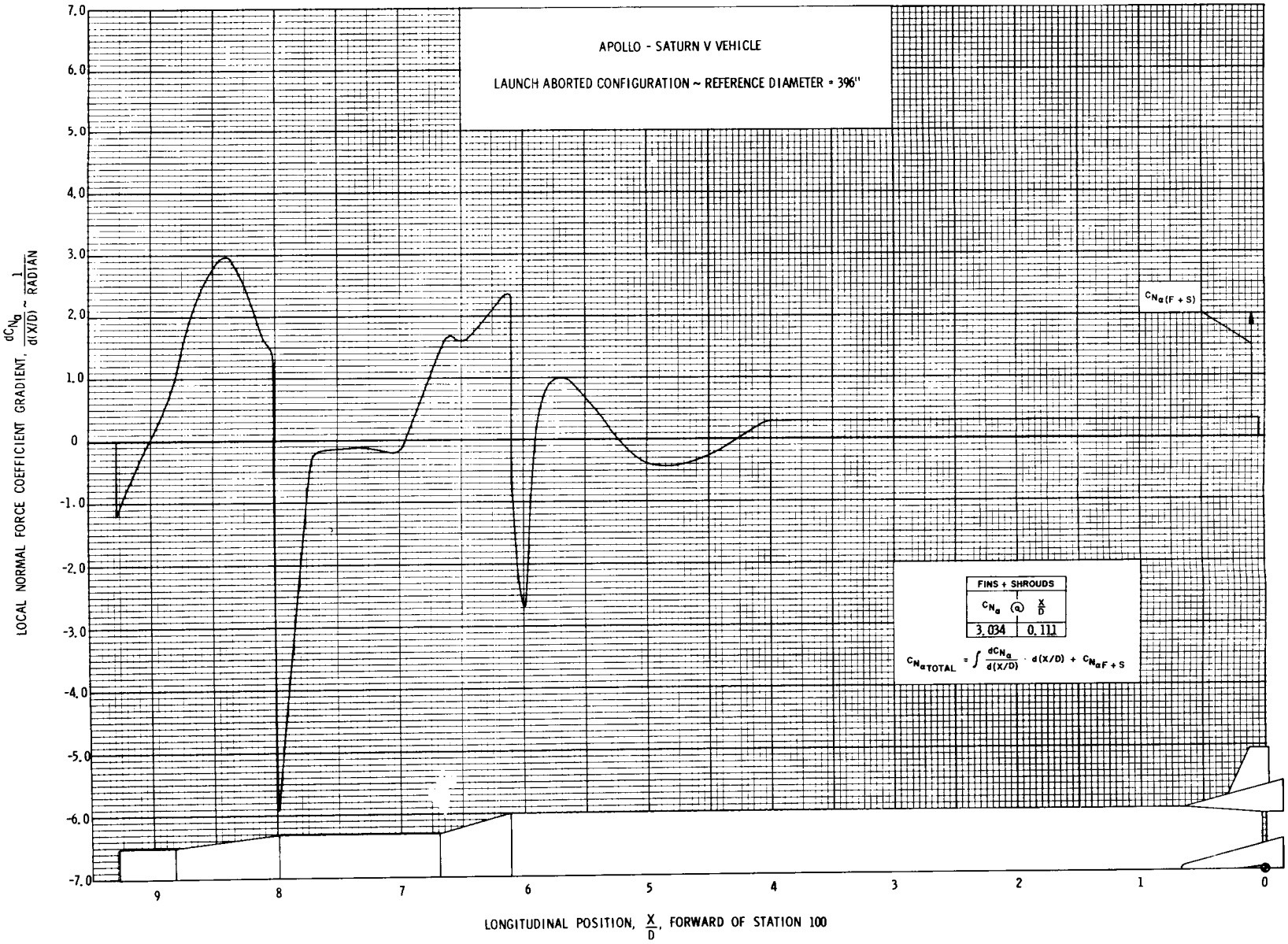

FIGURE 12 DISTRIBUTION OF LOCAL NORMAL FORCE COEFFICIENT GRADIENT, M = 1.00

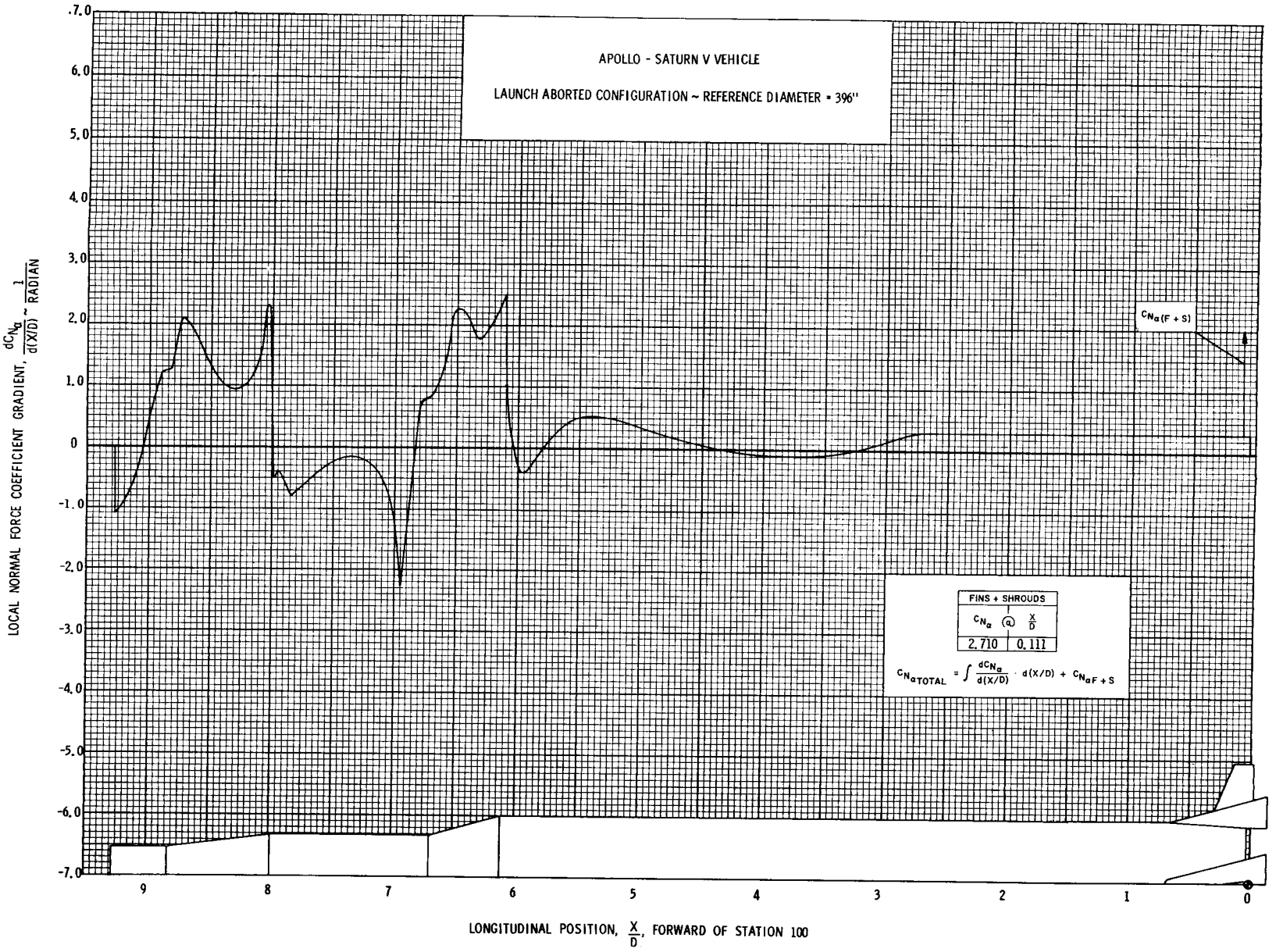

FIGURE 13 DISTRIBUTION OF LOCAL NORMAL FORCE COEFFICIENT GRADIENT, M = 1.20

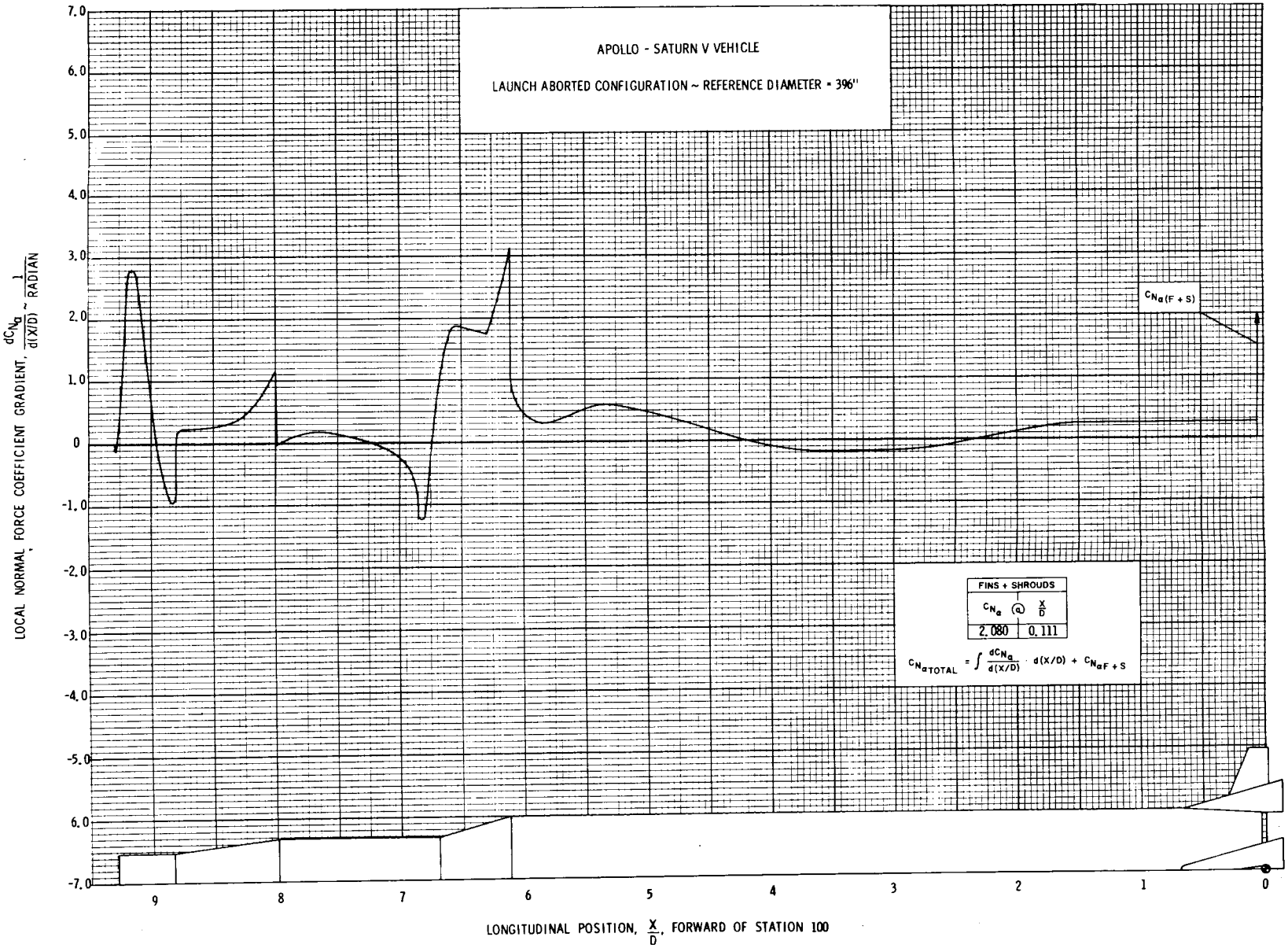

FIGURE 14 DISTRIBUTION OF LOCAL NORMAL FORCE COEFFICIENT GRADIENT, M = 1.50.

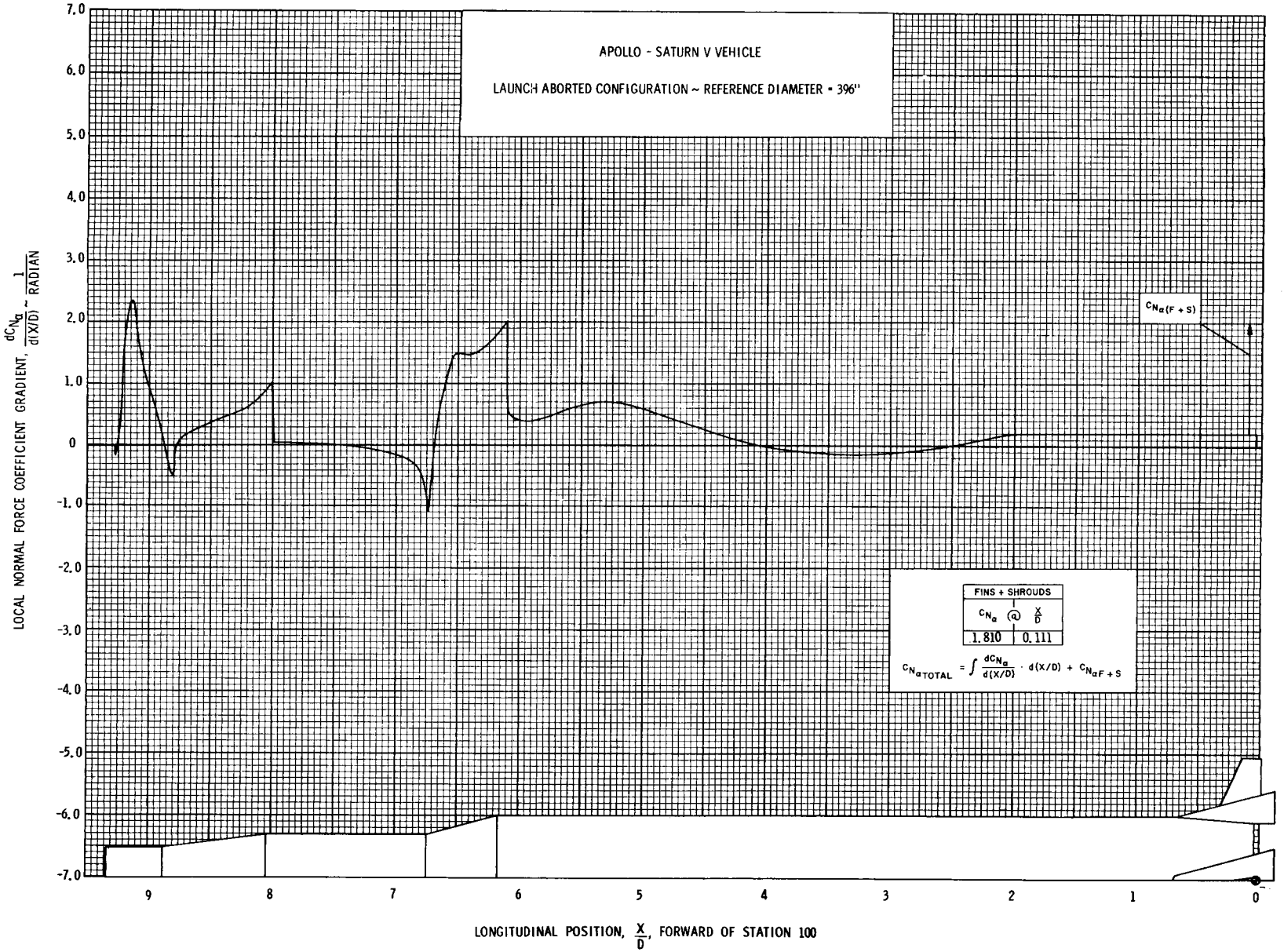

FIGURE 15 DISTRIBUTION OF LOCAL NORMAL FORCE COEFFICIENT GRADIENT, M = 1.76

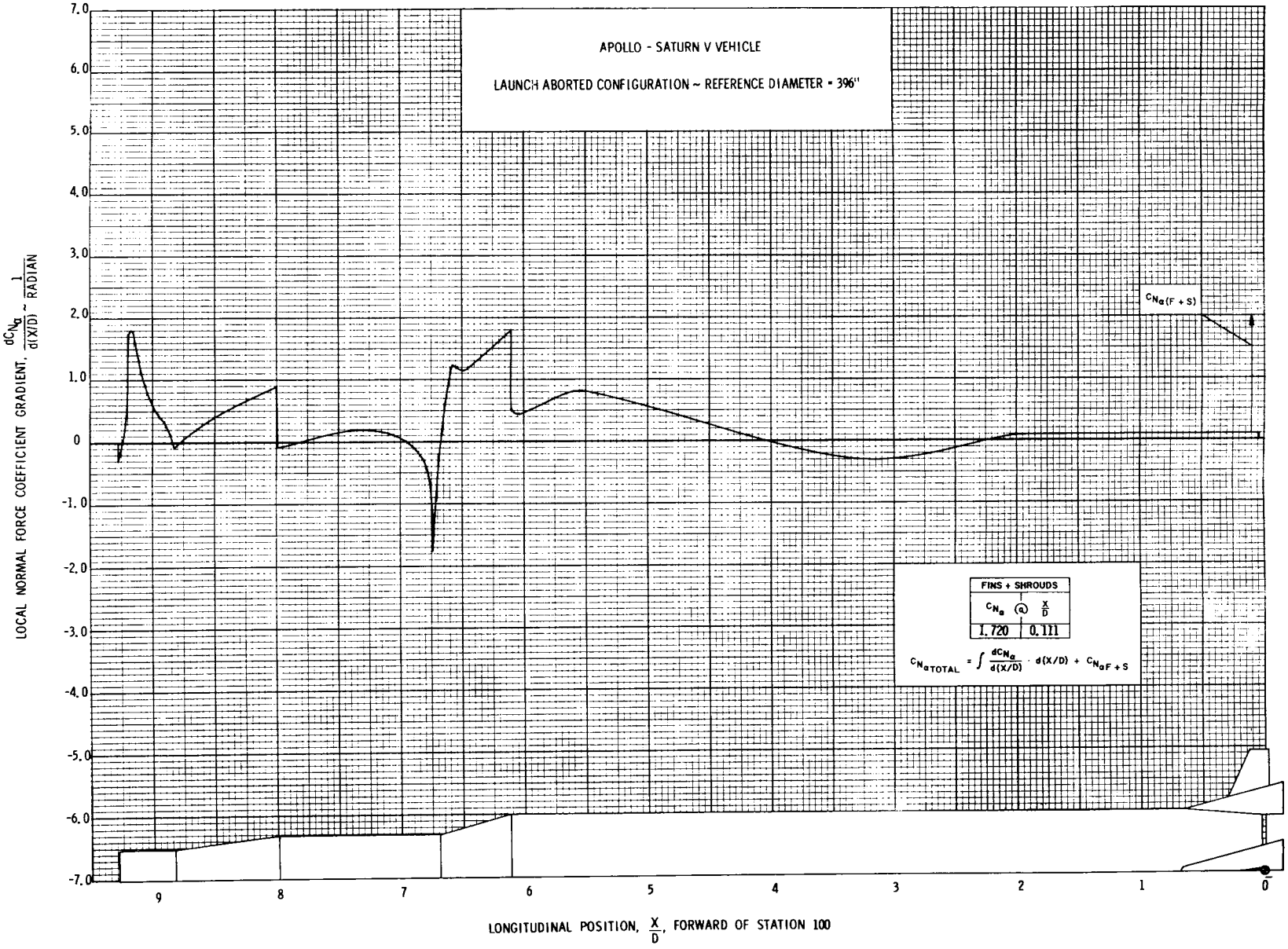

FIGURE 16 DISTRIBUTION OF LOCAL NORMAL FORCE COEFFICIENT GRADIENT, M = 2.00

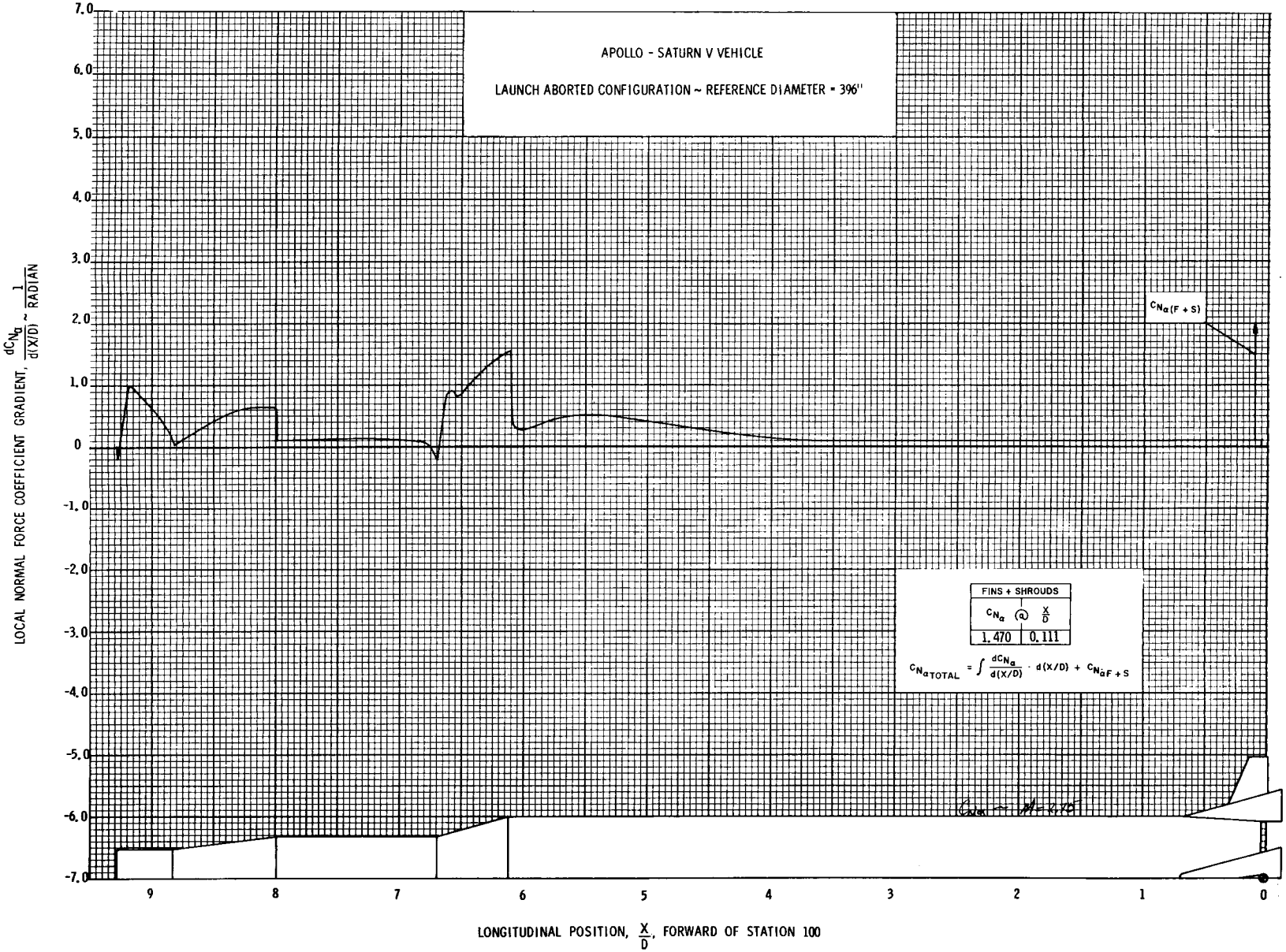

FIGURE 17 DISTRIBUTION OF LOCAL NORMAL FORCE COEFFICIENT GRADIENT, M = 2.75

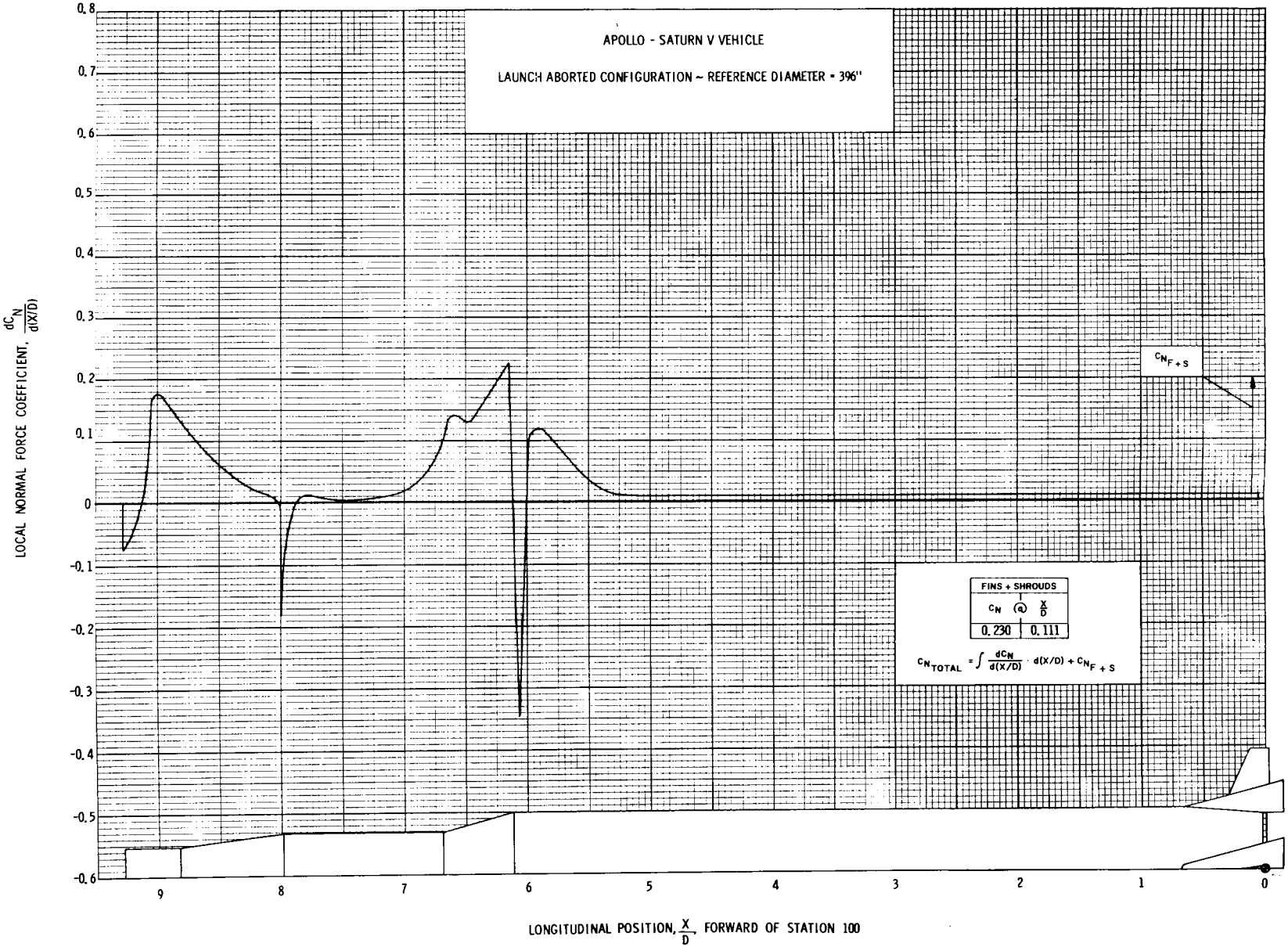

FIGURE 18 DISTRIBUTION OF LOCAL NORMAL FORCE COEFFICIENT, M = 0.50 ; α = 6°

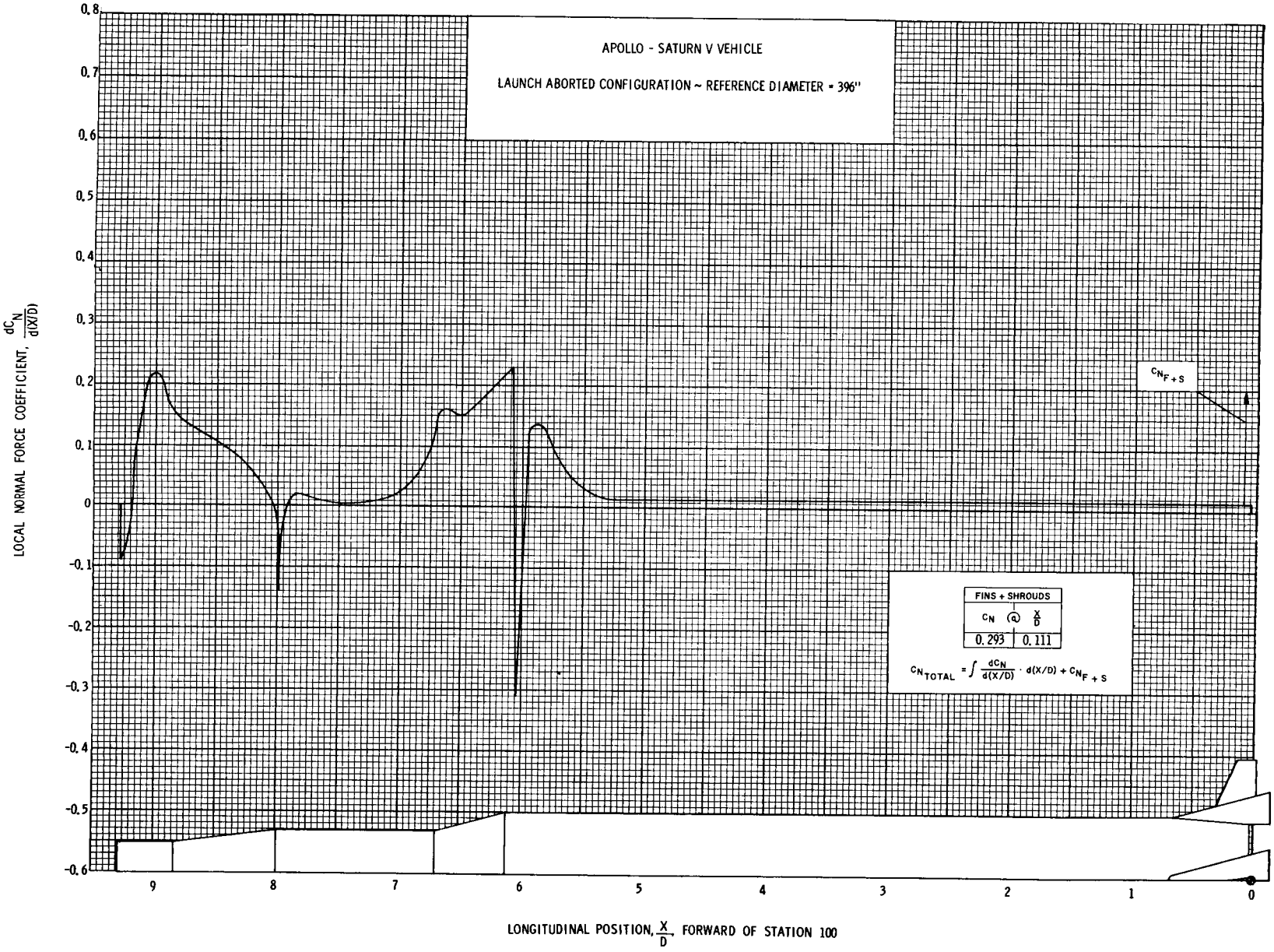

FIGURE 19 DISTRIBUTION OF LOCAL NORMAL FORCE COEFFICIENT, M = 0.50 ; α = 8°

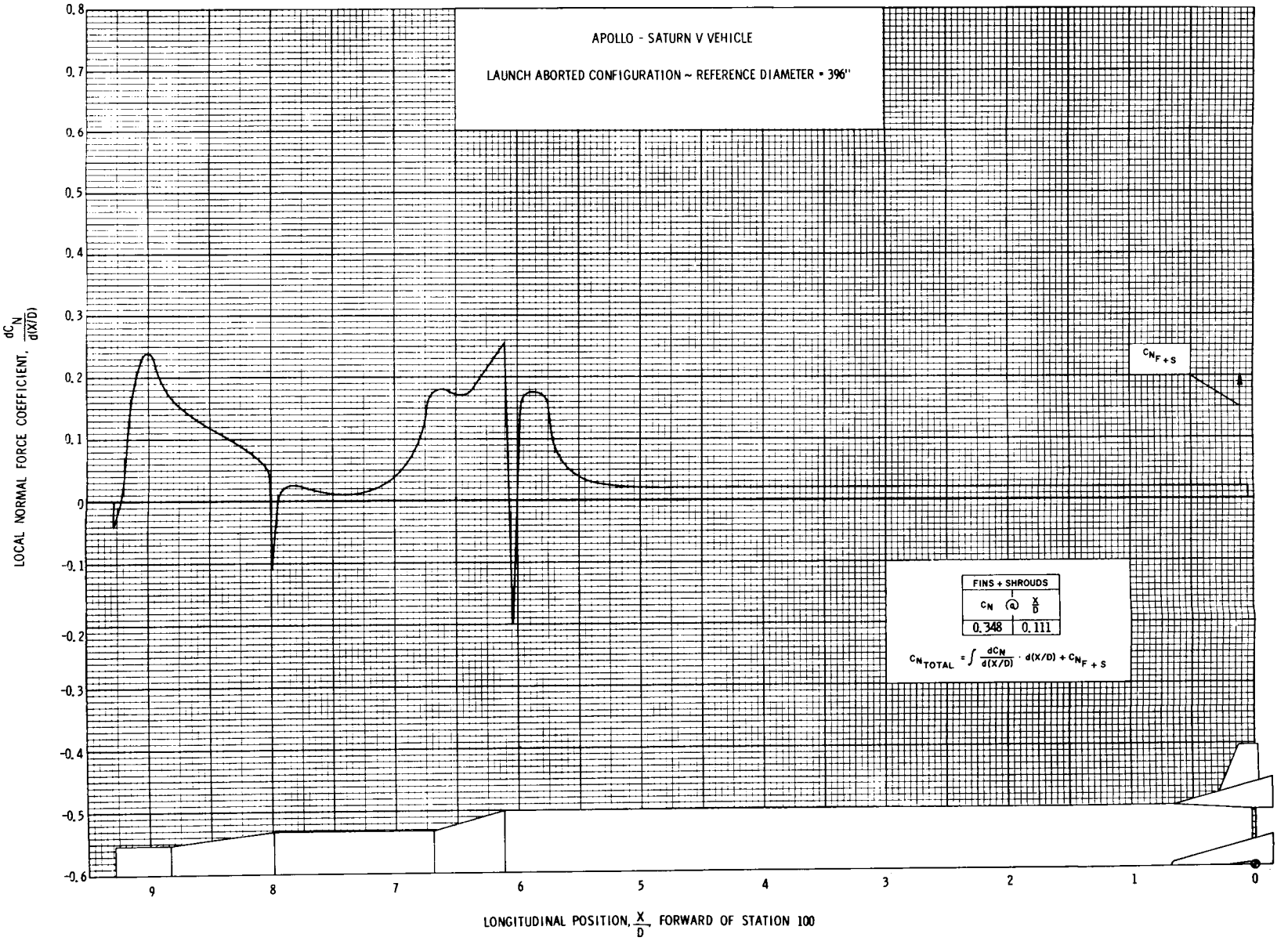

FIGURE 20 DISTRIBUTION OF LOCAL NORMAL FORCE COEFFICIENT, M = 0.50 ; $\alpha = 10°$

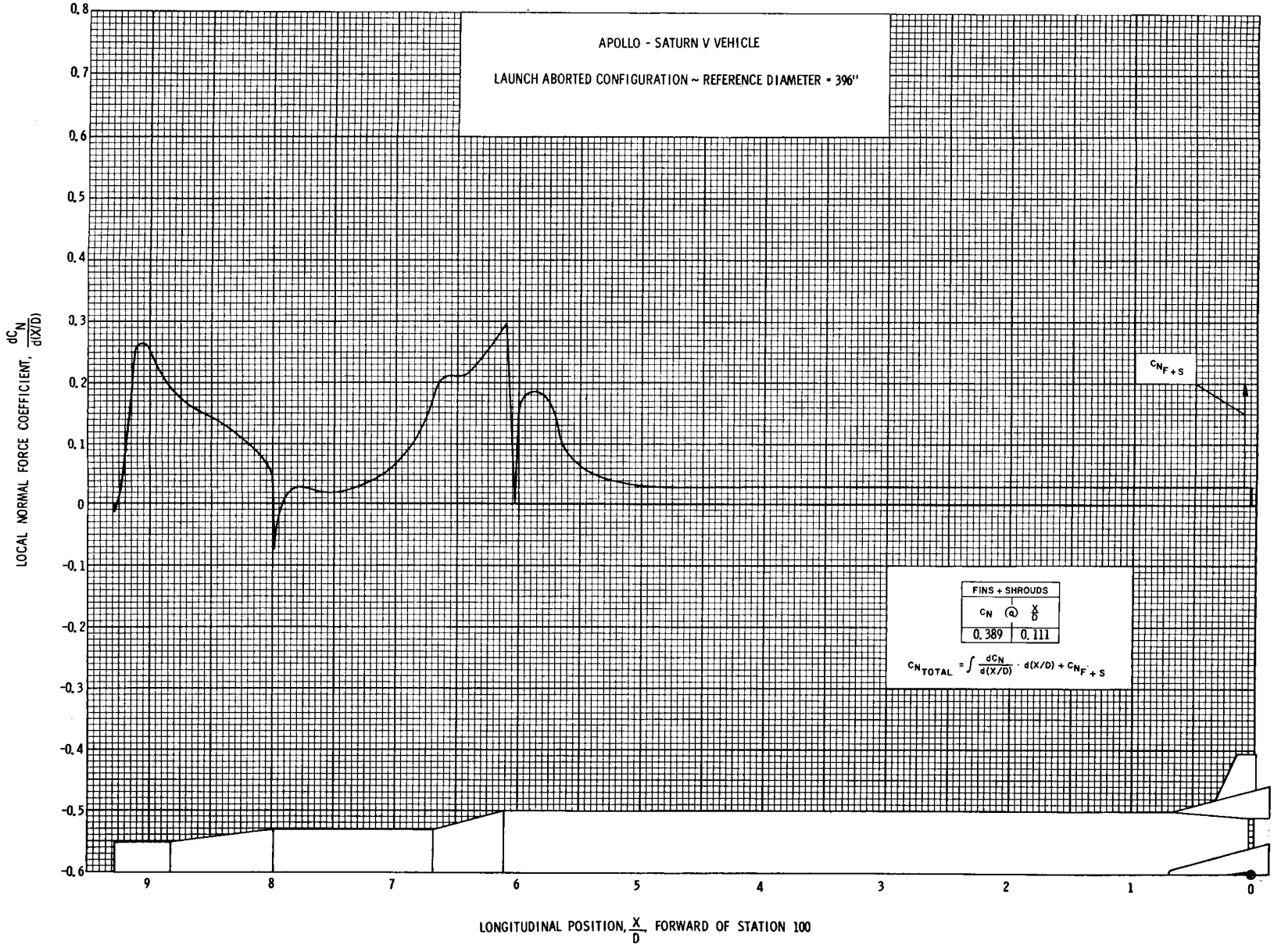

FIGURE 21 DISTRIBUTION OF LOCAL NORMAL FORCE COEFFICIENT, M = 0.50 ; α = 12°

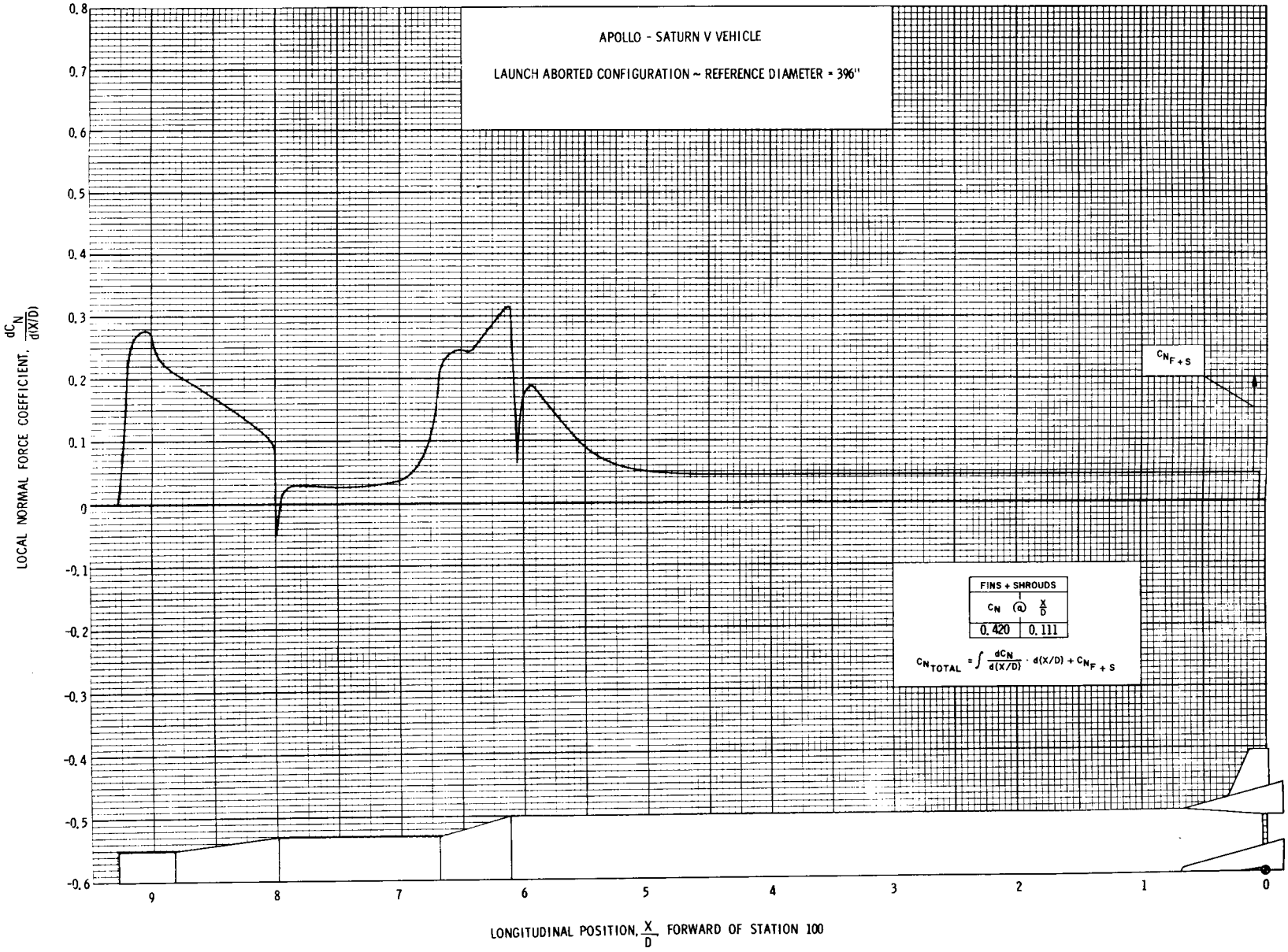

FIGURE 22 DISTRIBUTION OF LOCAL NORMAL FORCE COEFFICIENT, M = 0.50 ; $\alpha = 14^\circ$

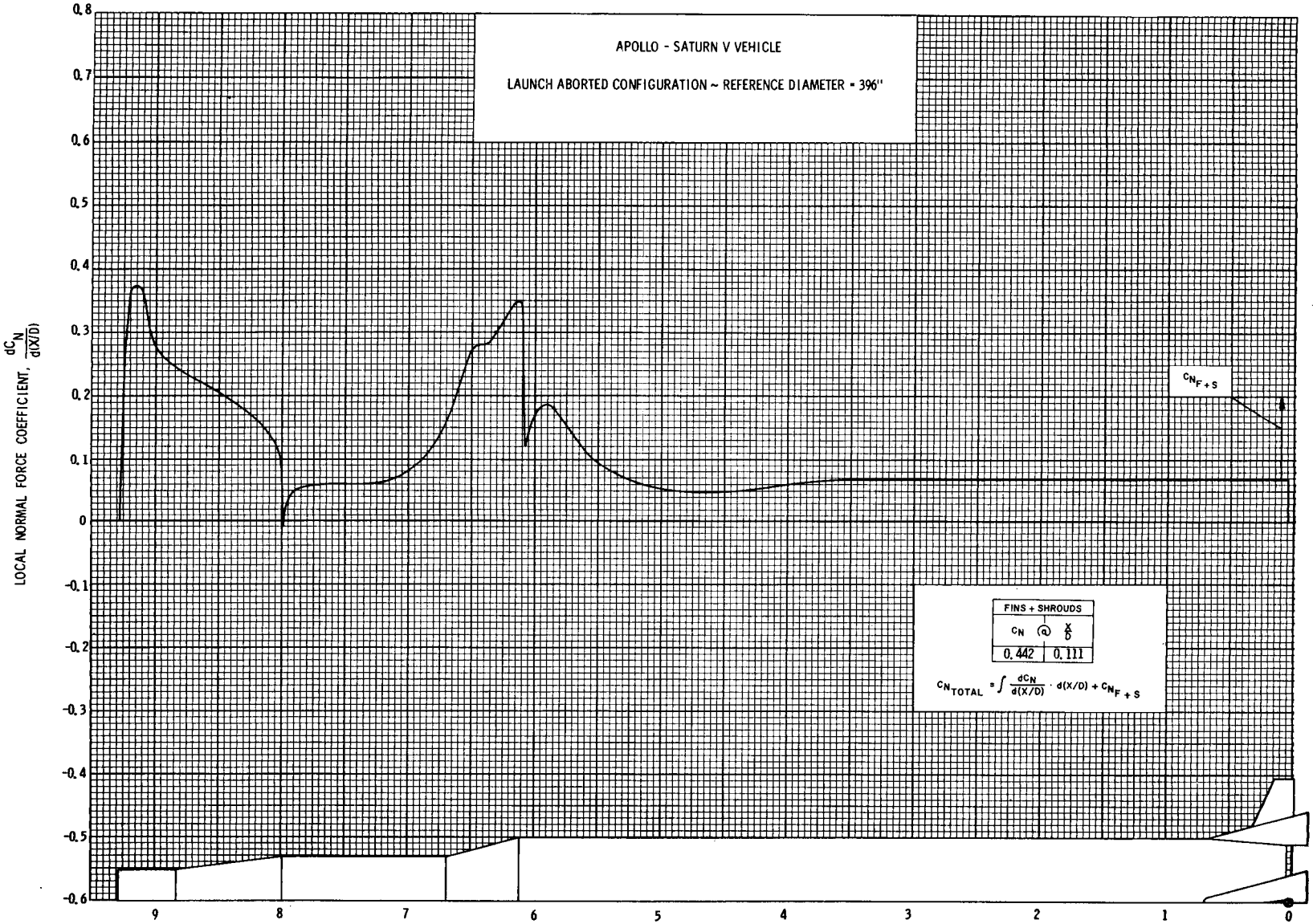

FIGURE 23 DISTRIBUTION OF LOCAL NORMAL FORCE COEFFICIENT, M = 0.50 ; $\alpha = 16°$

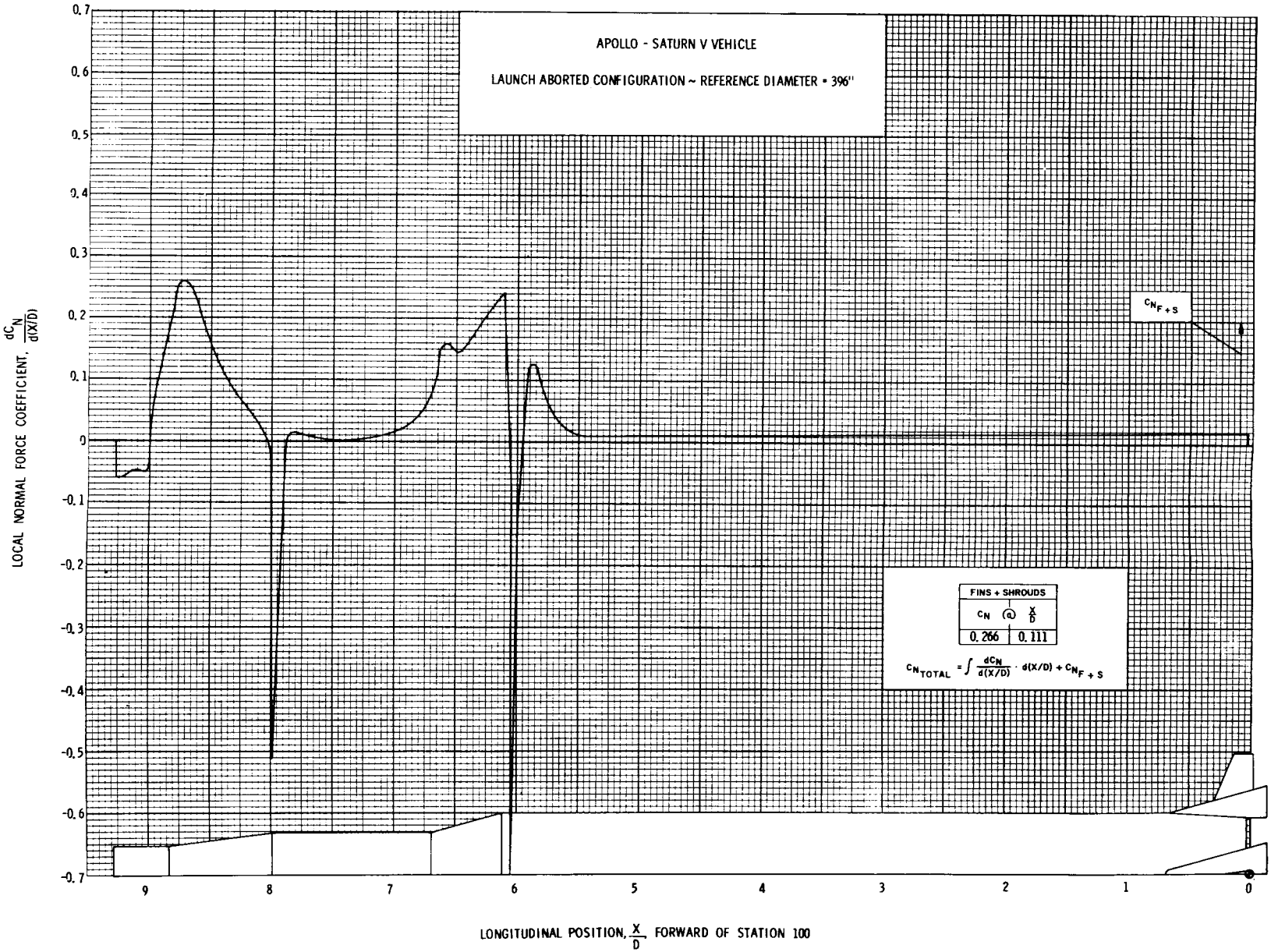

FIGURE 24 DISTRIBUTION OF LOCAL NORMAL FORCE COEFFICIENT, M = 0.80 ; $\alpha = 6^\circ$

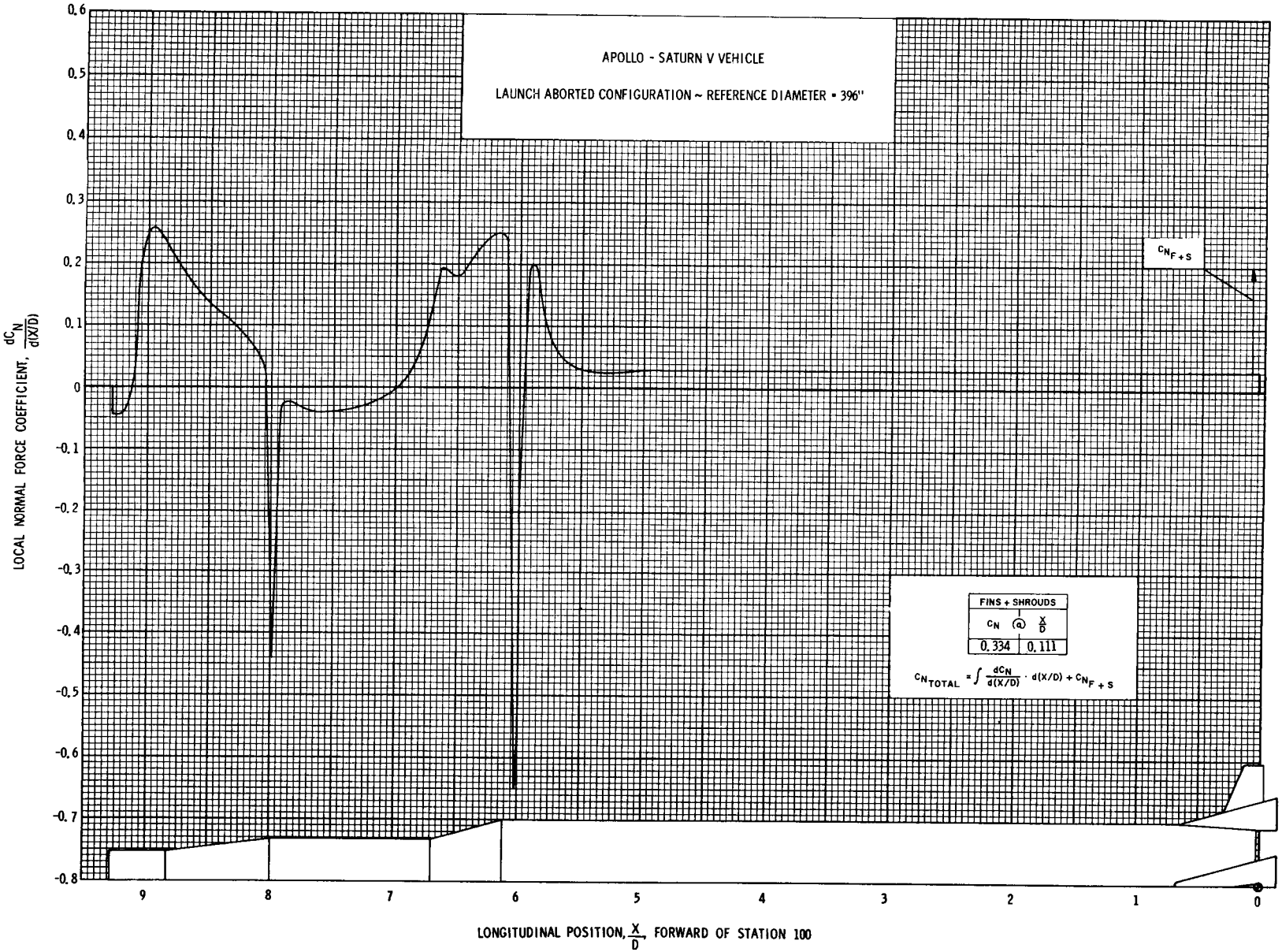

FIGURE 25 DISTRIBUTION OF LOCAL NORMAL FORCE COEFFICIENT, M = 0.80 ; $\alpha = 8°$

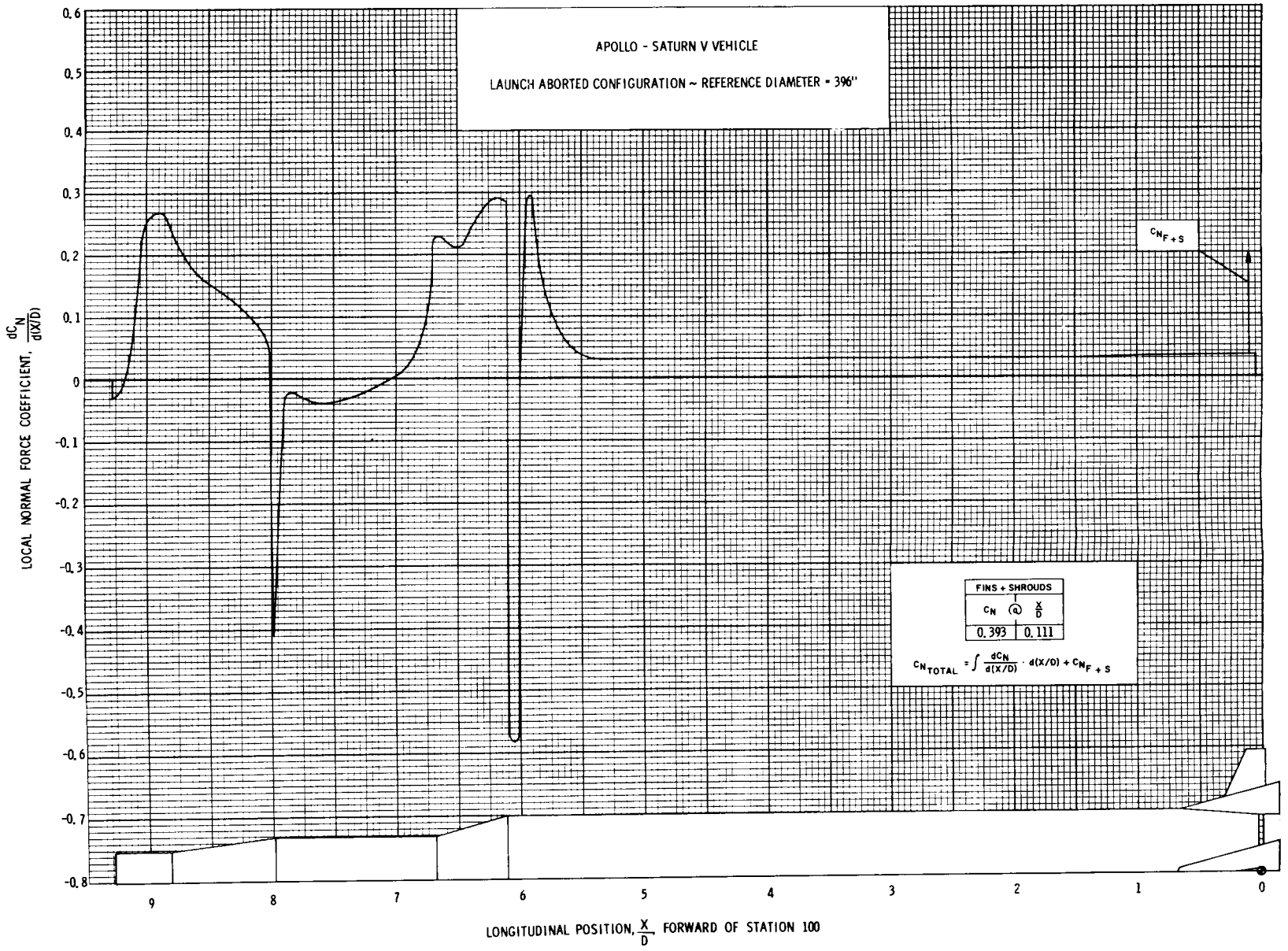

FIGURE 26 DISTRIBUTION OF LOCAL NORMAL FORCE COEFFICIENT, M = 0.80 ; $\alpha = 10^\circ$

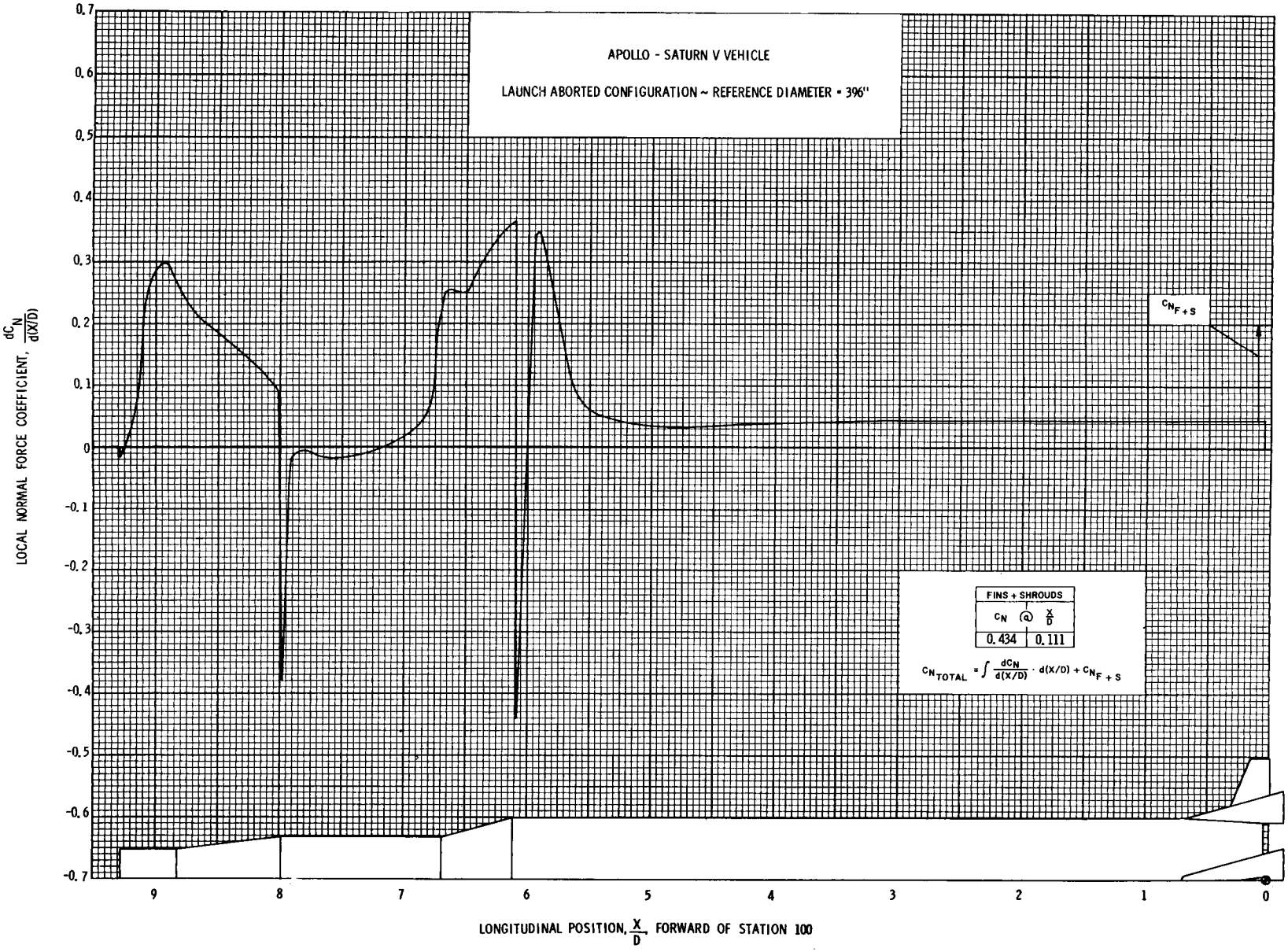

FIGURE 27 DISTRIBUTION OF LOCAL NORMAL FORCE COEFFICIENT, M = 0.80 ; $\alpha = 12^\circ$

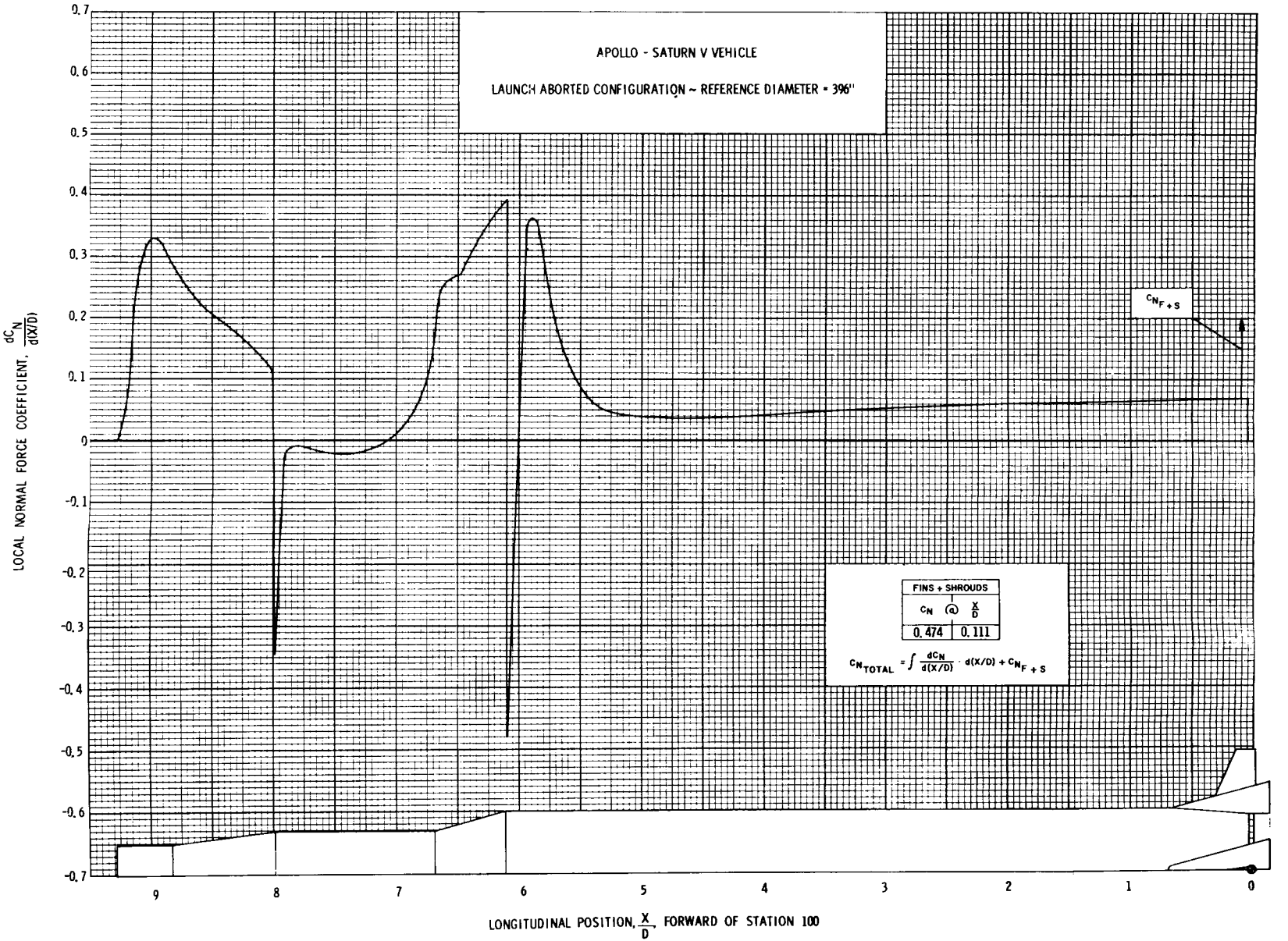

FIGURE 28 DISTRIBUTION OF LOCAL NORMAL FORCE COEFFICIENT, M = 0.80 ; $\alpha = 14^\circ$

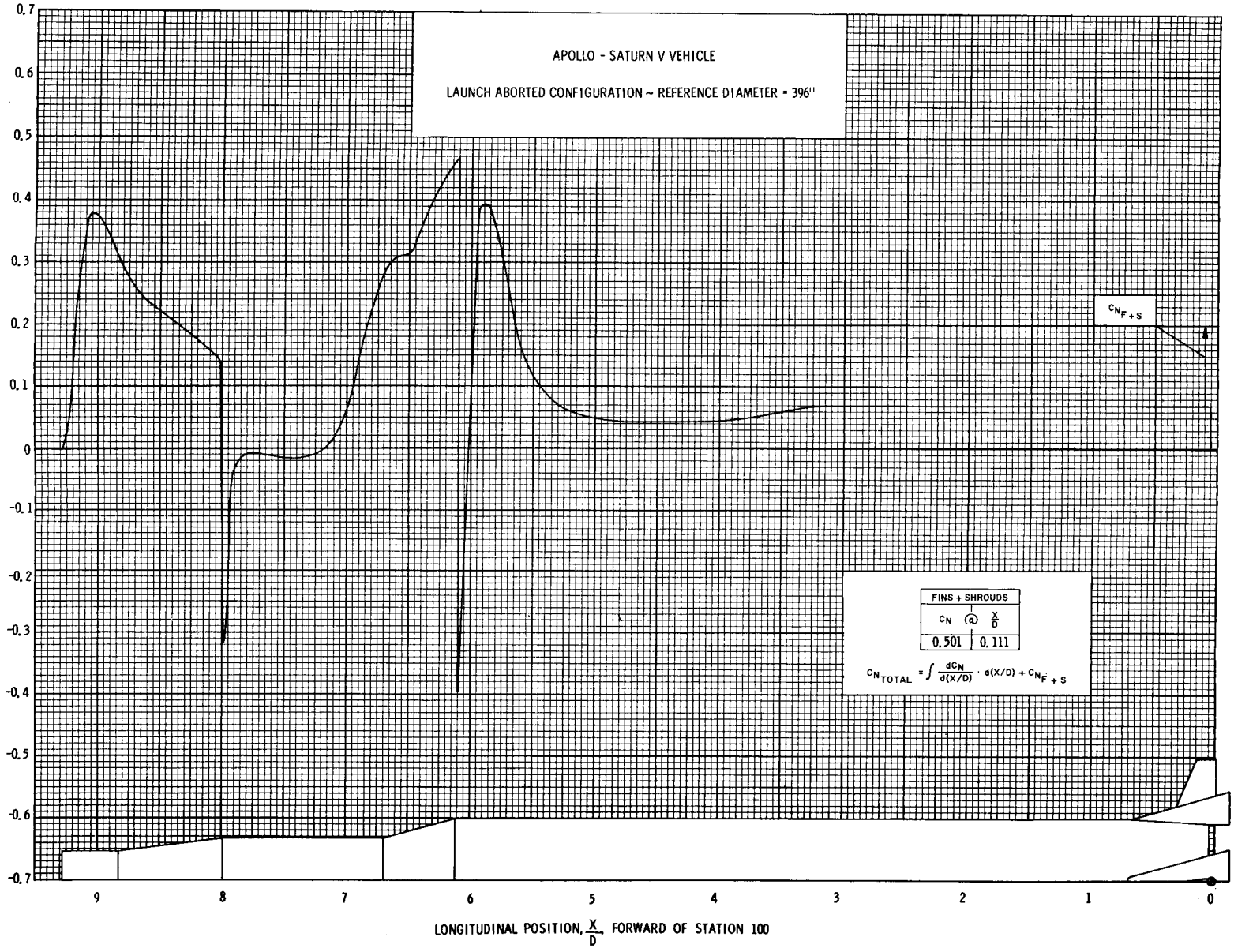

FIGURE 29 DISTRIBUTION OF LOCAL NORMAL FORCE COEFFICIENT, M = 0.80 ; $\alpha = 16^\circ$

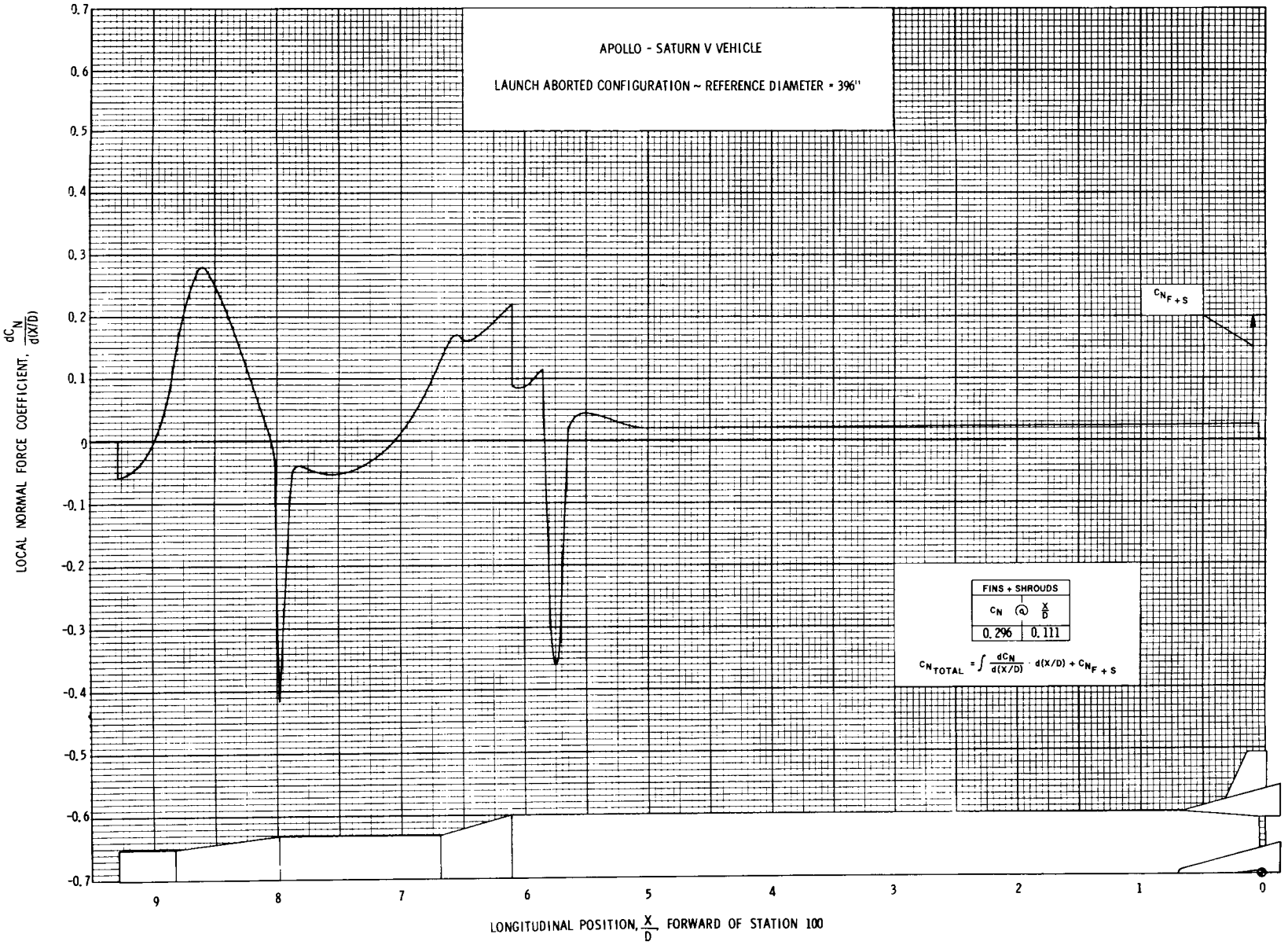

FIGURE 30 DISTRIBUTION OF LOCAL NORMAL FORCE COEFFICIENT, $M = 0.90$; $\alpha = 6°$

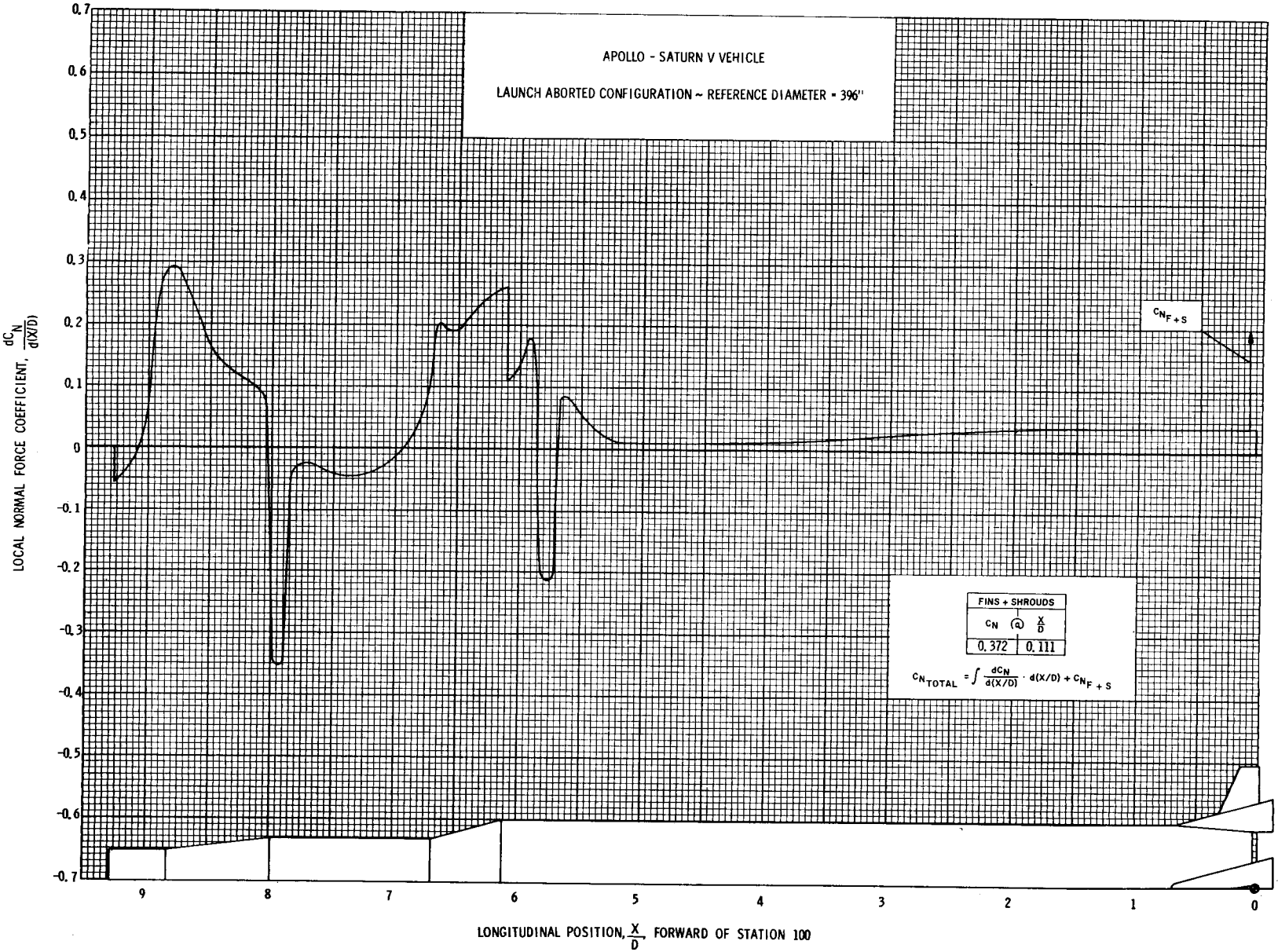

FIGURE 31 DISTRIBUTION OF LOCAL NORMAL FORCE COEFFICIENT, M = 0.90 ; α = 8°

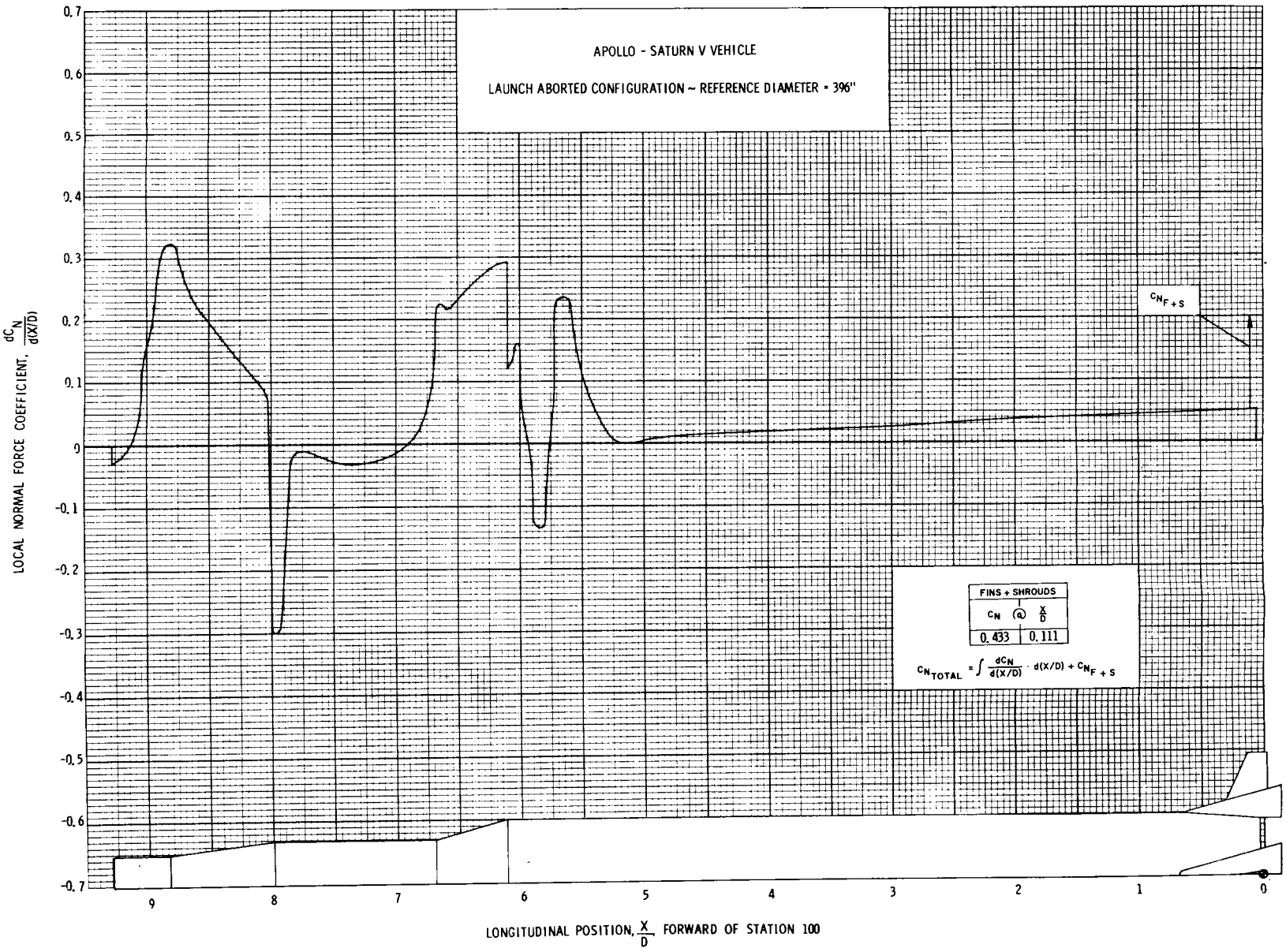

FIGURE 32 DISTRIBUTION OF LOCAL NORMAL FORCE COEFFICIENT, M = 0.90 ; $\alpha = 10°$

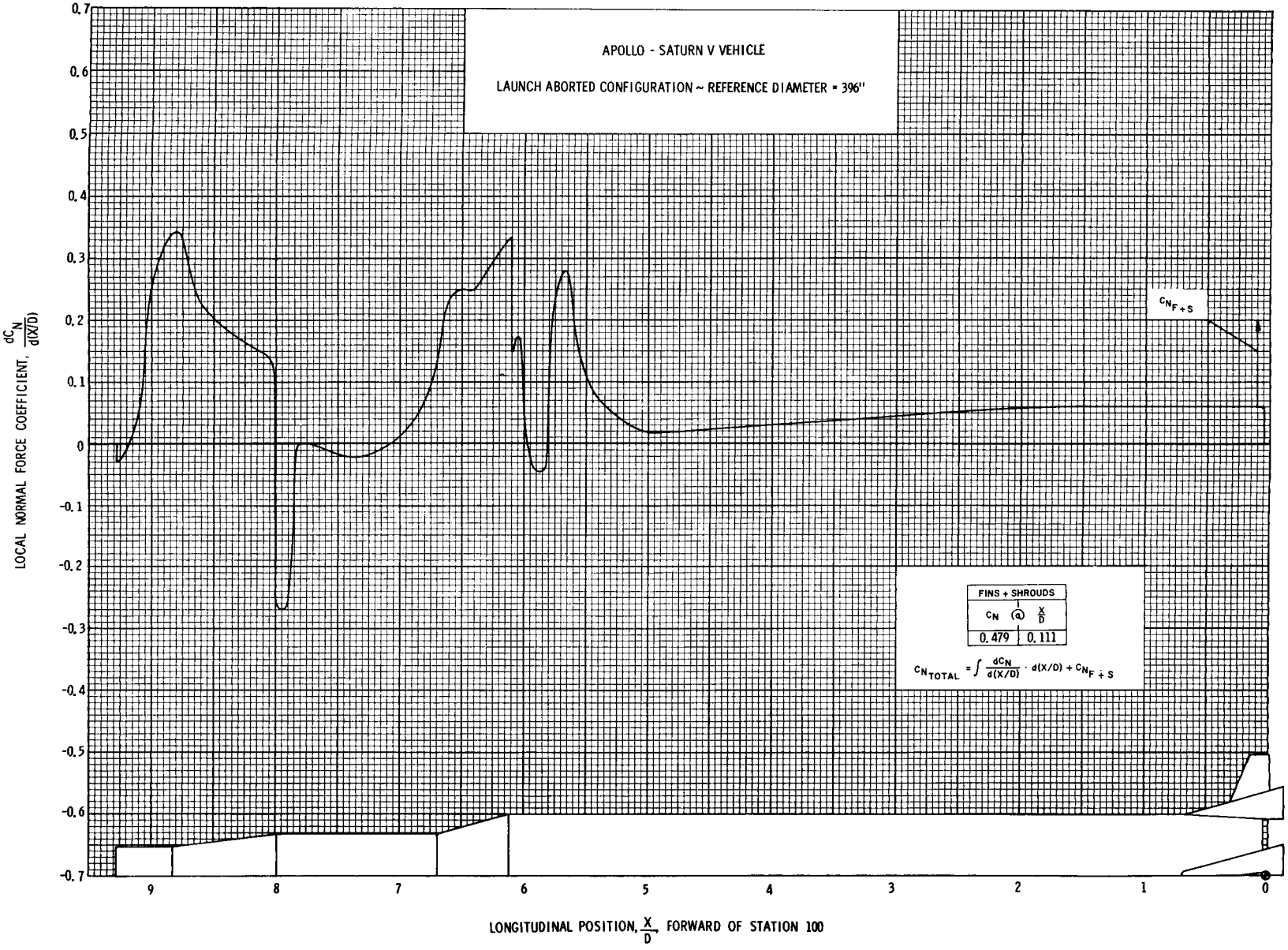

FIGURE 33 DISTRIBUTION OF LOCAL NORMAL FORCE COEFFICIENT, M = 0.90 ; $\alpha = 12^\circ$

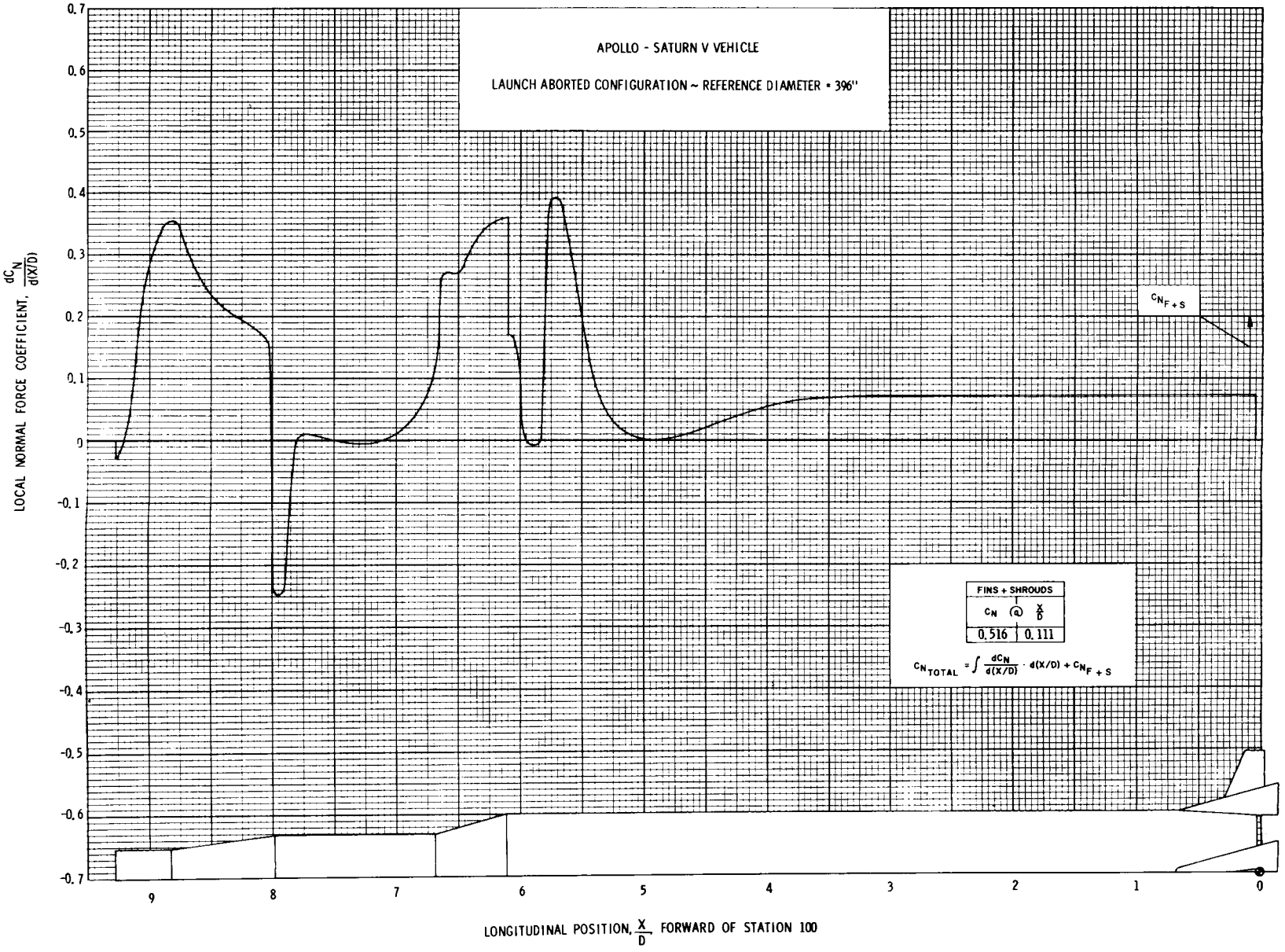

FIGURE 34 DISTRIBUTION OF LOCAL NORMAL FORCE COEFFICIENT, M = 0.90 ; $\alpha = 14^\circ$

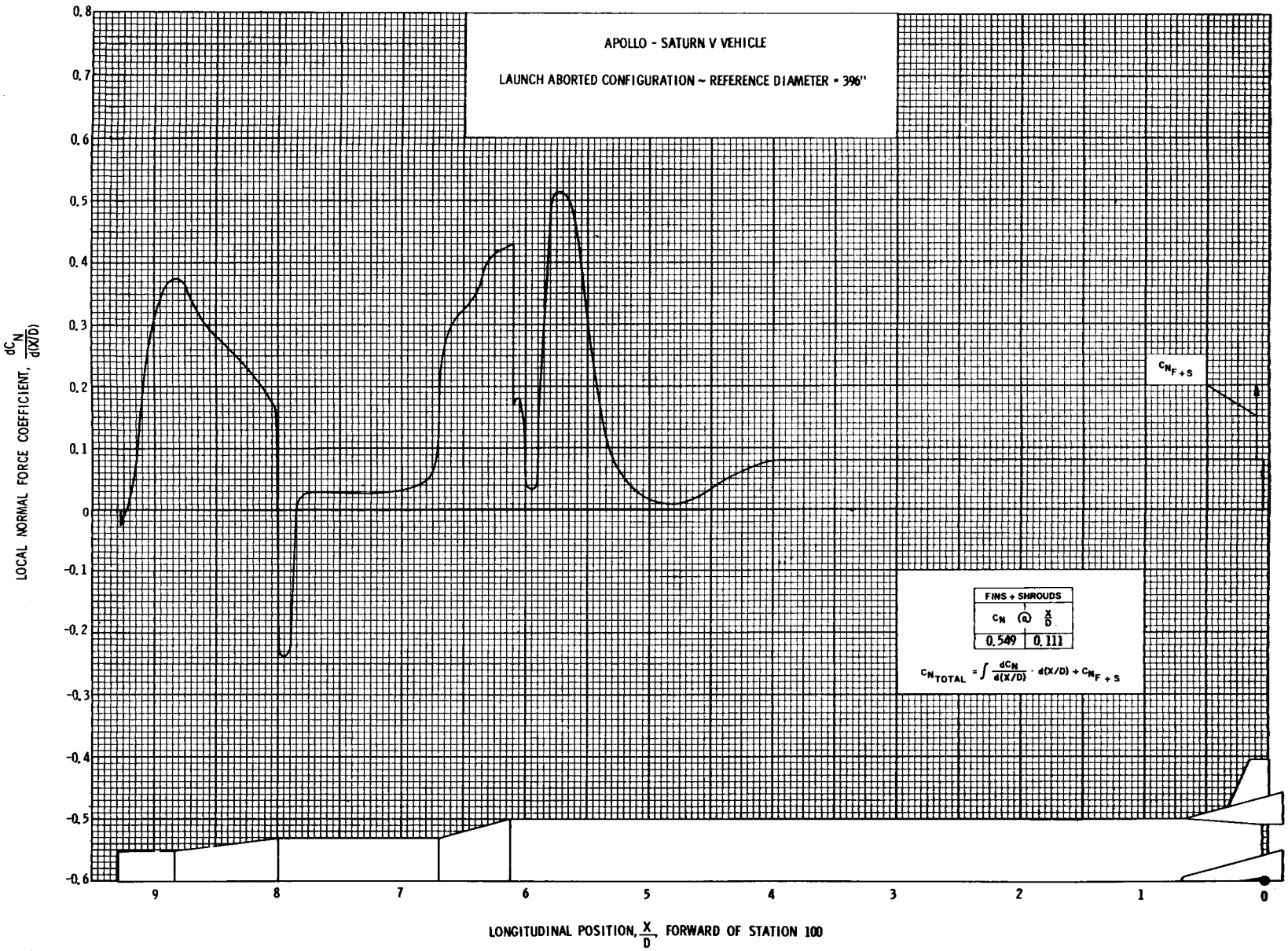

FIGURE 35 DISTRIBUTION OF LOCAL NORMAL FORCE COEFFICIENT, M = 0.90 ; $\alpha = 16^\circ$

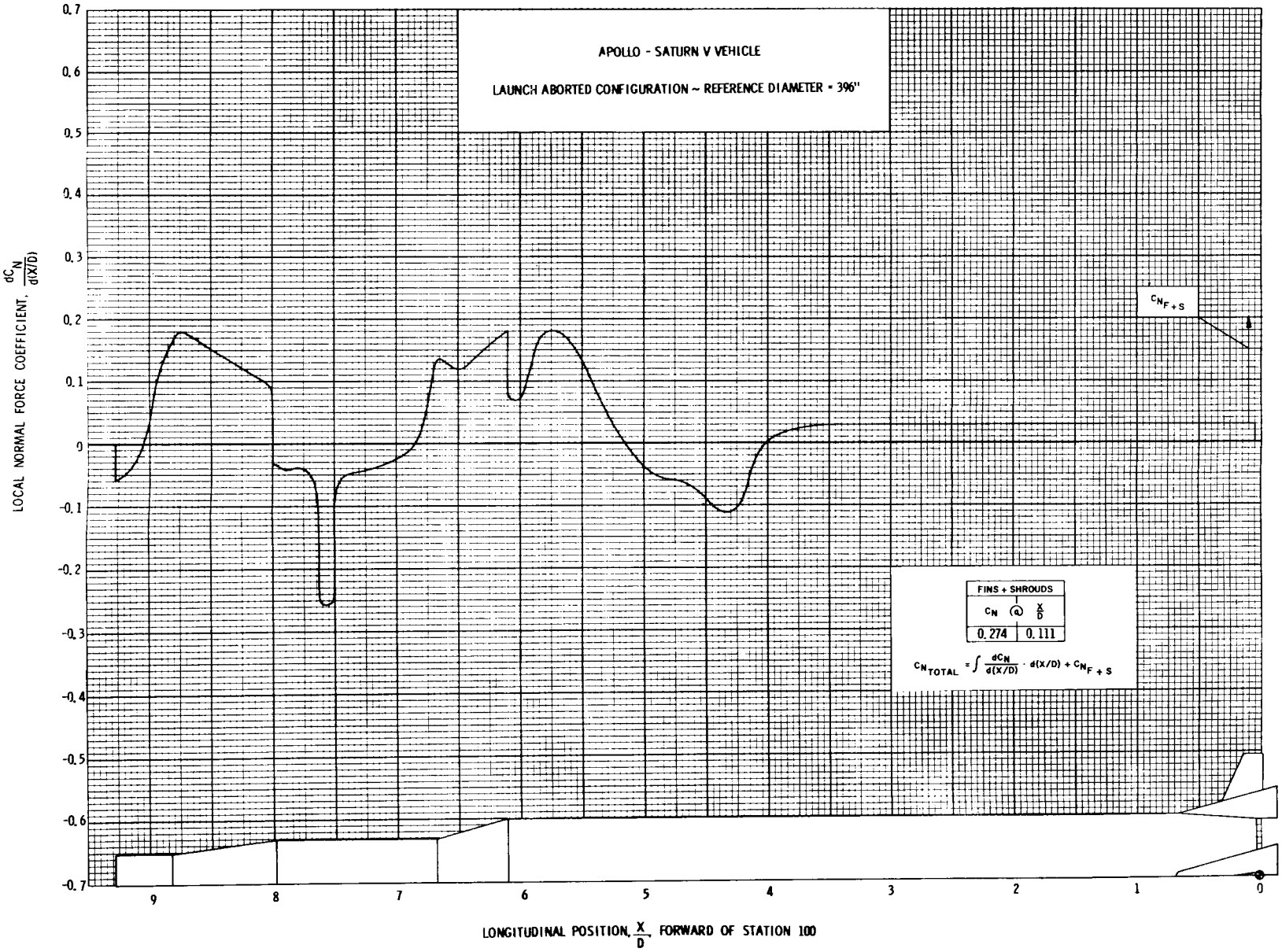

FIGURE 36 DISTRIBUTION OF LOCAL NORMAL FORCE COEFFICIENT, M = 1.00 ; $\alpha = 6^\circ$

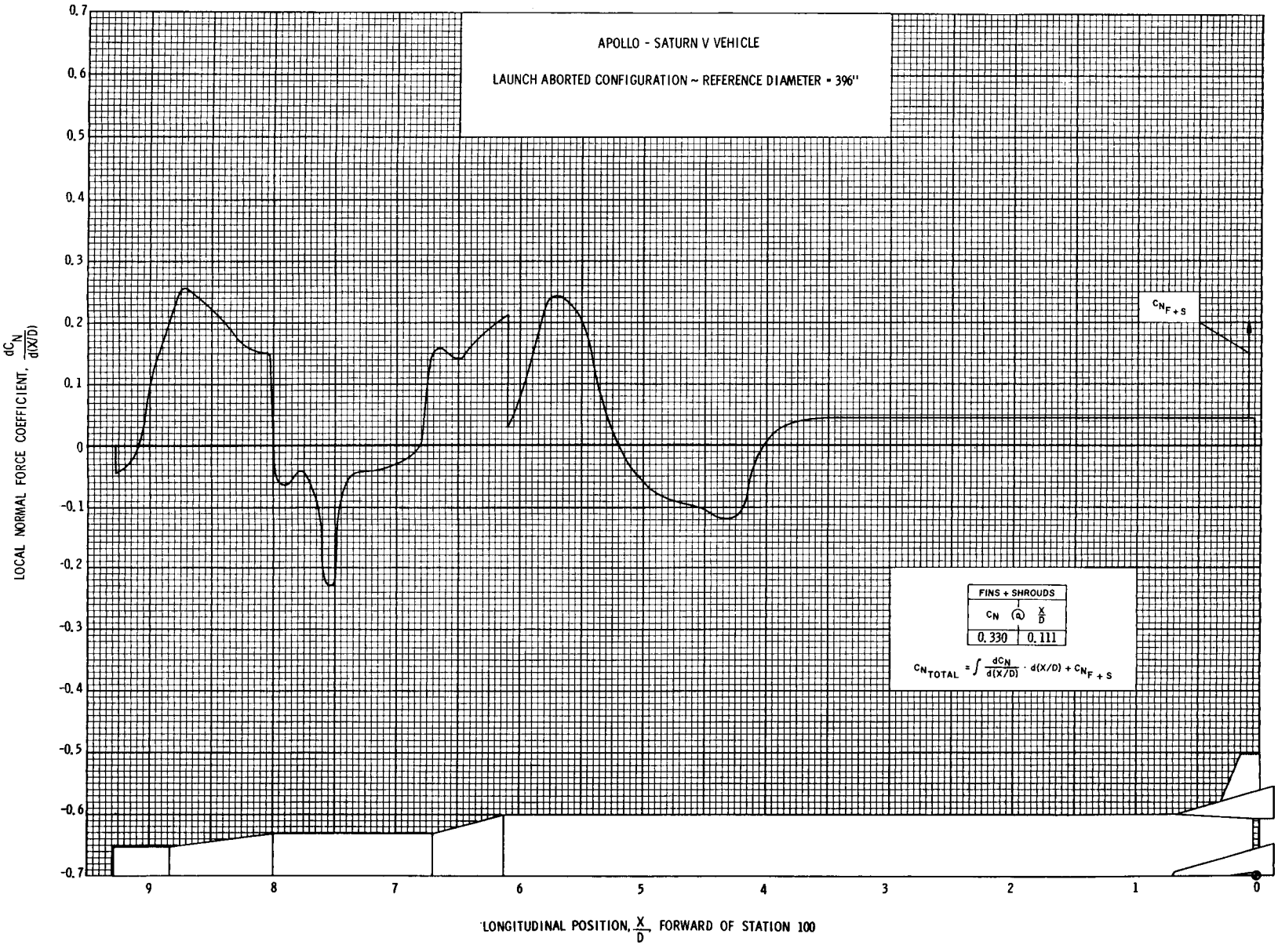

FIGURE 37 DISTRIBUTION OF LOCAL NORMAL FORCE COEFFICIENT, M = 1.00 ; $\alpha = 8°$

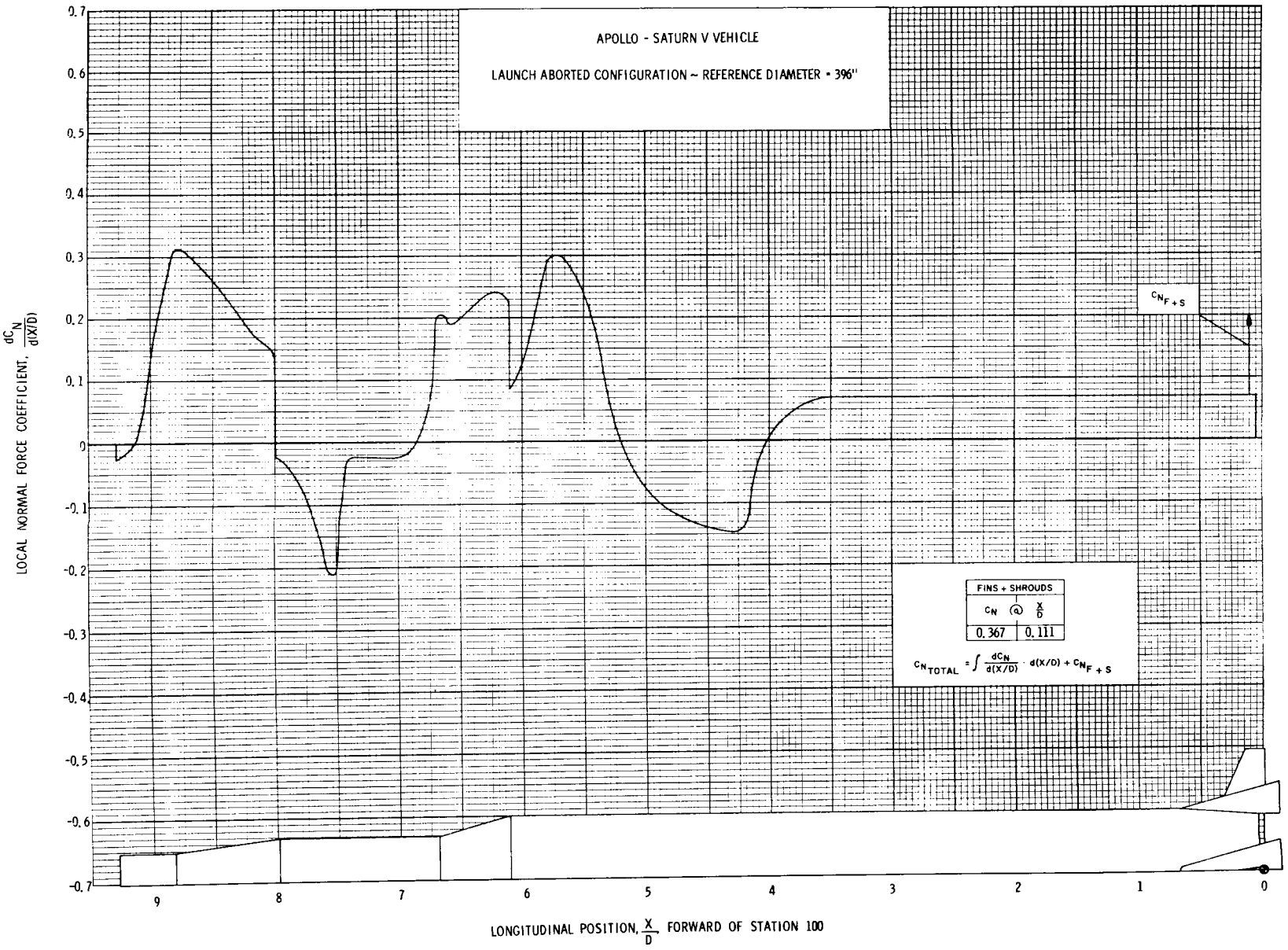

FIGURE 38 DISTRIBUTION OF LOCAL NORMAL FORCE COEFFICIENT, M = 1.00 ; $\alpha = 10^\circ$

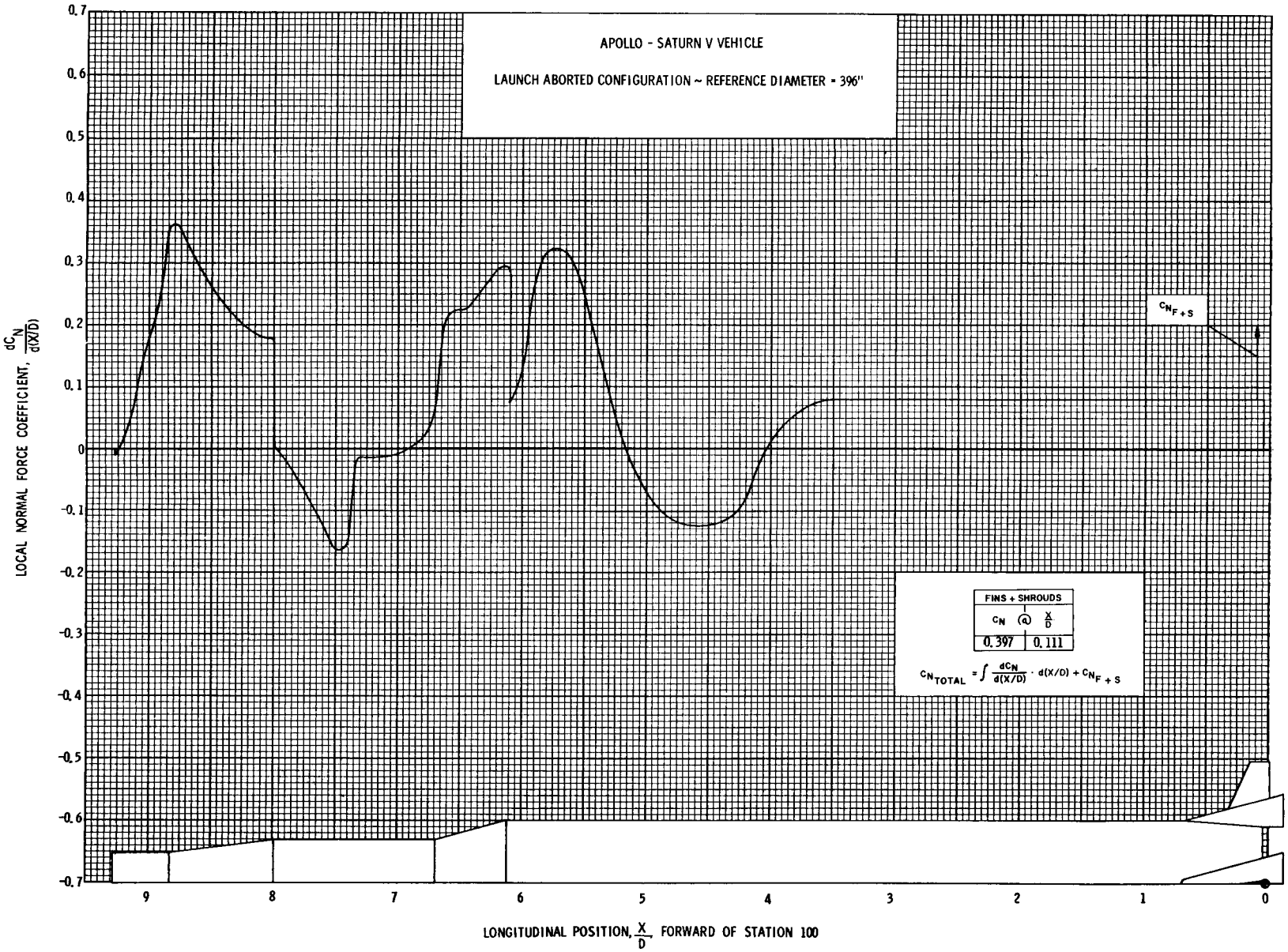

FIGURE 39 DISTRIBUTION OF LOCAL NORMAL FORCE COEFFICIENT, M = 1.00 ; $\alpha = 12^\circ$

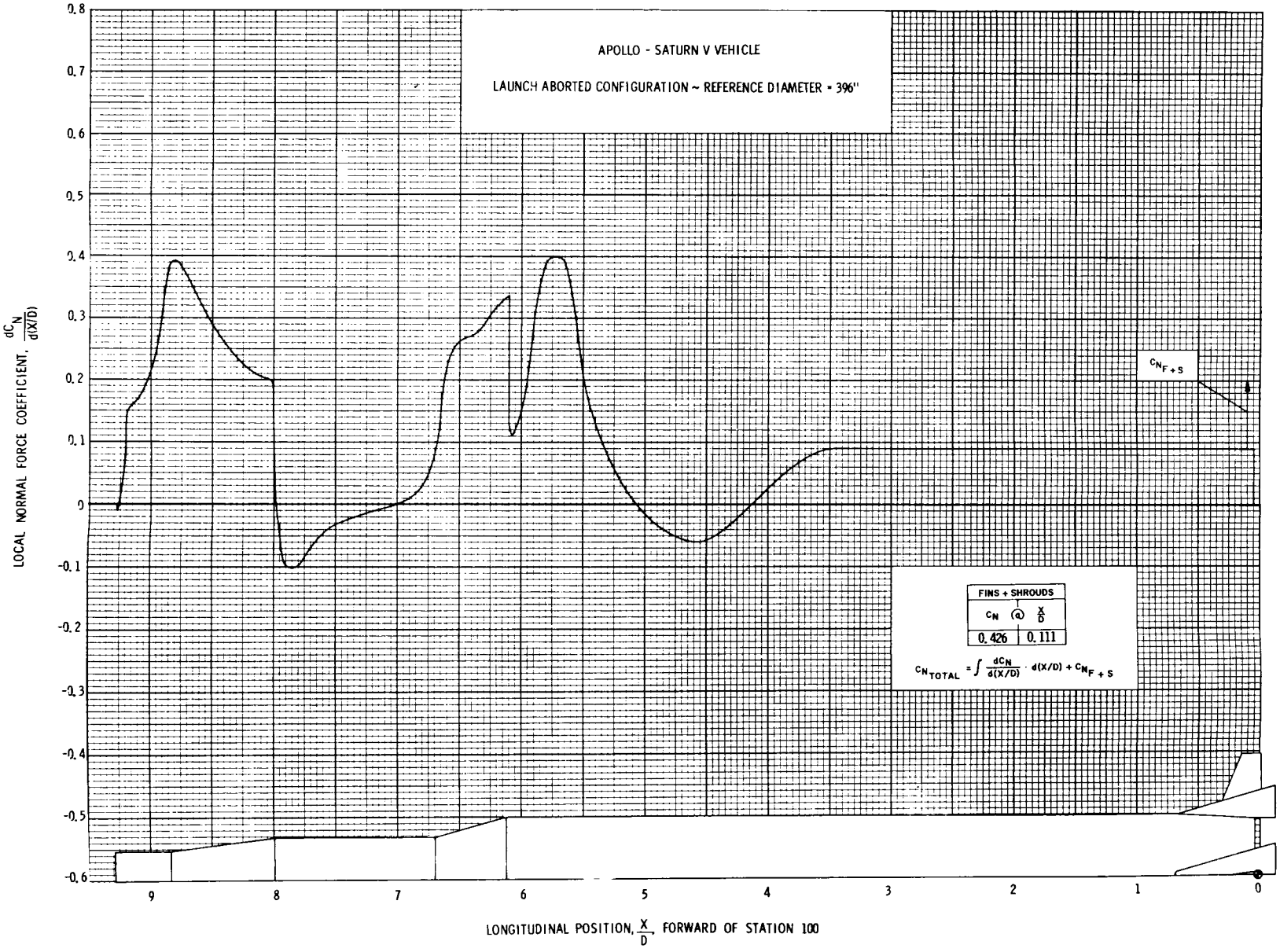

FIGURE 40 DISTRIBUTION OF LOCAL NORMAL FORCE COEFFICIENT, M = 1.00 ; $\alpha = 14^\circ$

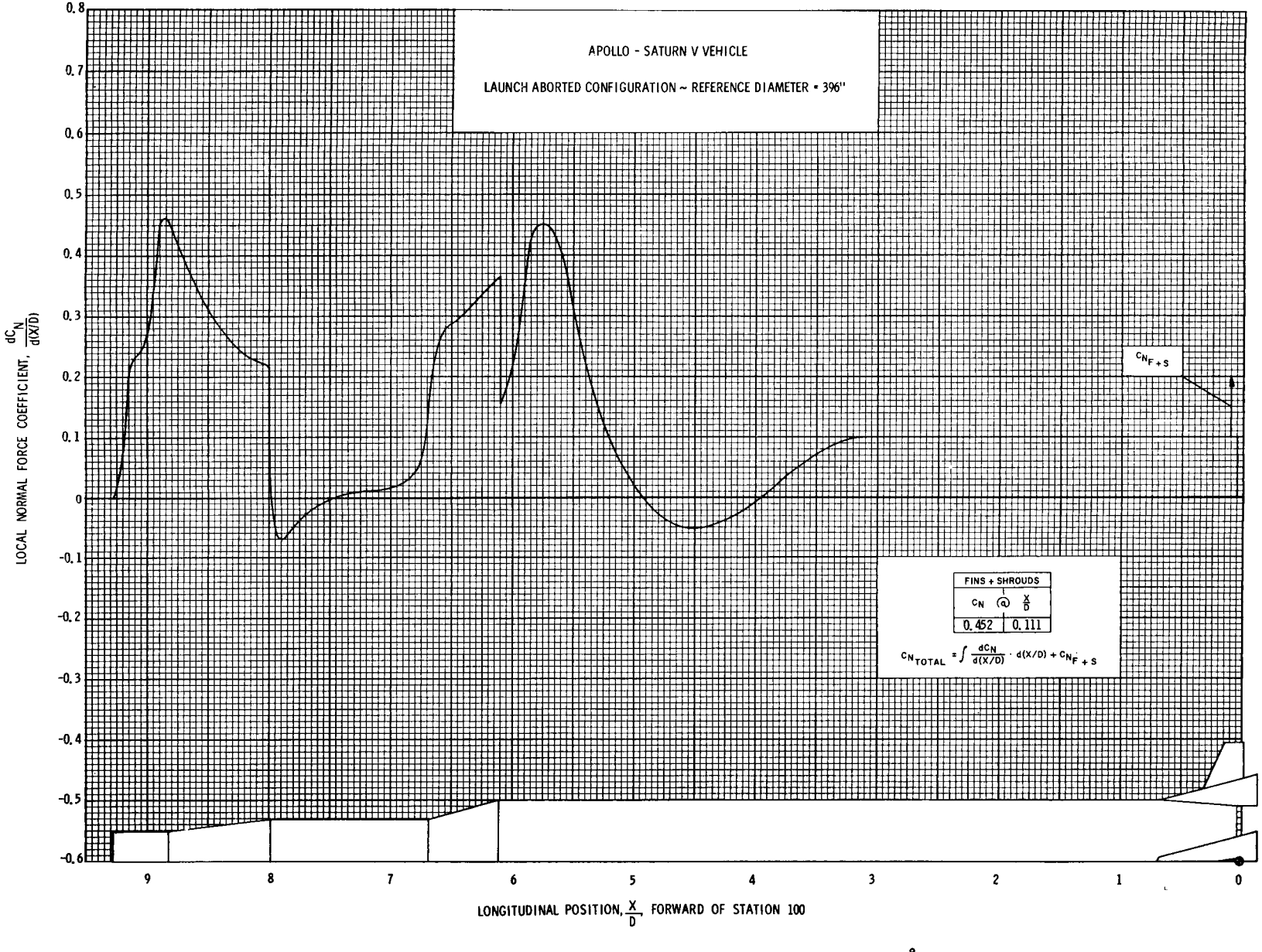

FIGURE 41 DISTRIBUTION OF LOCAL NORMAL FORCE COEFFICIENT, M = 1.00 ; $\alpha = 16^\circ$

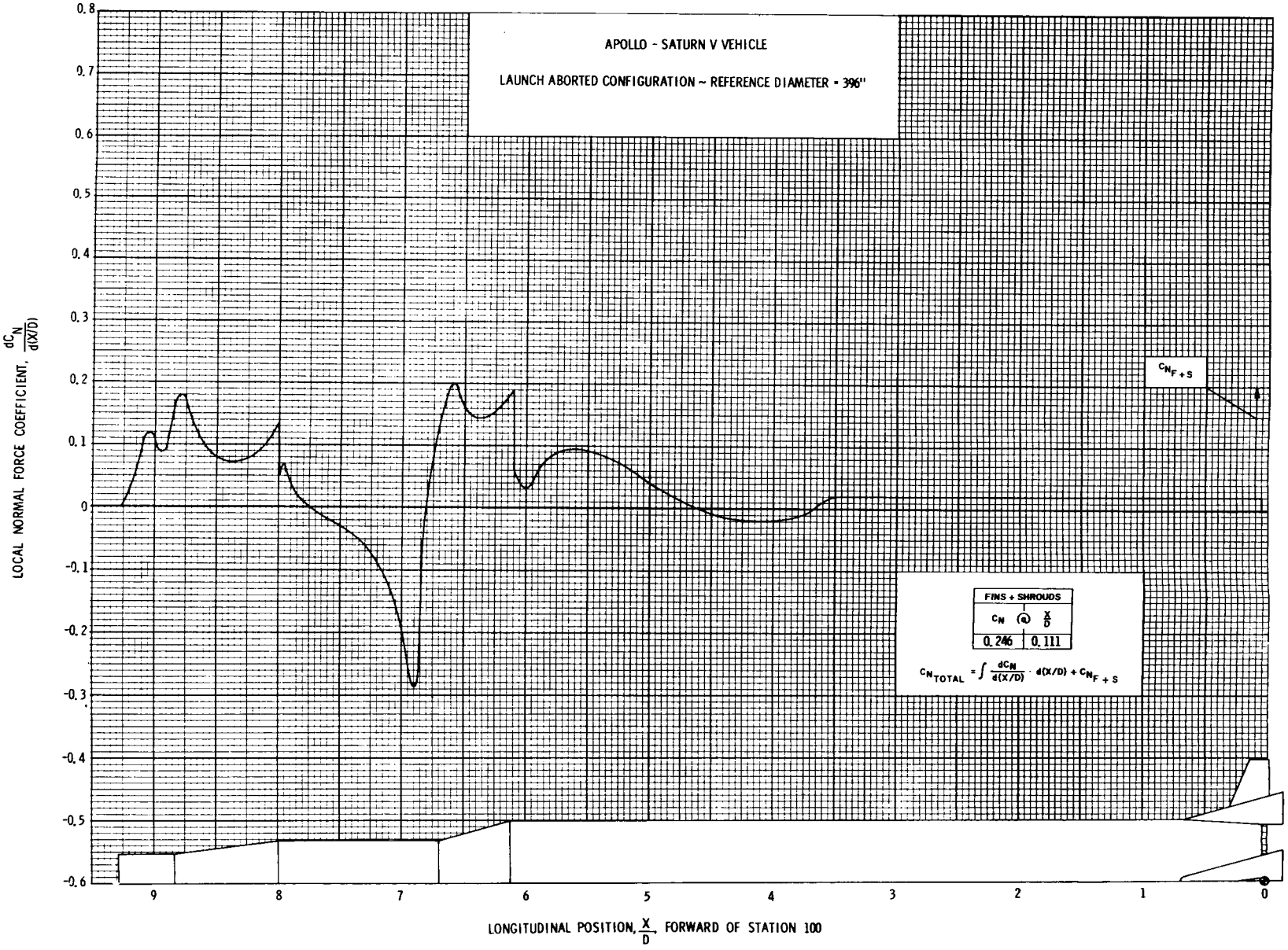

FIGURE 42 DISTRIBUTION OF LOCAL NORMAL FORCE COEFFICIENT, M = 1.20 ; α = 6°

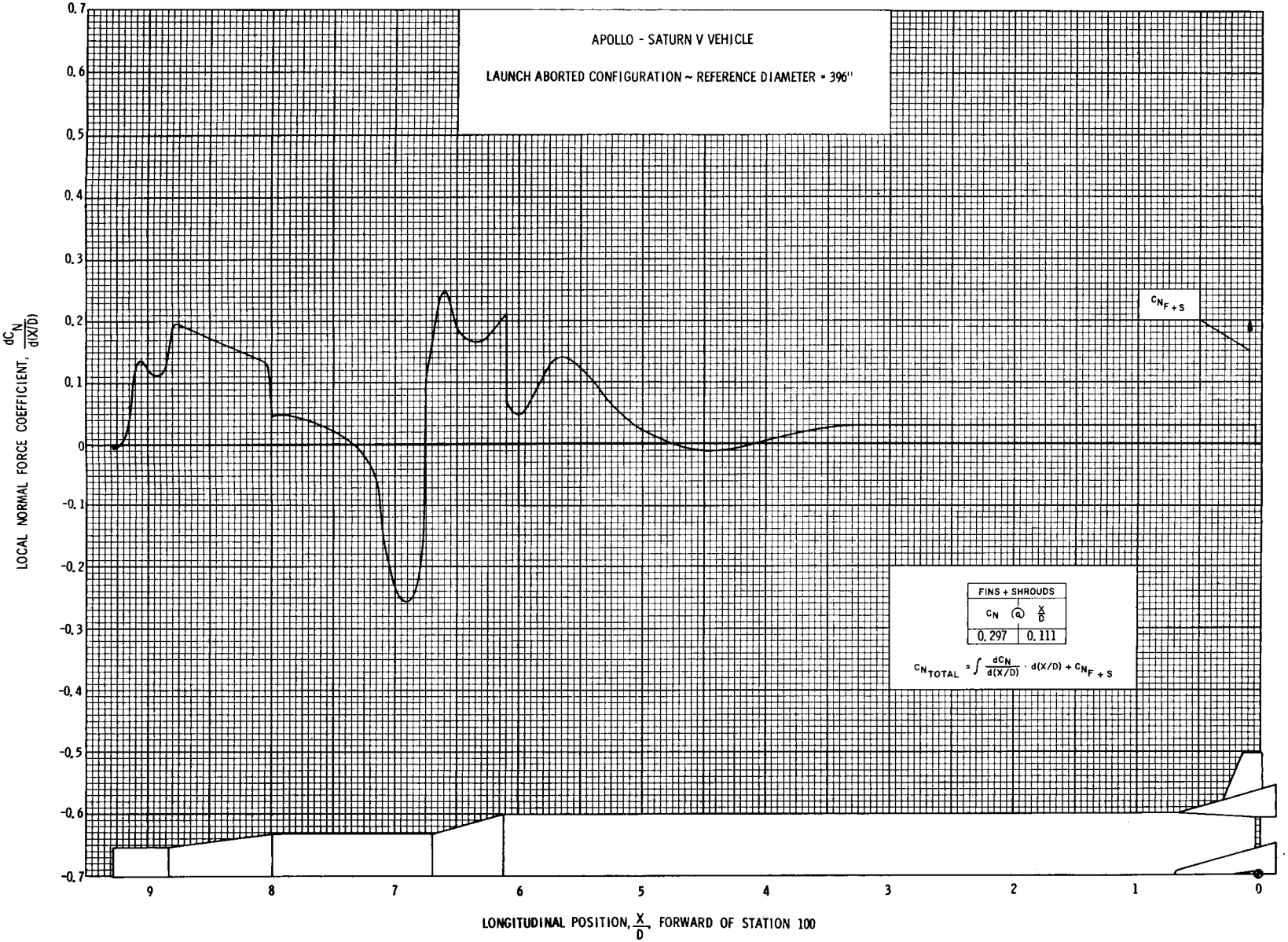

FIGURE 43 DISTRIBUTION OF LOCAL NORMAL FORCE COEFFICIENT, M = 1.20 ; $\alpha = 8°$

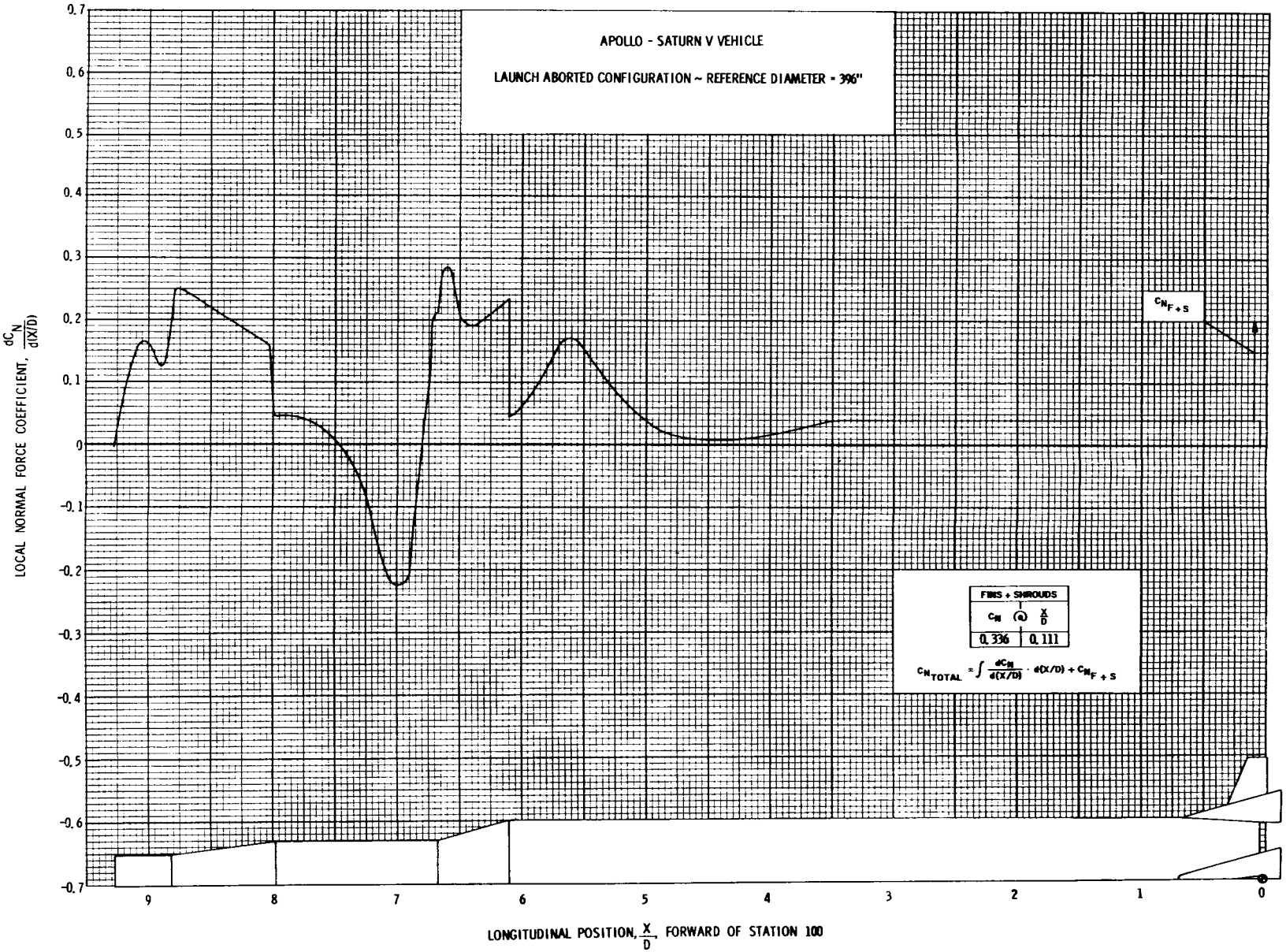

FIGURE 44 DISTRIBUTION OF LOCAL NORMAL FORCE COEFFICIENT, M = 1.20 ; $\alpha = 10^\circ$

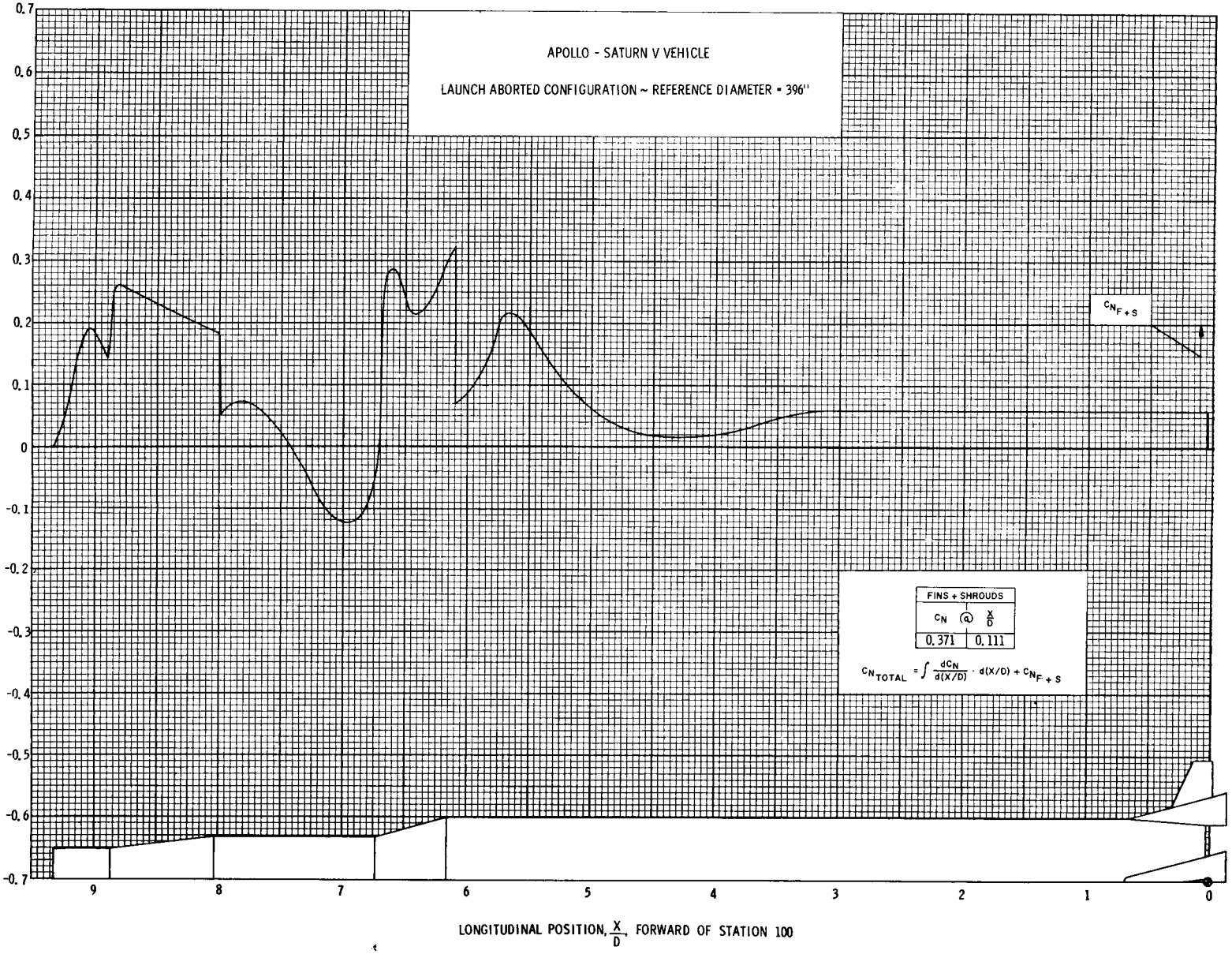

FIGURE 45 DISTRIBUTION OF LOCAL NORMAL FORCE COEFFICIENT, M = 1.20 ; α = 12°

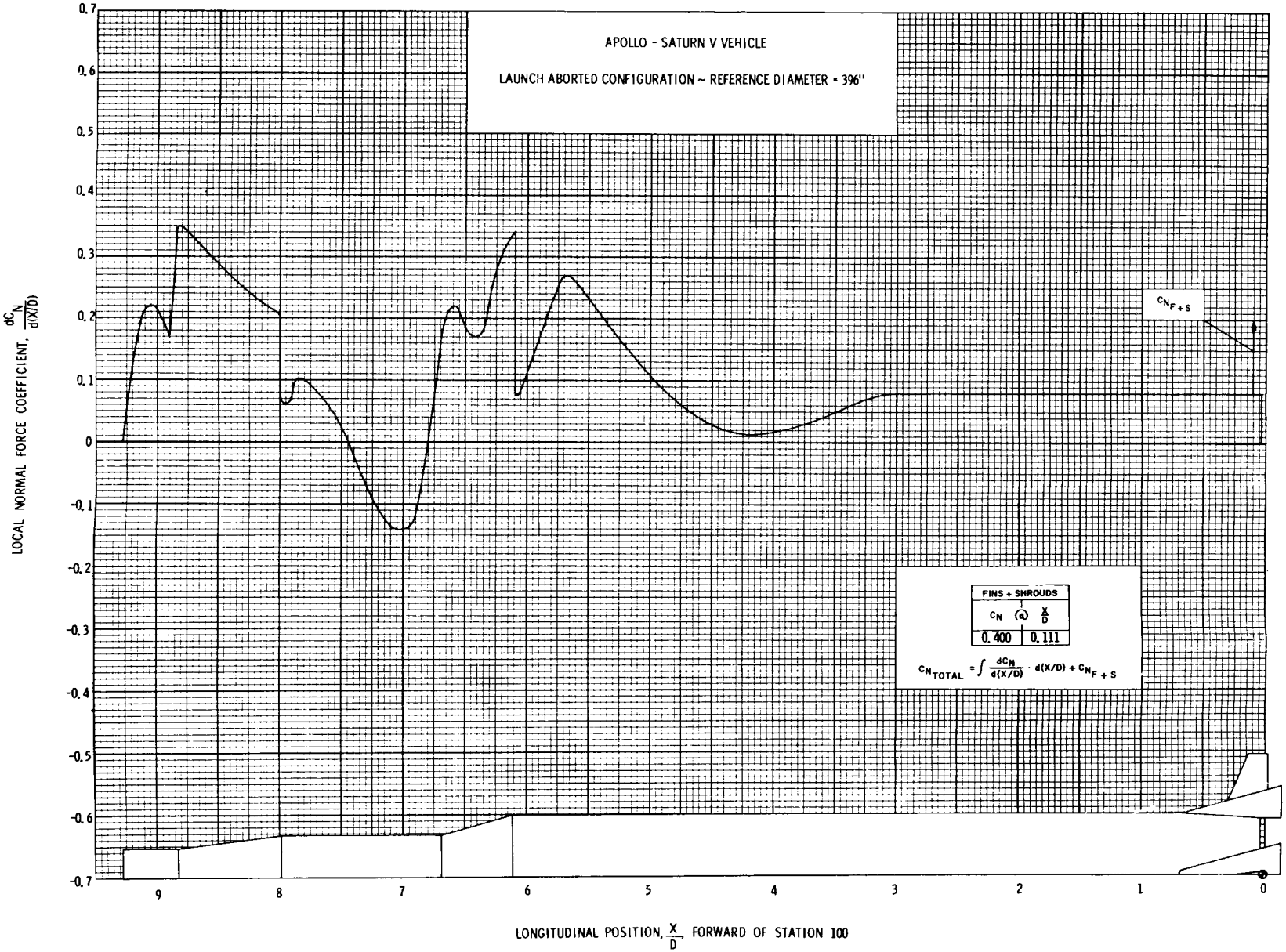

FIGURE 46 DISTRIBUTION OF LOCAL NORMAL FORCE COEFFICIENT, M = 1.20 ; $\alpha = 14^\circ$

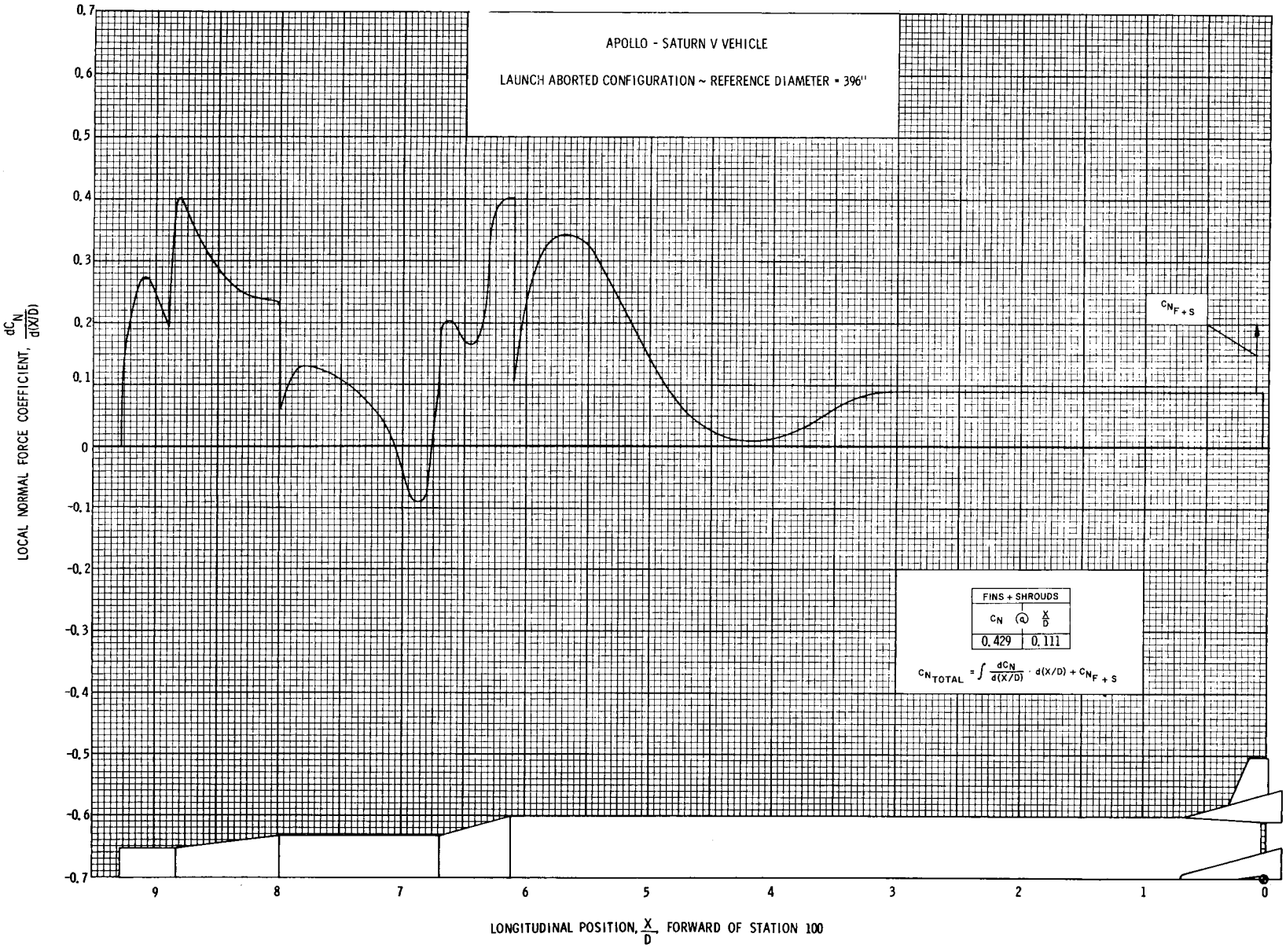

FIGURE 47 DISTRIBUTION OF LOCAL NORMAL FORCE COEFFICIENT, M = 1.20 ; $\alpha = 16^\circ$

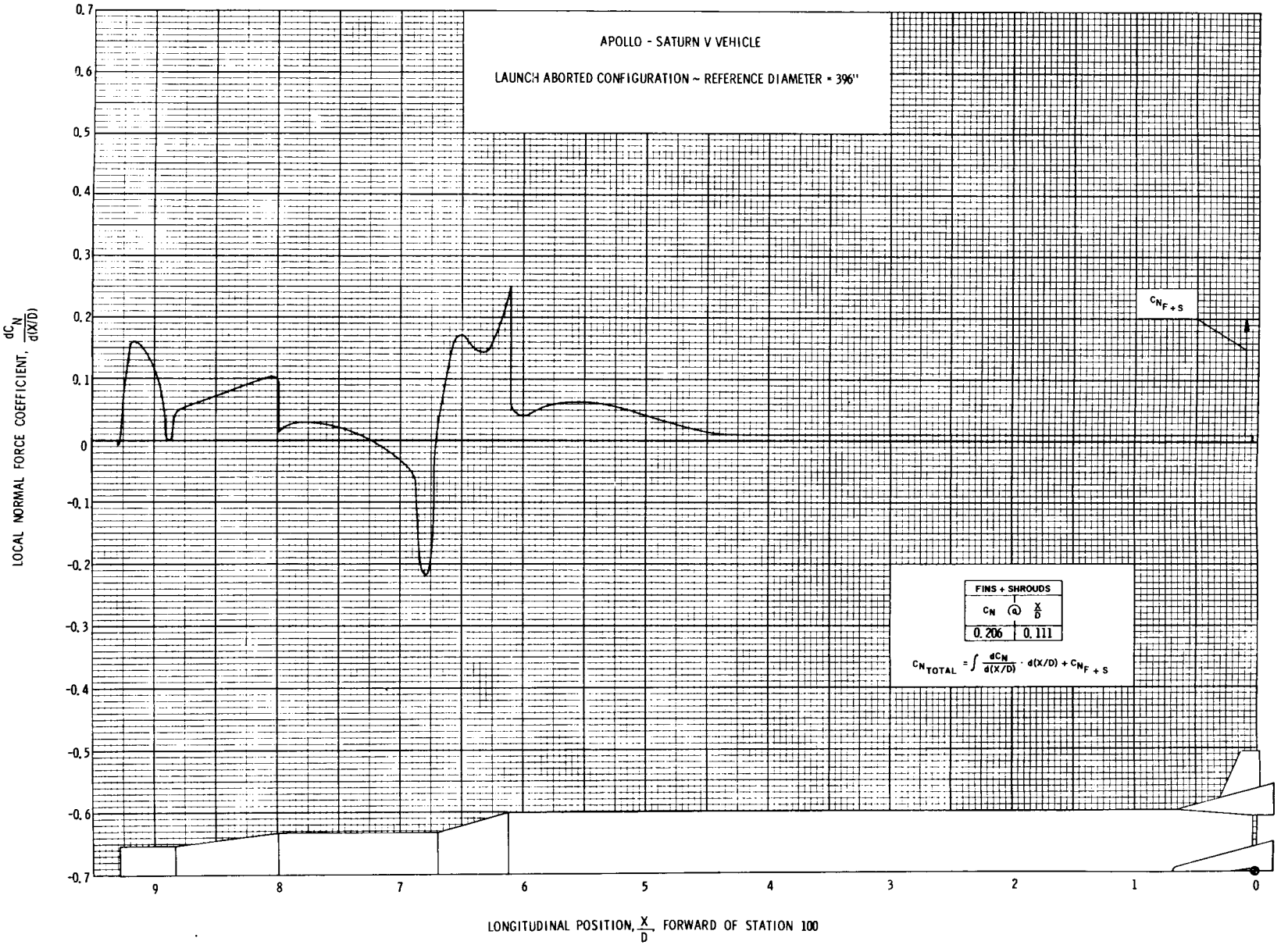

FIGURE 48 DISTRIBUTION OF LOCAL NORMAL FORCE COEFFICIENT, $M = 1.50$; $\alpha = 6^\circ$

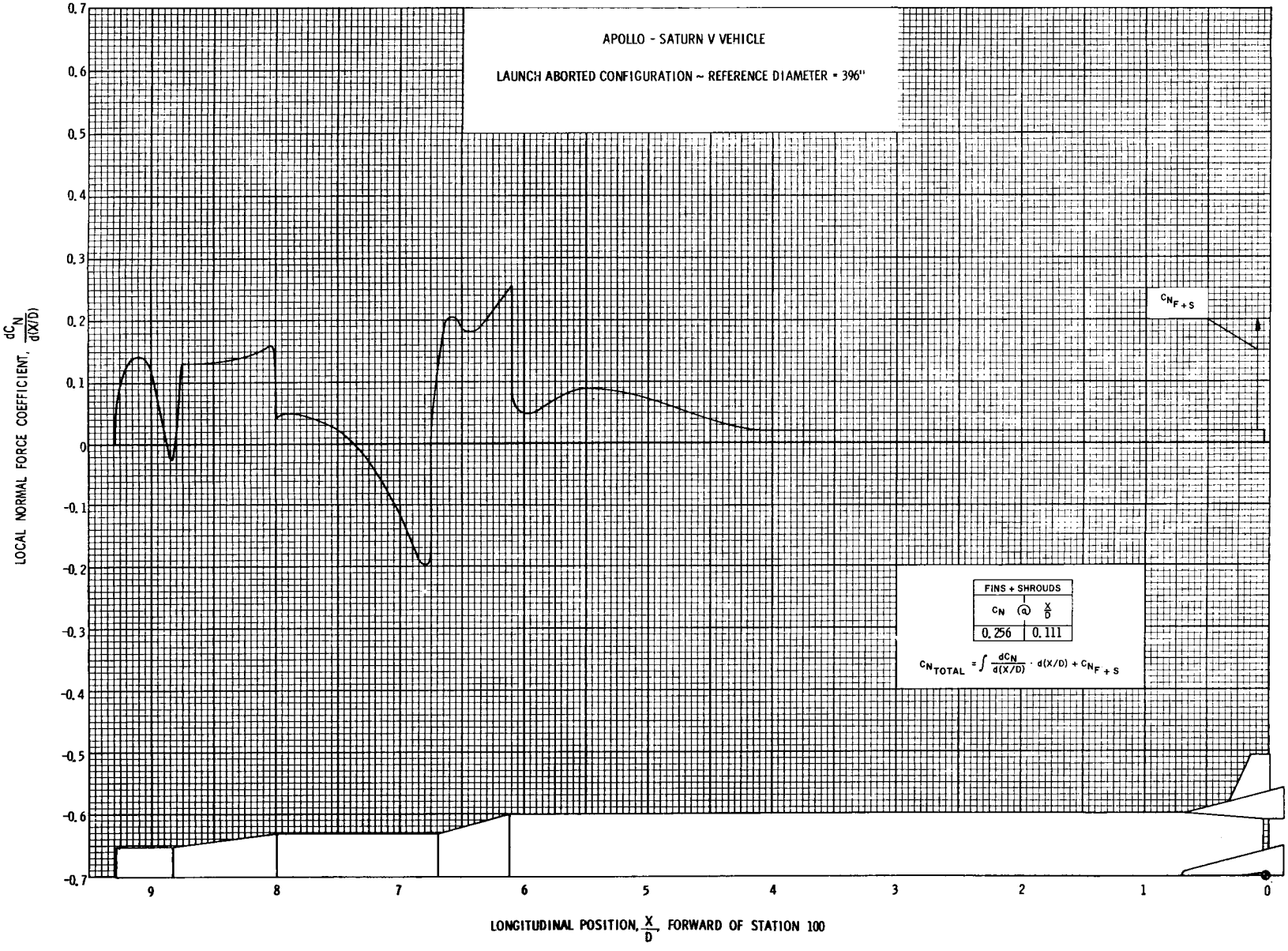

FIGURE 49 DISTRIBUTION OF LOCAL NORMAL FORCE COEFFICIENT, M = 1.50 ; α = 8°

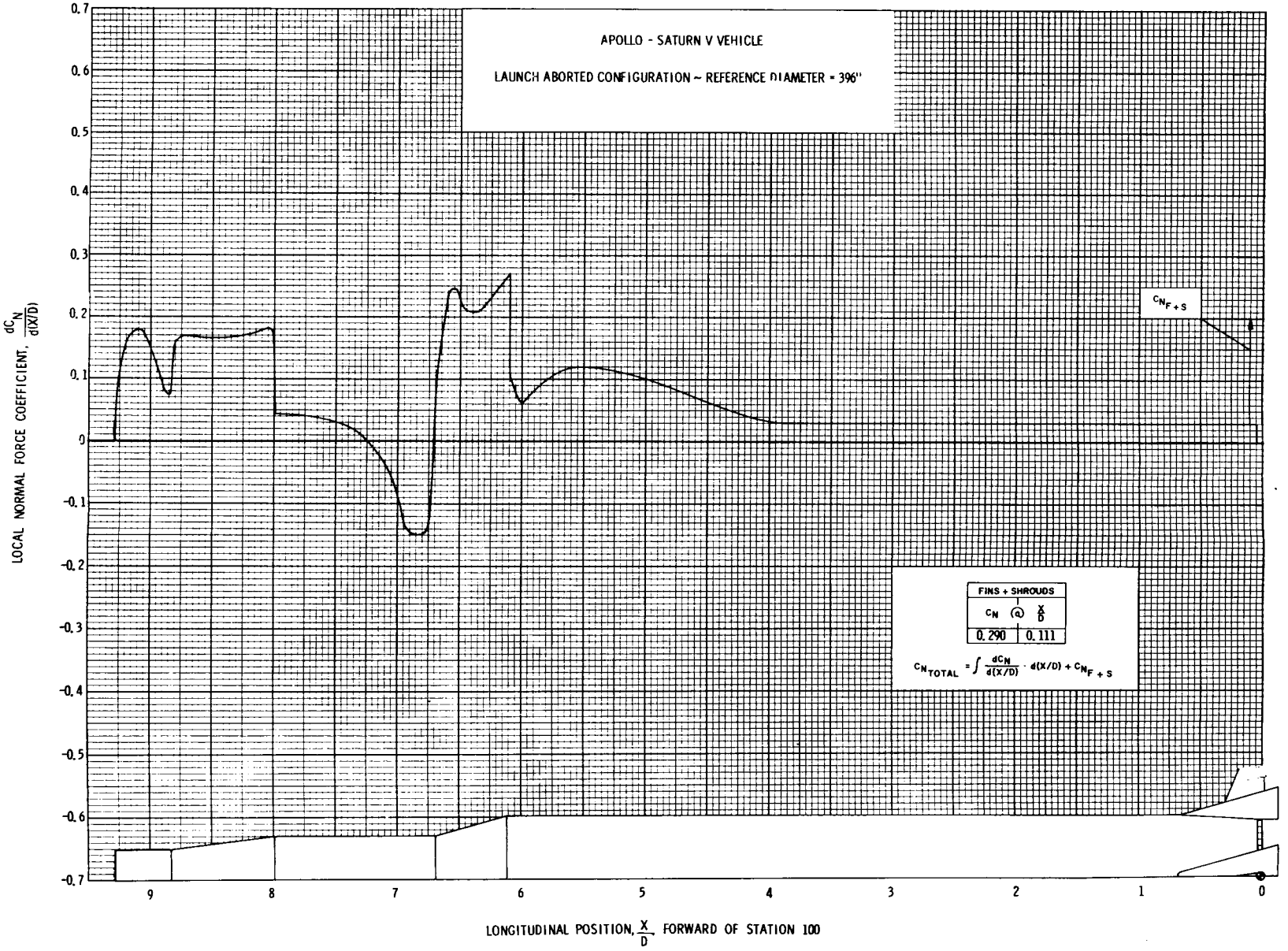

FIGURE 50 DISTRIBUTION OF LOCAL NORMAL FORCE COEFFICIENT, M = 1.50 ; $\alpha = 10°$

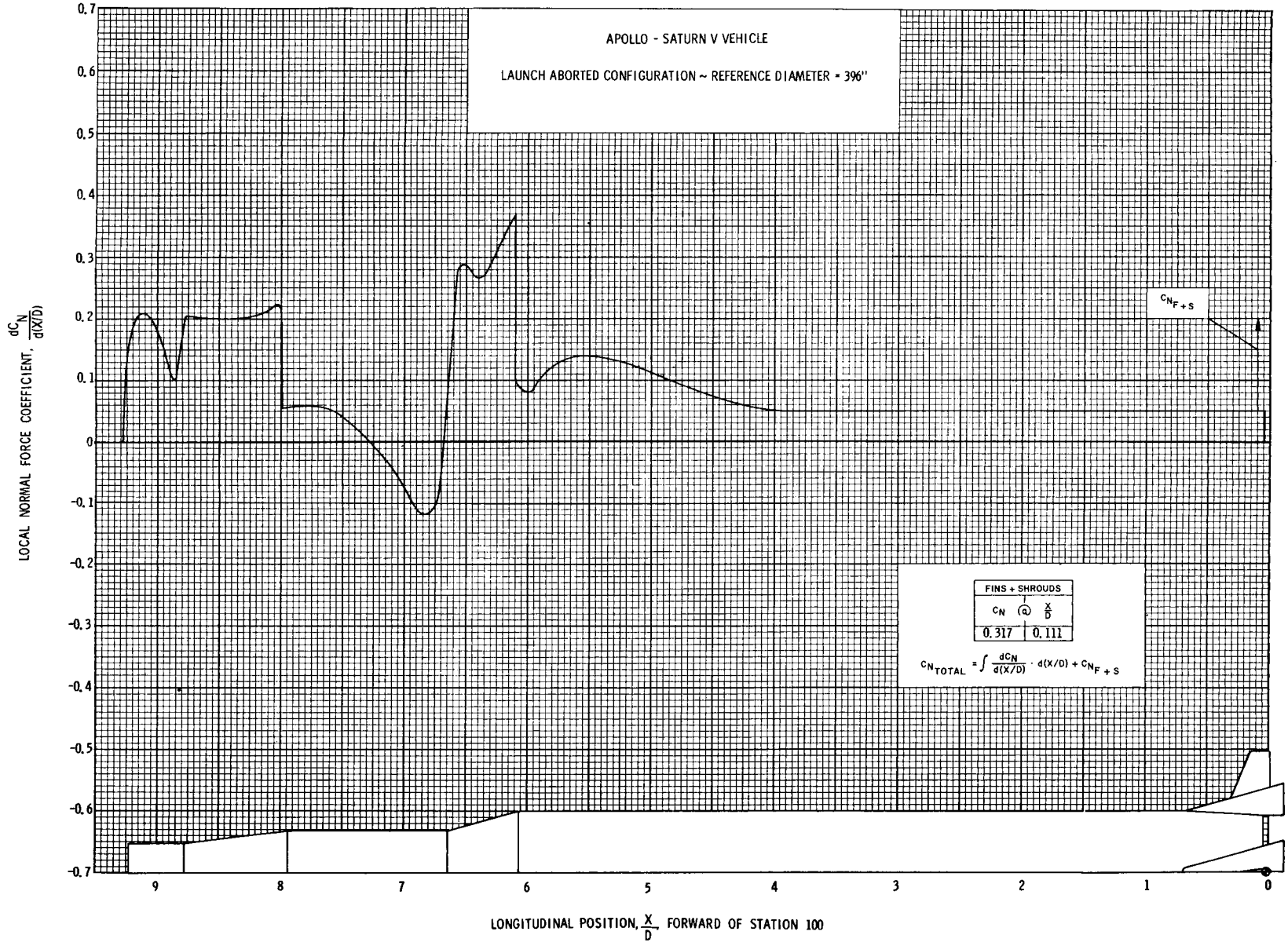

FIGURE 51 DISTRIBUTION OF LOCAL NORMAL FORCE COEFFICIENT, M = 1.50 ; $\alpha = 12°$

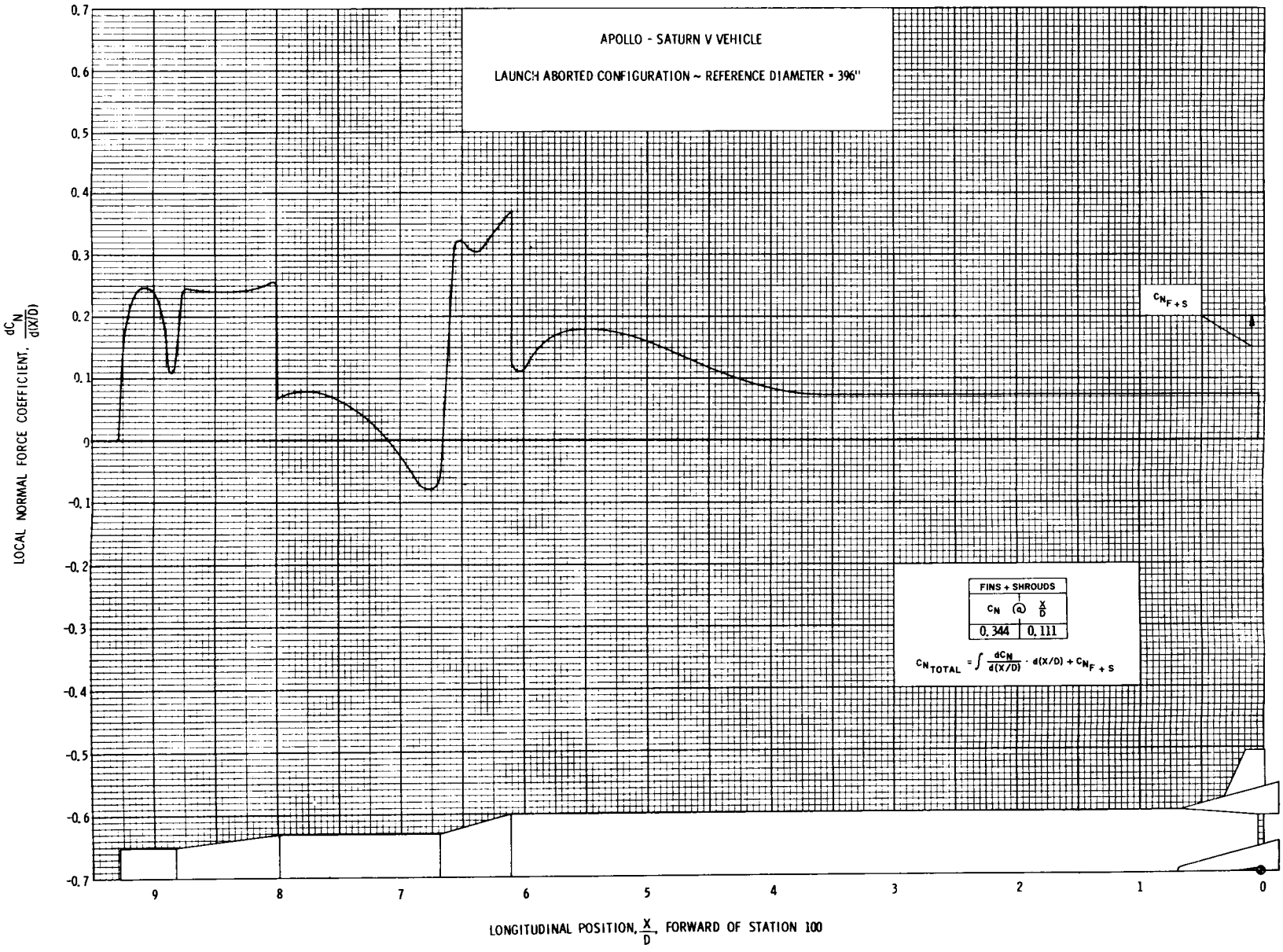

FIGURE 52 DISTRIBUTION OF LOCAL NORMAL FORCE COEFFICIENT, $M = 1.50$; $\alpha = 14^\circ$

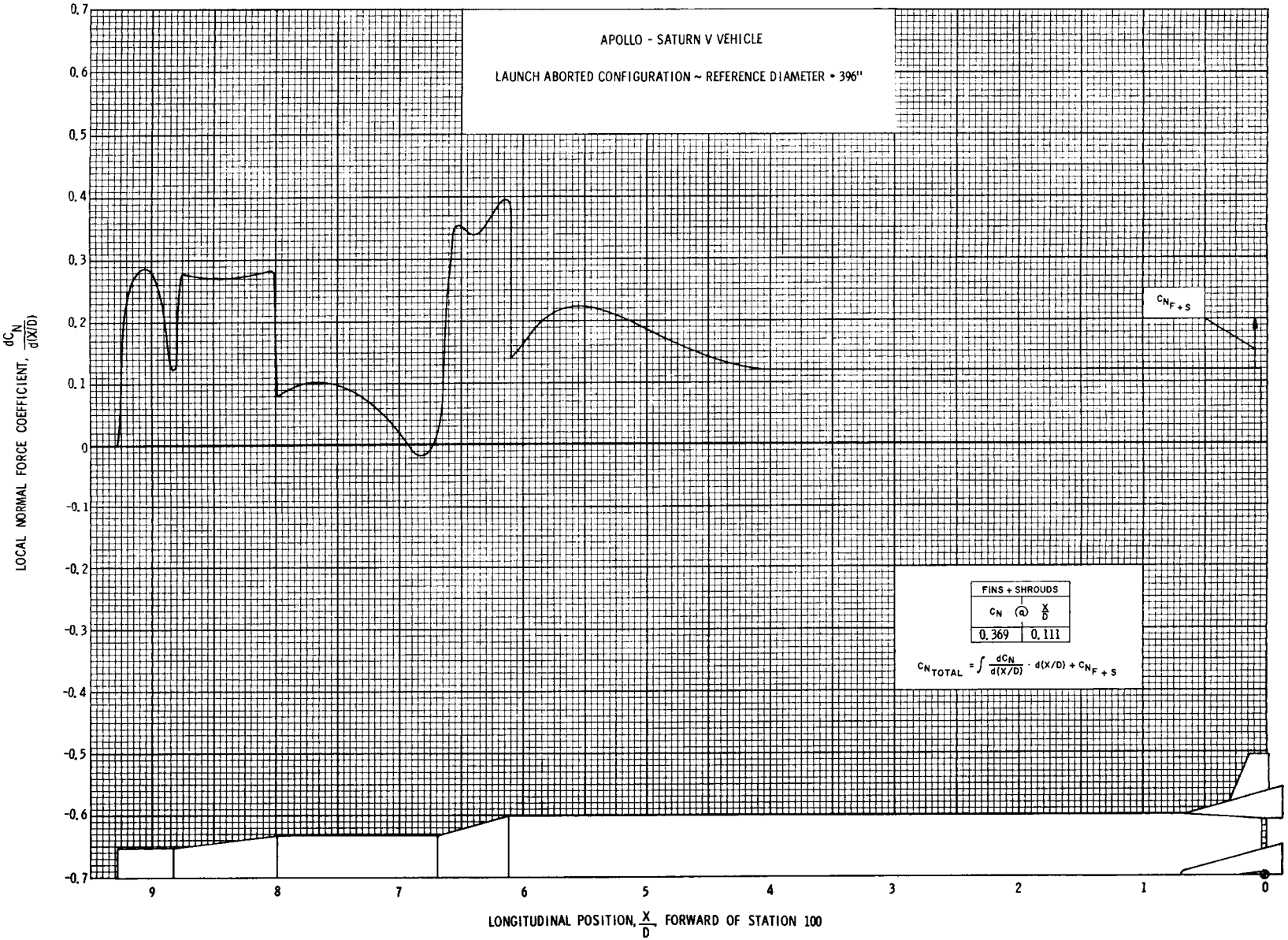

FIGURE 53 DISTRIBUTION OF LOCAL NORMAL FORCE COEFFICIENT, M = 1.50 ; α = 16°

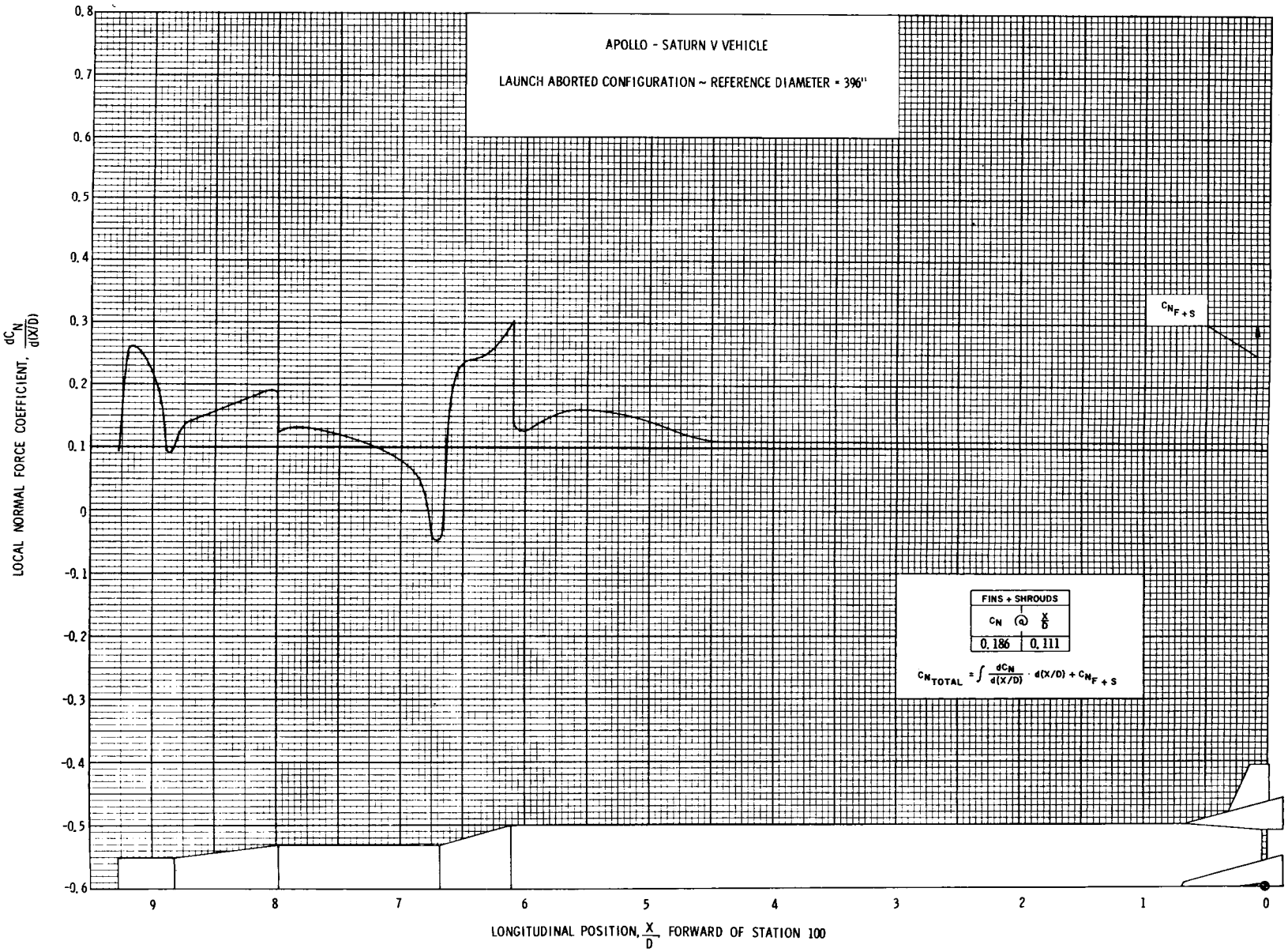

FIGURE 54 DISTRIBUTION OF LOCAL NORMAL FORCE COEFFICIENT, M = 1.70 ; $\alpha = 6^\circ$

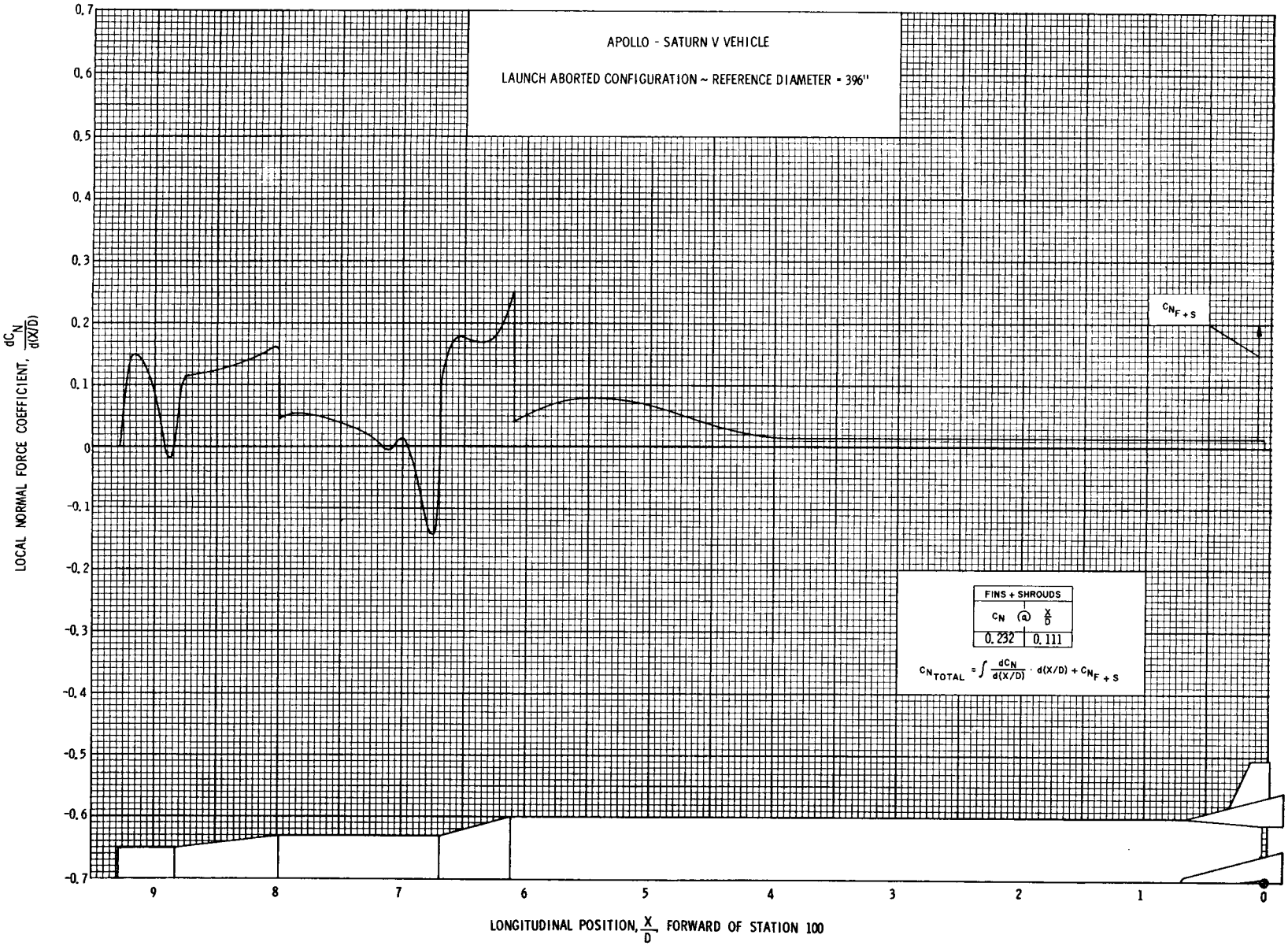

FIGURE 55 DISTRIBUTION OF LOCAL NORMAL FORCE COEFFICIENT, M = 1.70 ; $\alpha = 8°$

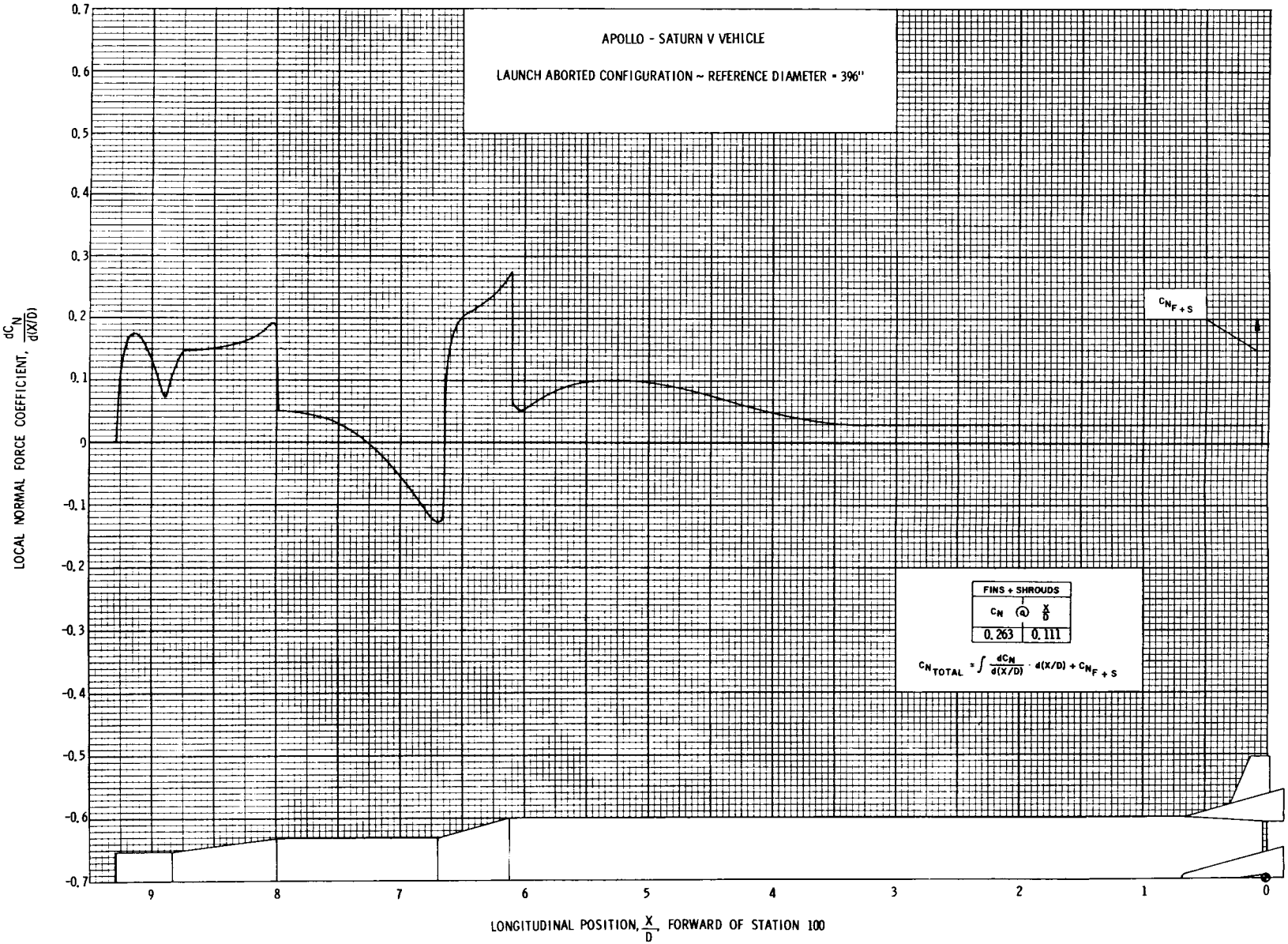

FIGURE 56 DISTRIBUTION OF LOCAL NORMAL FORCE COEFFICIENT, M = 1.70 ; $\alpha = 10^\circ$

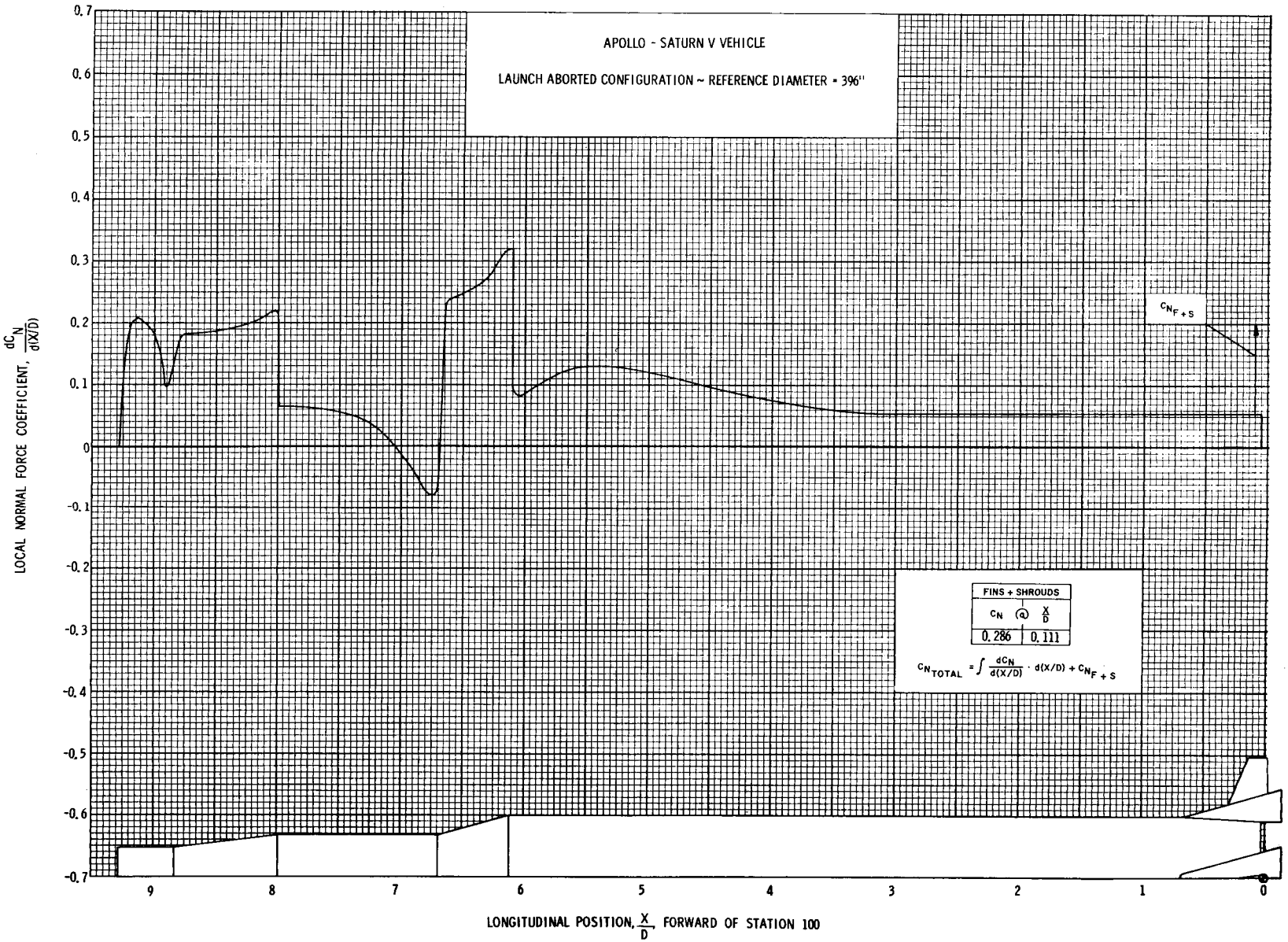

FIGURE 57 DISTRIBUTION OF LOCAL NORMAL FORCE COEFFICIENT, M = 1.70 ; $\alpha = 12^\circ$

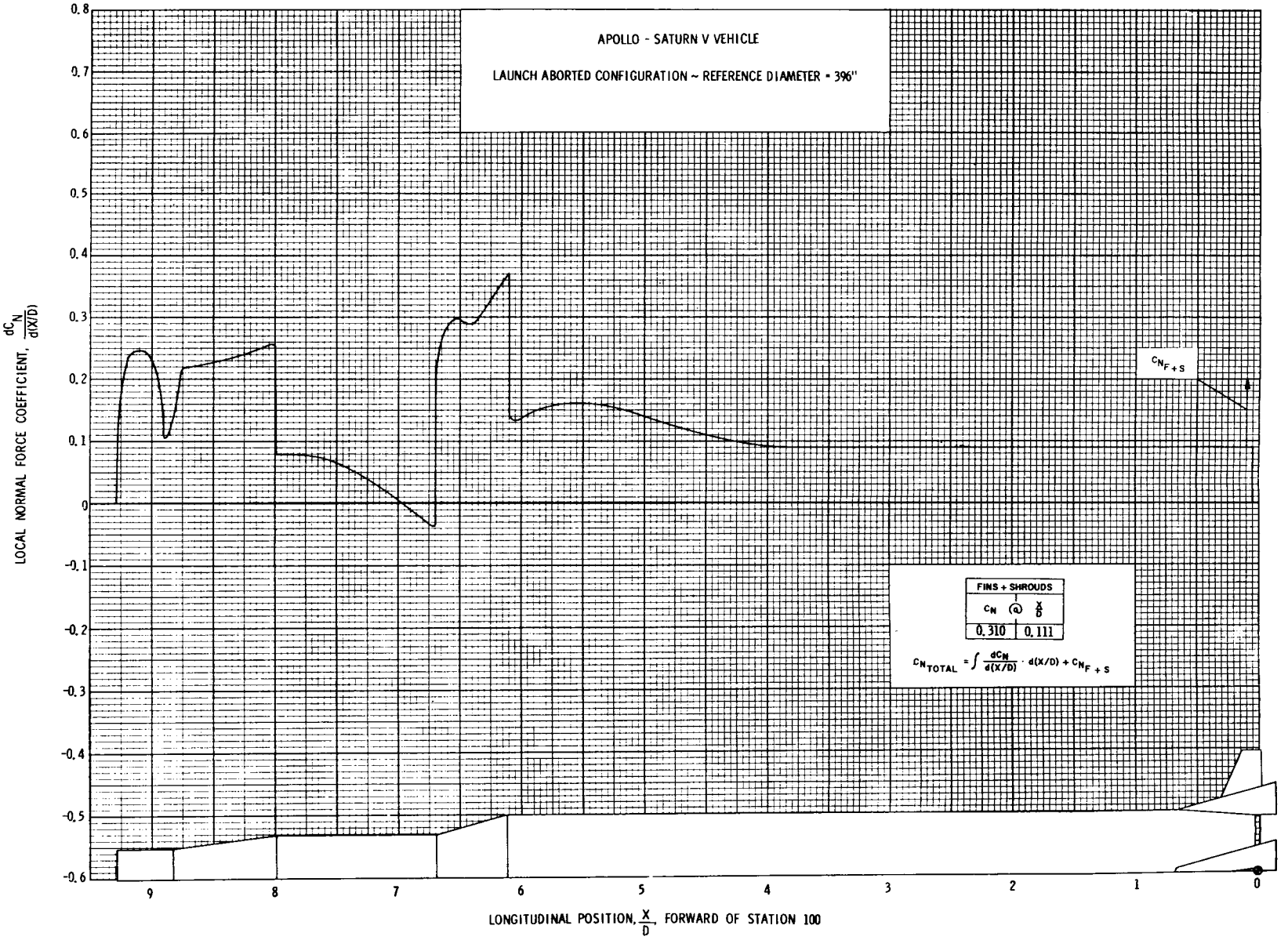

FIGURE 58 DISTRIBUTION OF LOCAL NORMAL FORCE COEFFICIENT, M = 1.70 ; $\alpha = 14°$

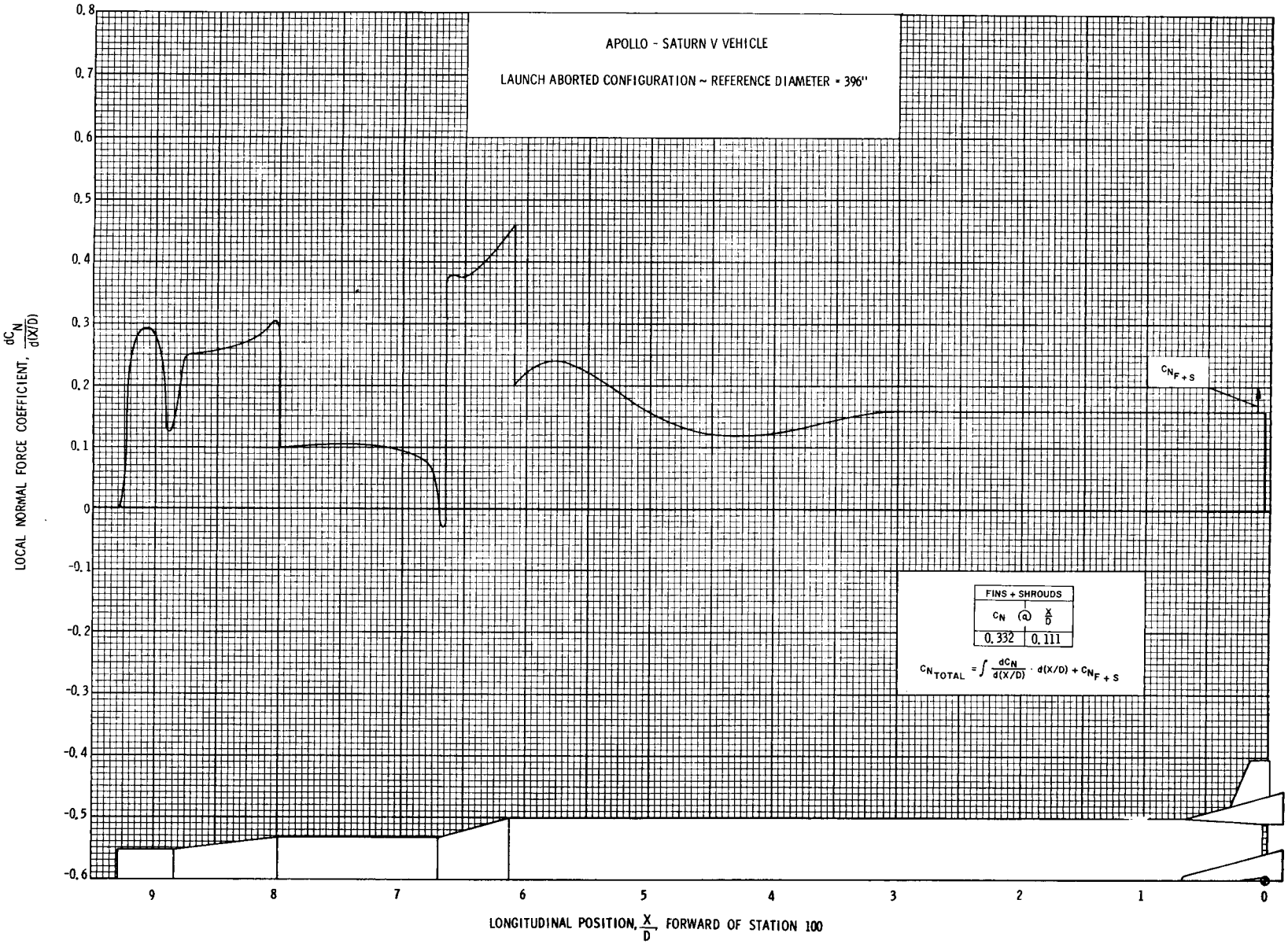

FIGURE 59 DISTRIBUTION OF LOCAL NORMAL FORCE COEFFICIENT, M = 1.70 ; $\alpha = 16°$

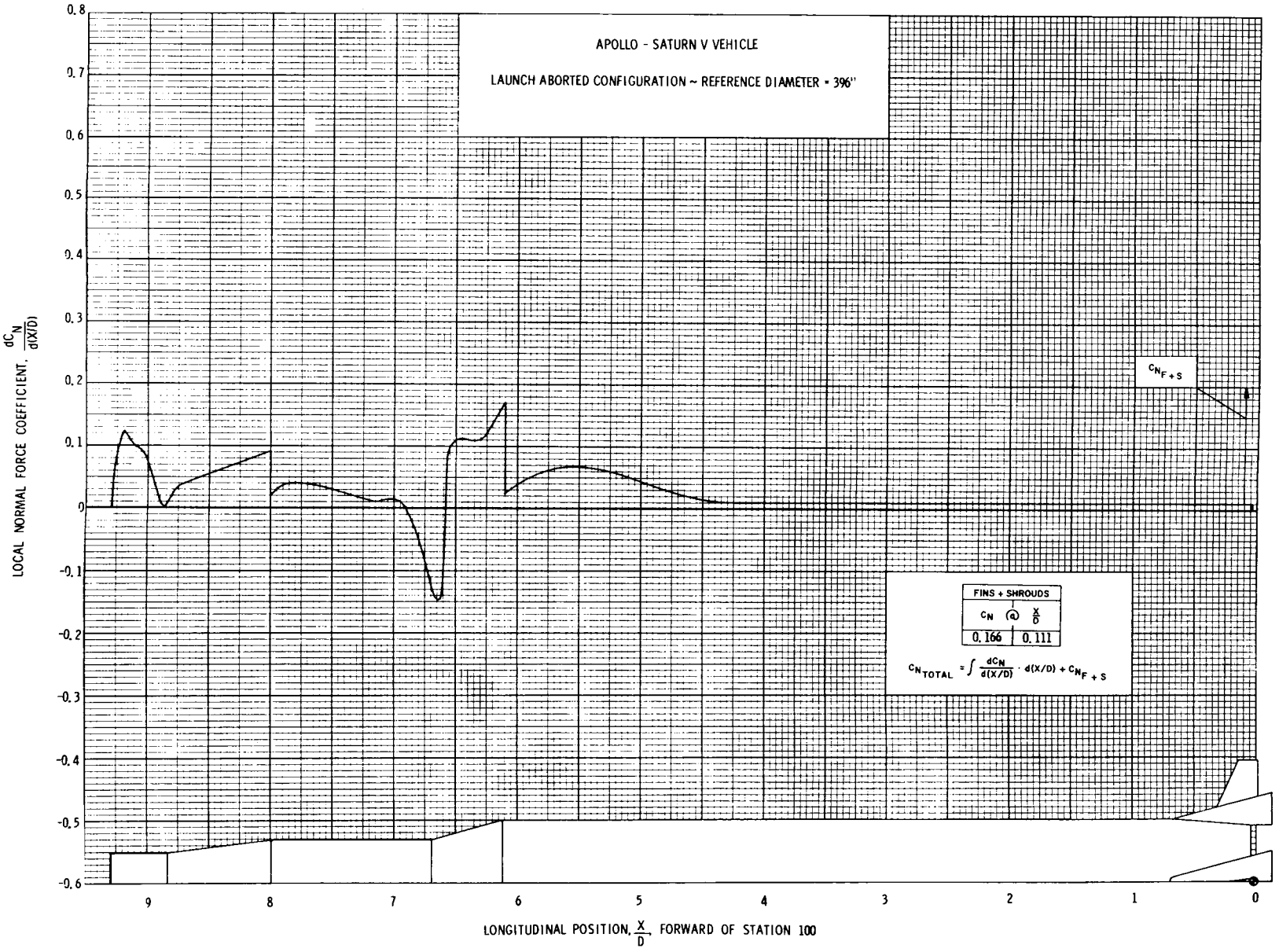

FIGURE 60 DISTRIBUTION OF LOCAL NORMAL FORCE COEFFICIENT, M = 2.00 ; $\alpha = 6^\circ$

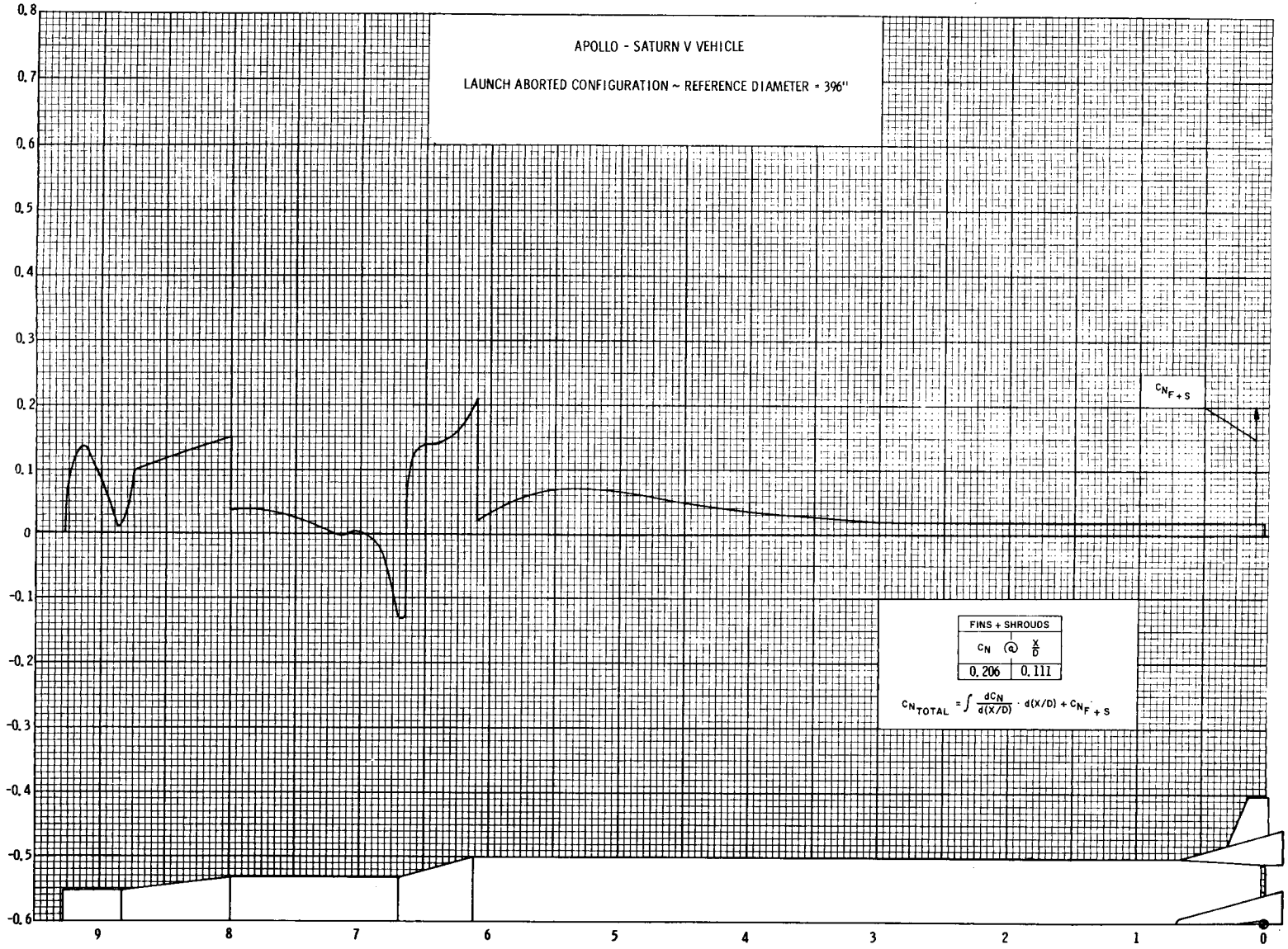

FIGURE 61 DISTRIBUTION OF LOCAL NORMAL FORCE COEFFICIENT, M = 2.00 ; $\alpha = 8°$

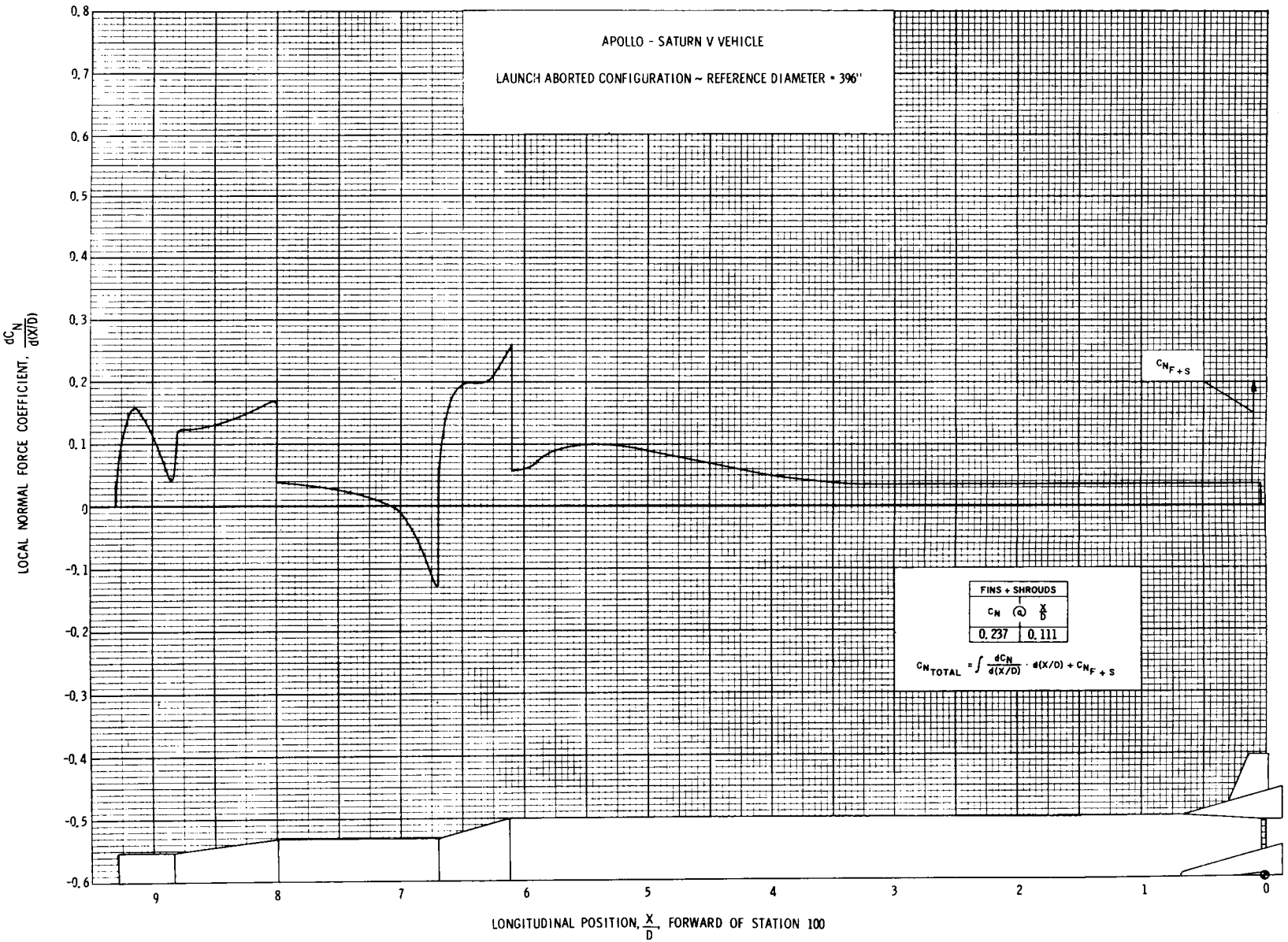

FIGURE 62 DISTRIBUTION OF LOCAL NORMAL FORCE COEFFICIENT, M = 2.00 ; $\alpha = 10^\circ$

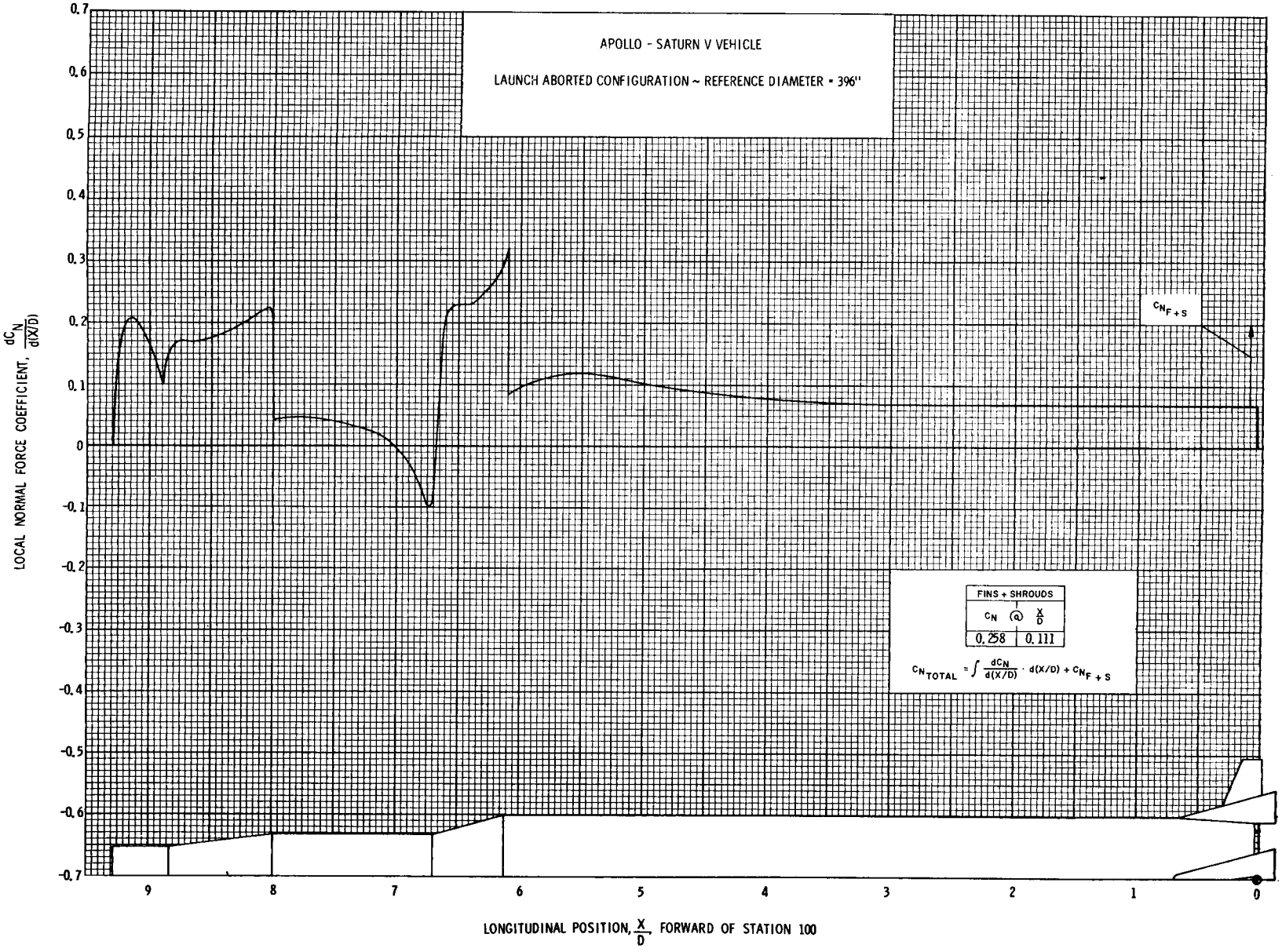

FIGURE 63 DISTRIBUTION OF LOCAL NORMAL FORCE COEFFICIENT, M = 2.00 ; $\alpha = 12^\circ$

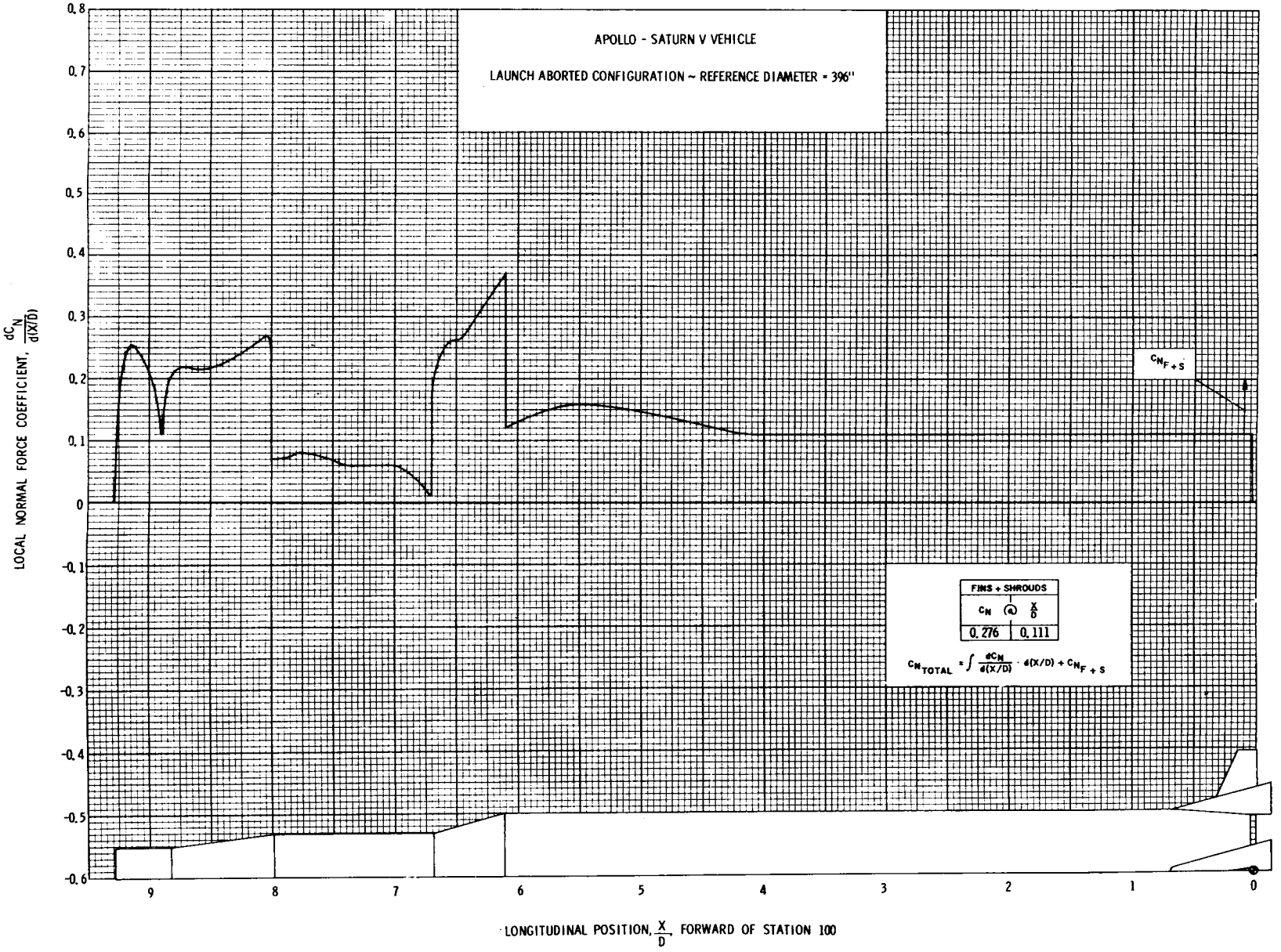

FIGURE 64 DISTRIBUTION OF LOCAL NORMAL FORCE COEFFICIENT, M = 2.00 ; $\alpha = 14^\circ$

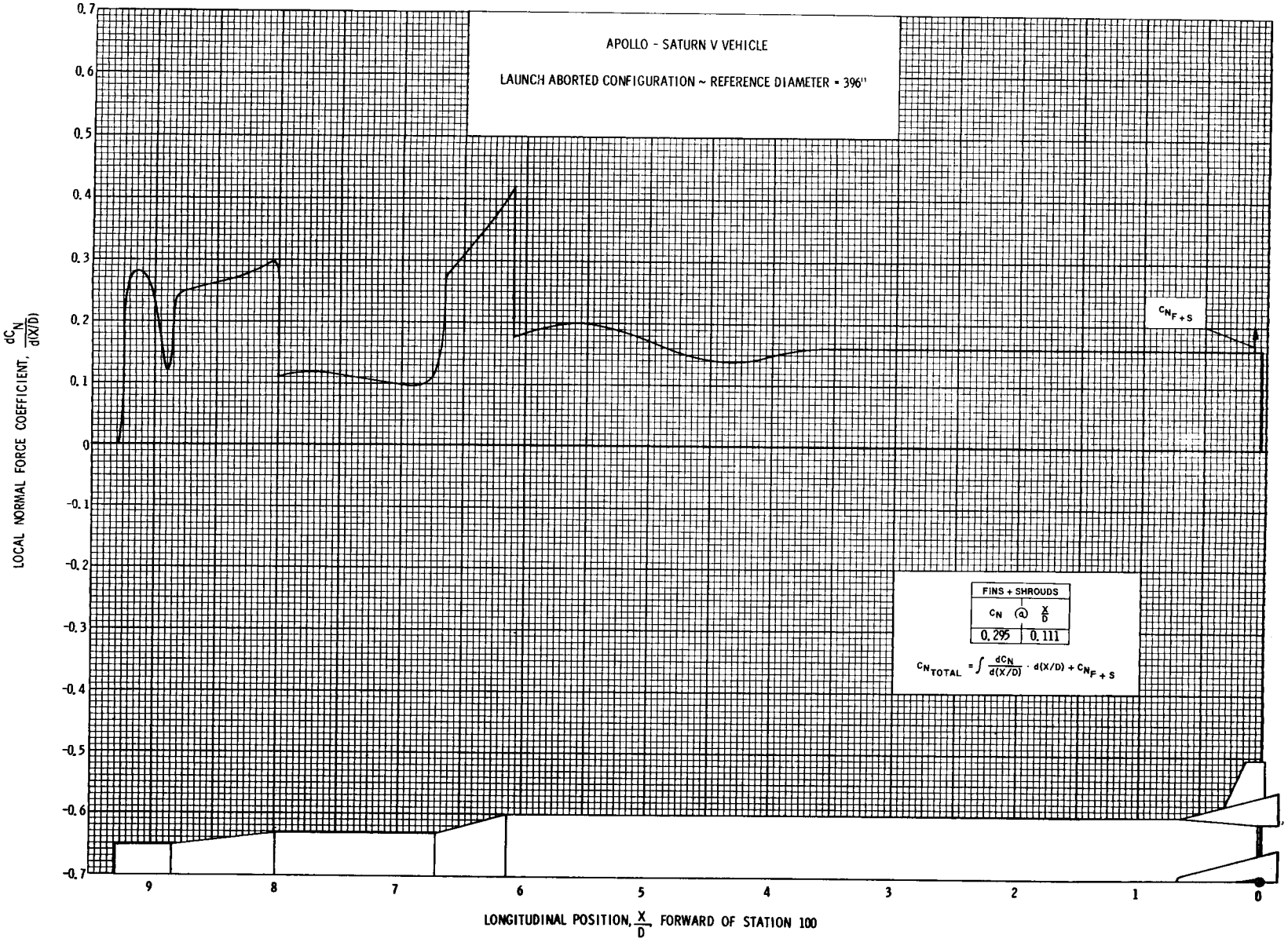

FIGURE 65 DISTRIBUTION OF LOCAL NORMAL FORCE COEFFICIENT, M = 2.00 ; α = 16°

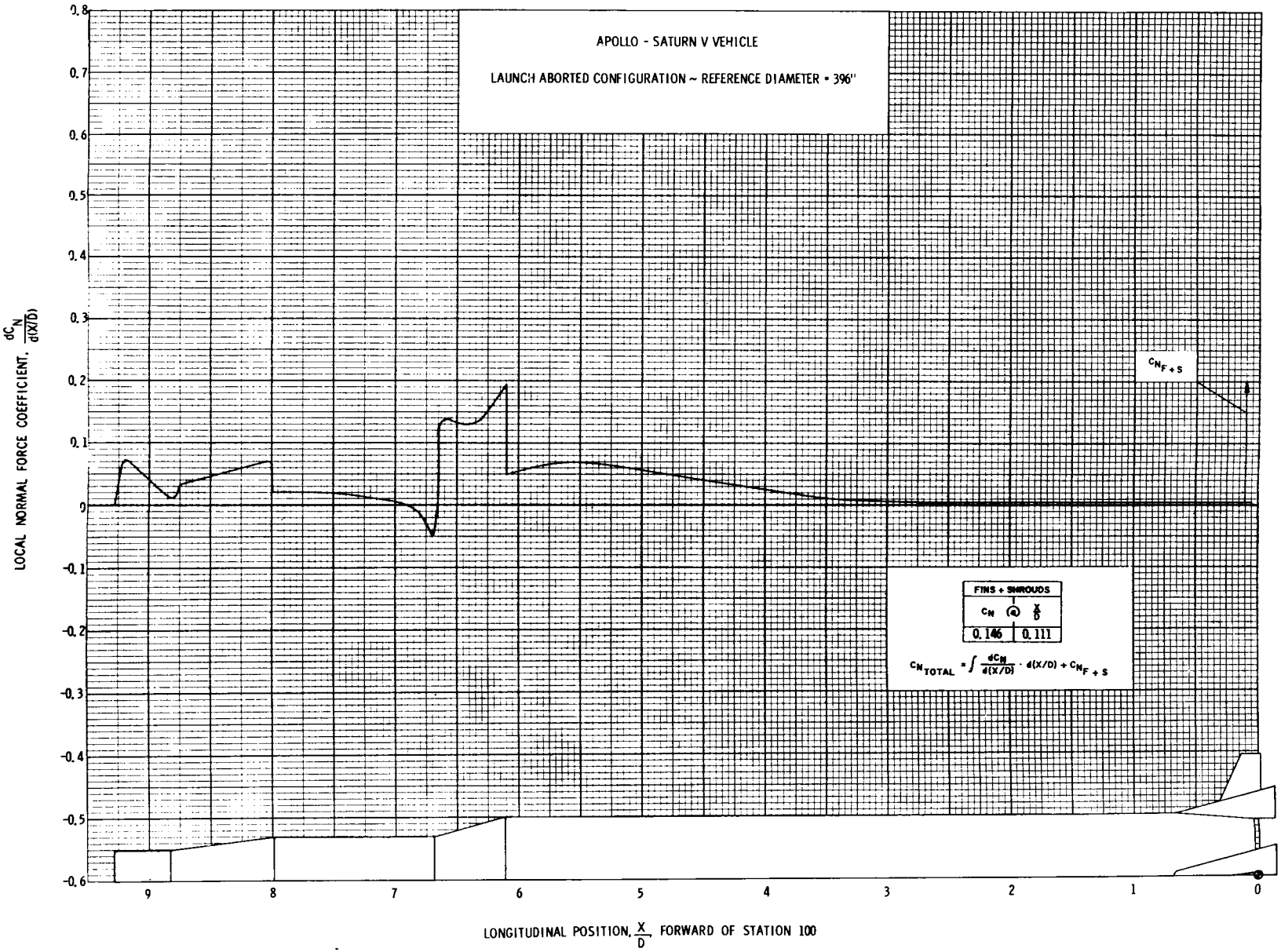

FIGURE 66 DISTRIBUTION OF LOCAL NORMAL FORCE COEFFICIENT, M = 2.75 ; $\alpha = 6^\circ$

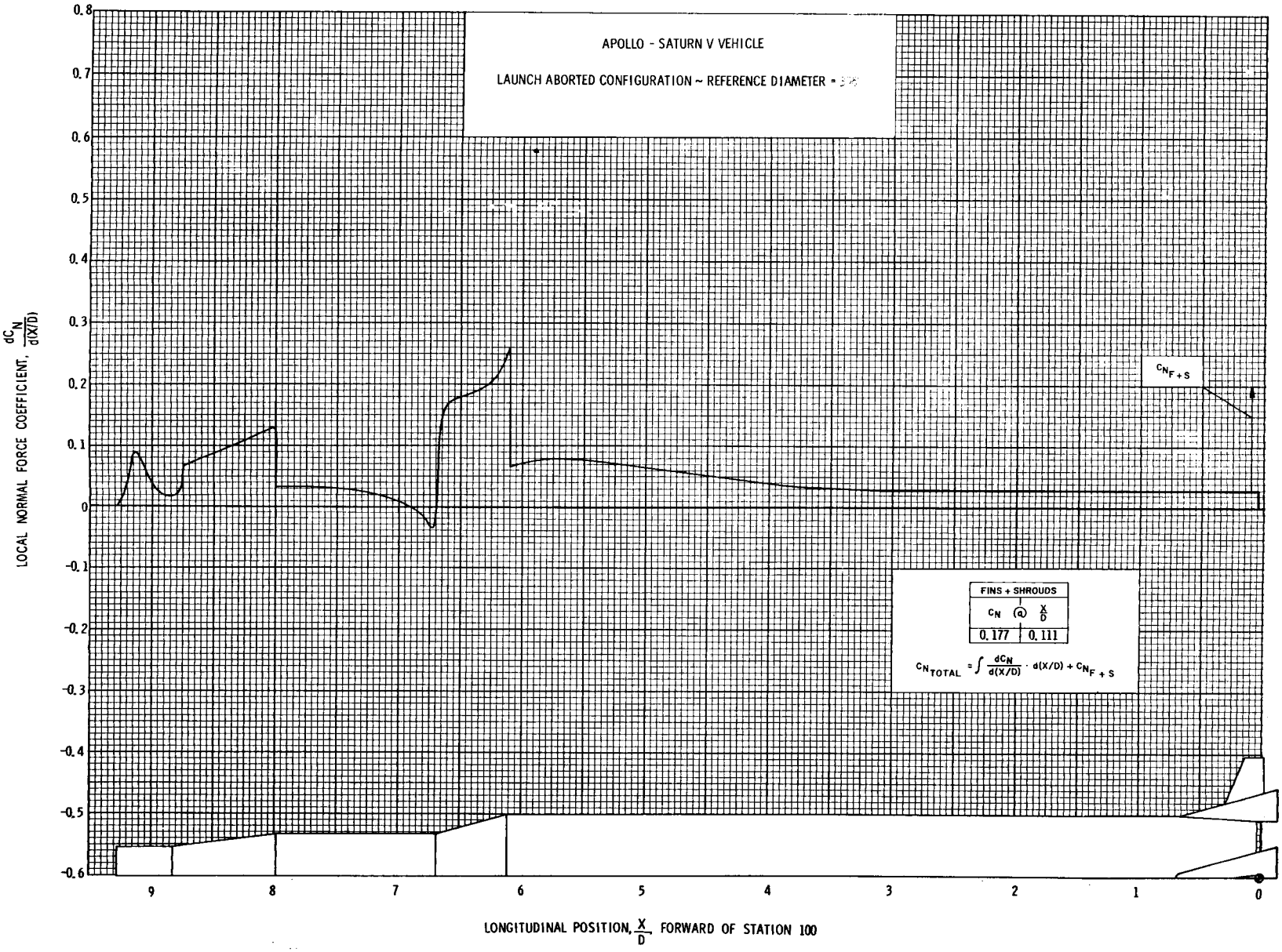

FIGURE 67 DISTRIBUTION OF LOCAL NORMAL FORCE COEFFICIENT, M = 2.75 ; $\alpha = 8°$

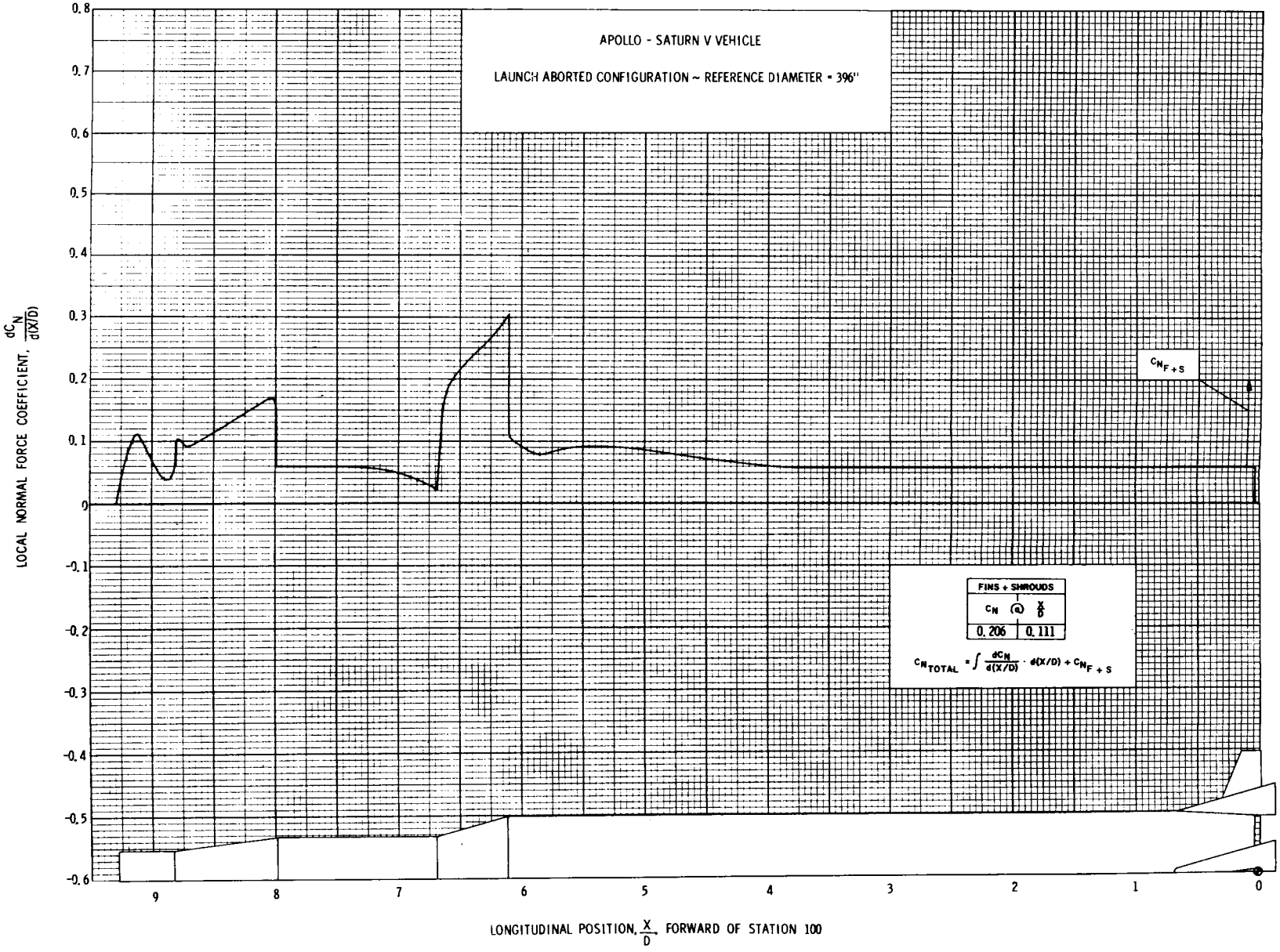

FIGURE 68 DISTRIBUTION OF LOCAL NORMAL FORCE COEFFICIENT, $M = 2.75$; $\alpha = 10^\circ$

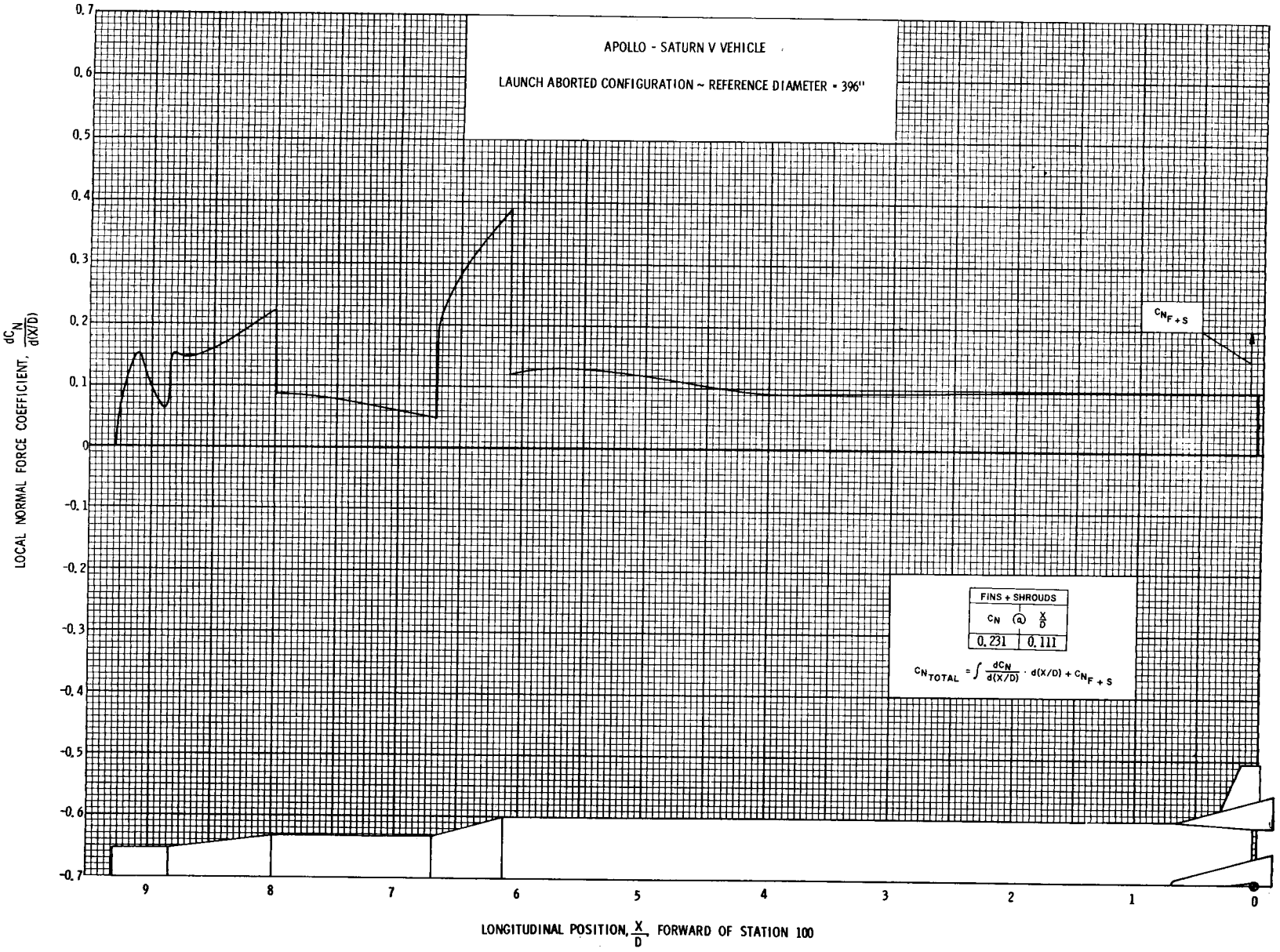

FIGURE 69 DISTRIBUTION OF LOCAL NORMAL FORCE COEFFICIENT, M = 2.75 ; $\alpha = 12^\circ$

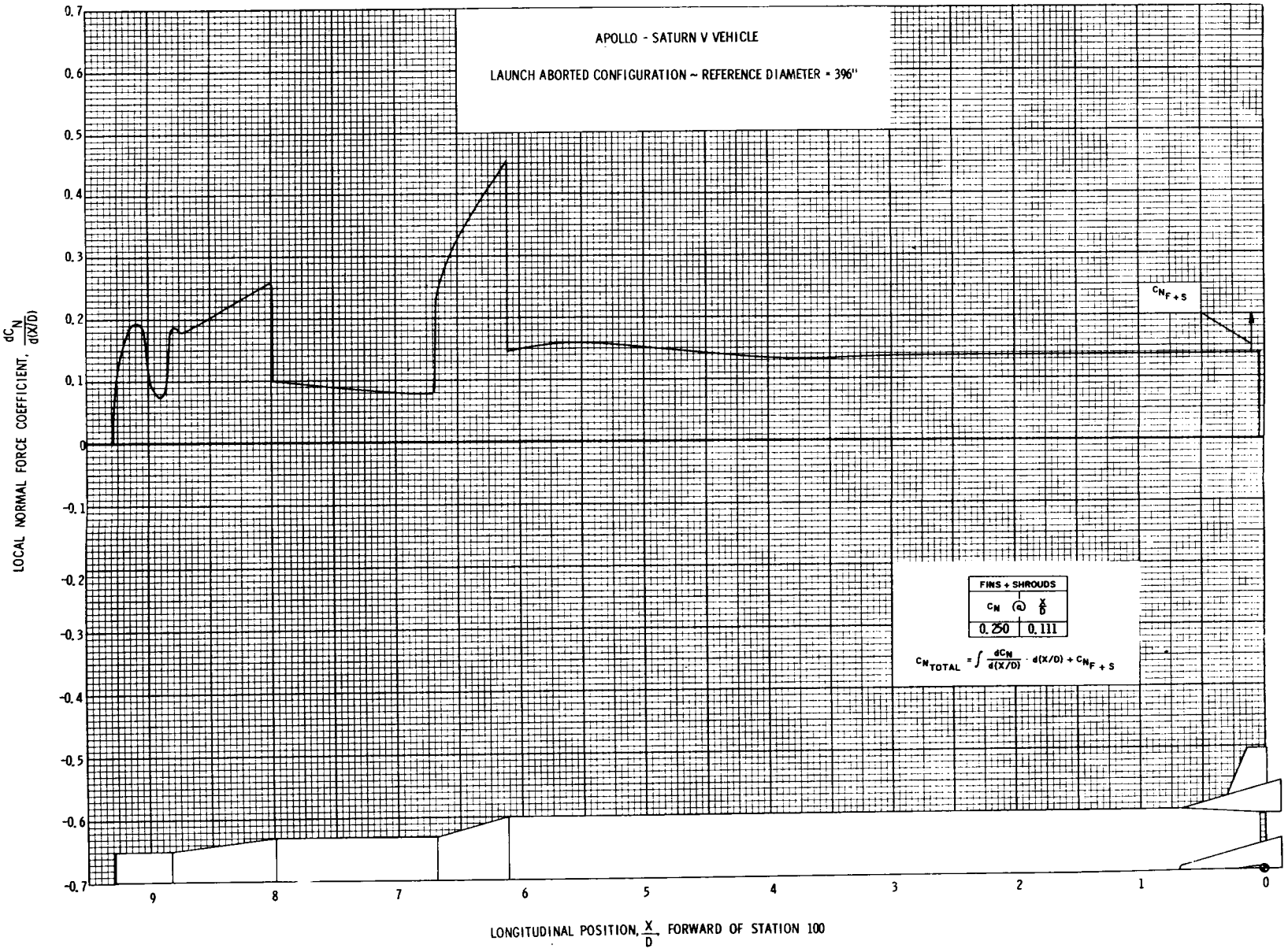

FIGURE 70 DISTRIBUTION OF LOCAL NORMAL FORCE COEFFICIENT, M = 2.75 ; $\alpha = 14^\circ$

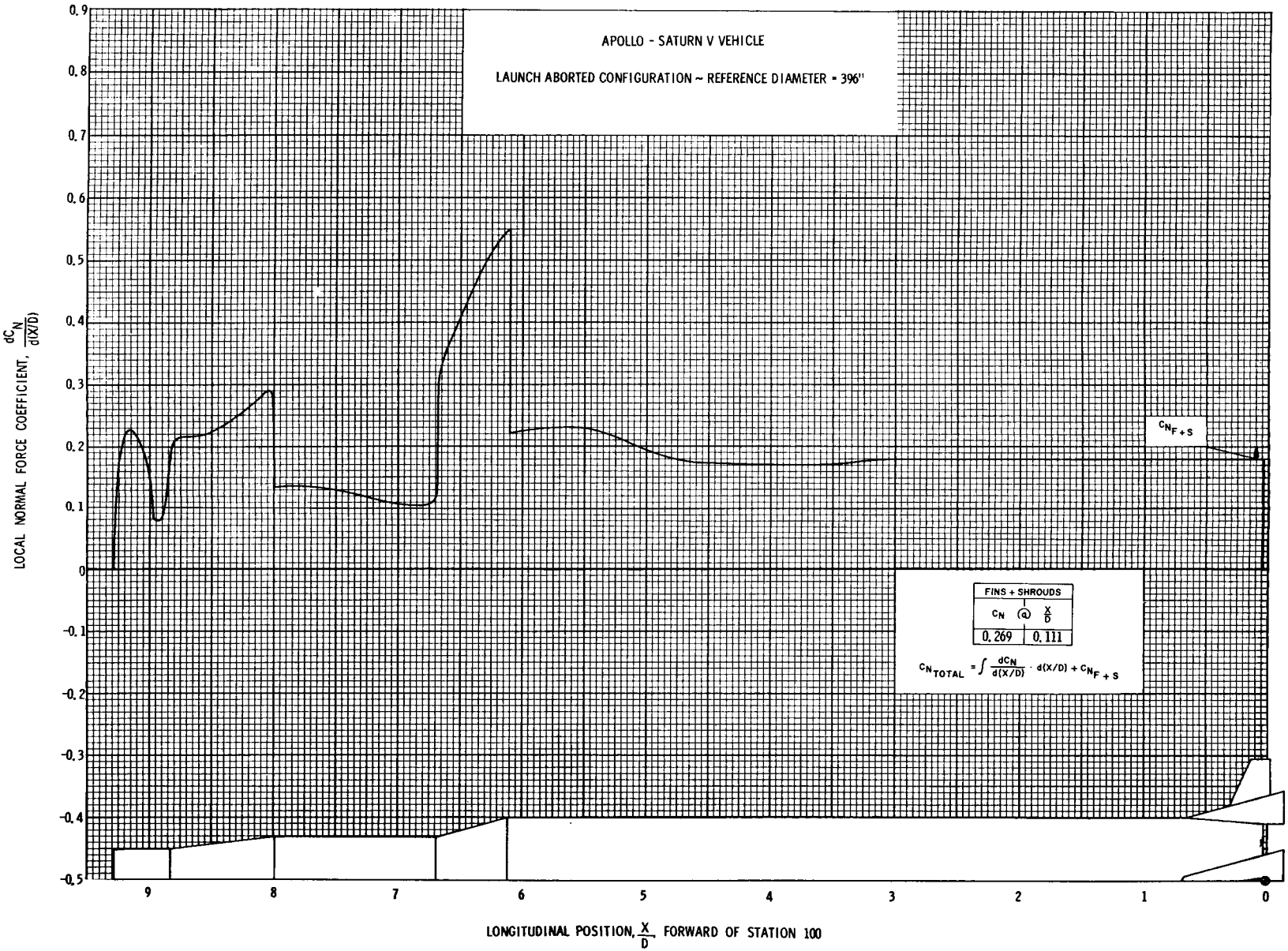

FIGURE 71 DISTRIBUTION OF LOCAL NORMAL FORCE COEFFICIENT, $M = 2.75$: $\alpha = 16^\circ$

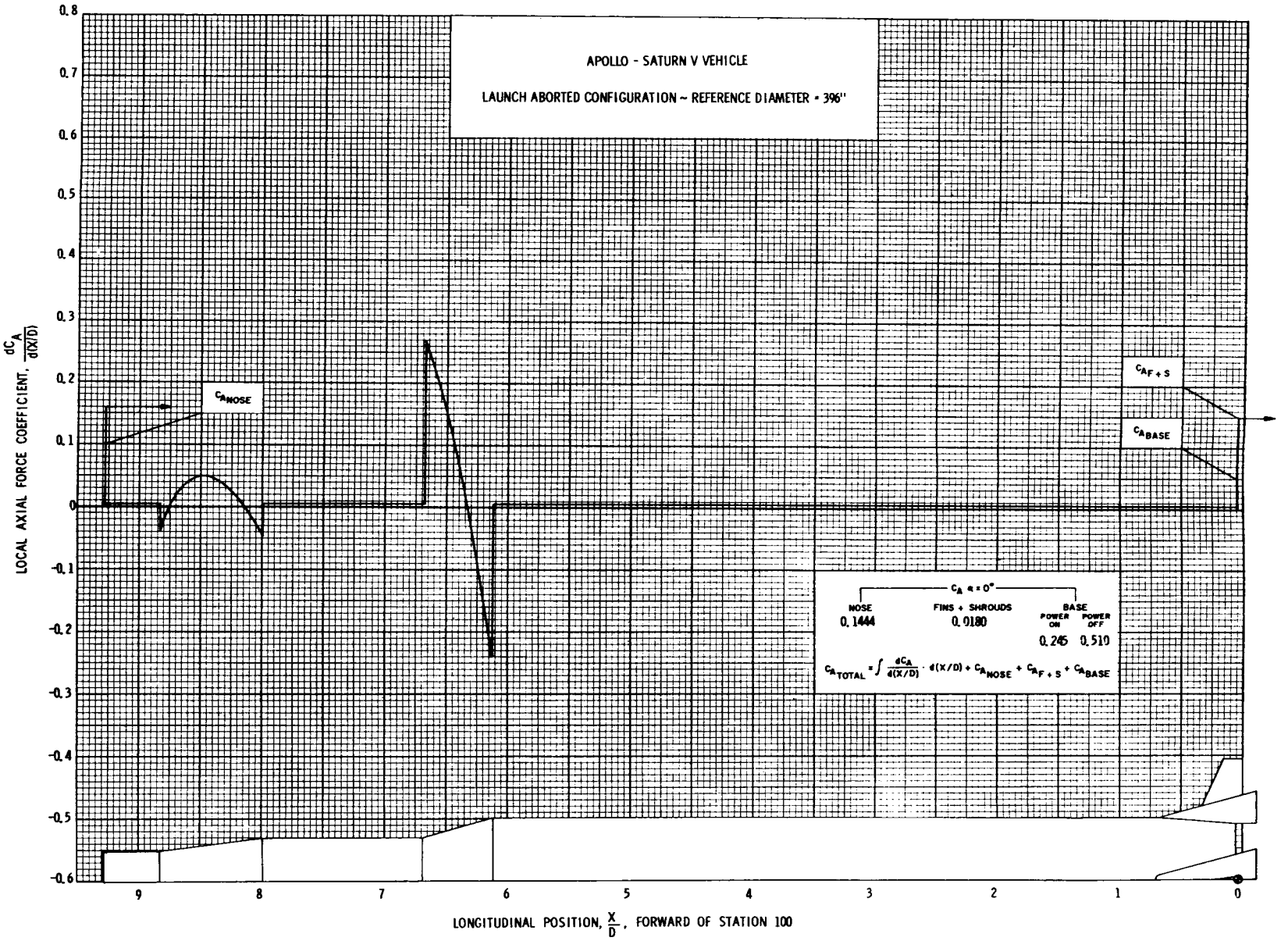

FIGURE 72 DISTRIBUTION OF LOCAL AXIAL FORCE COEFFICIENT, M = 0.50

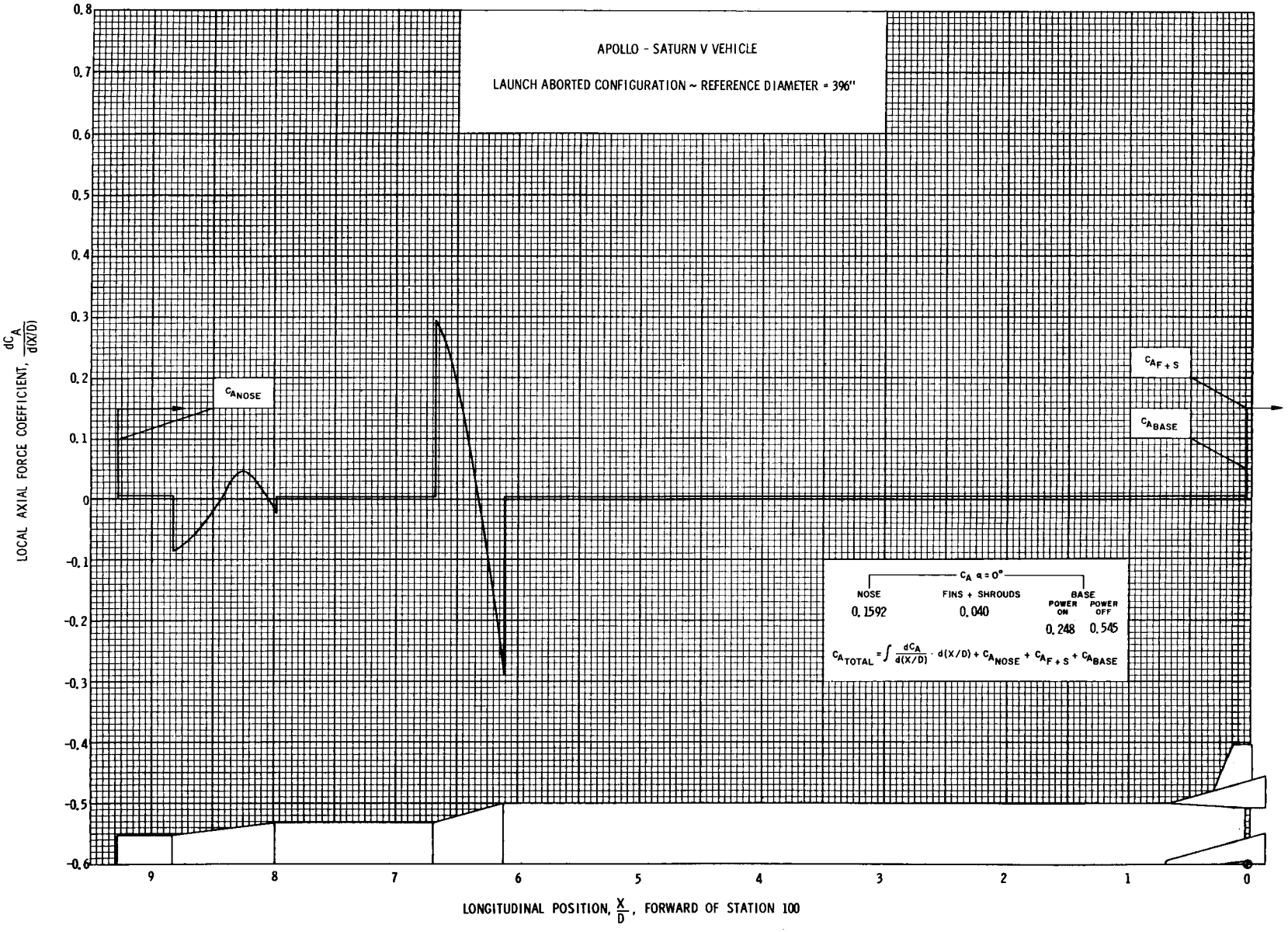

FIGURE 73 DISTRIBUTION OF LOCAL AXIAL FORCE COEFFICIENT, M = 0.80

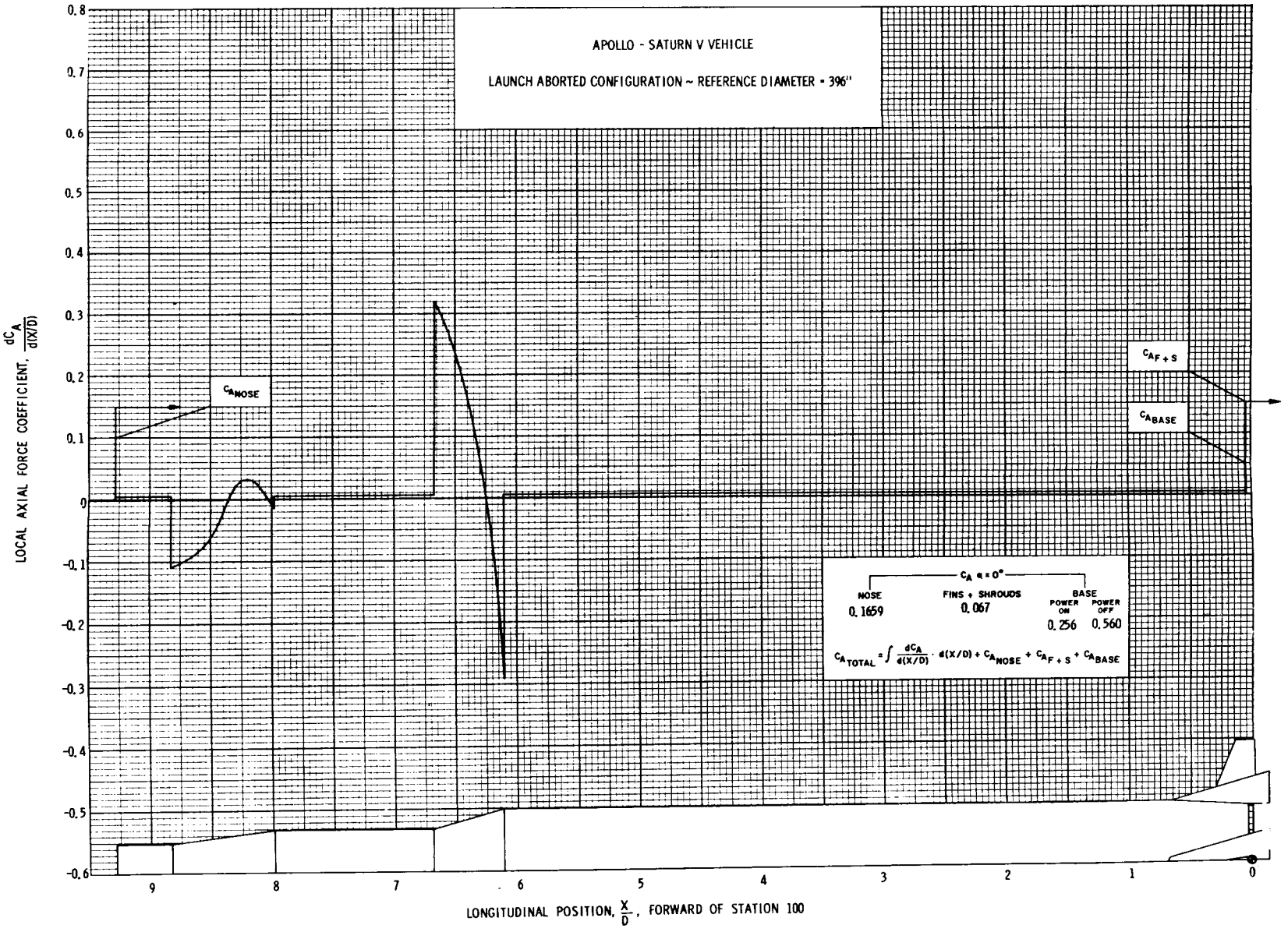

FIGURE 74 DISTRIBUTION OF LOCAL AXIAL FORCE COEFFICIENT, M = 0.90

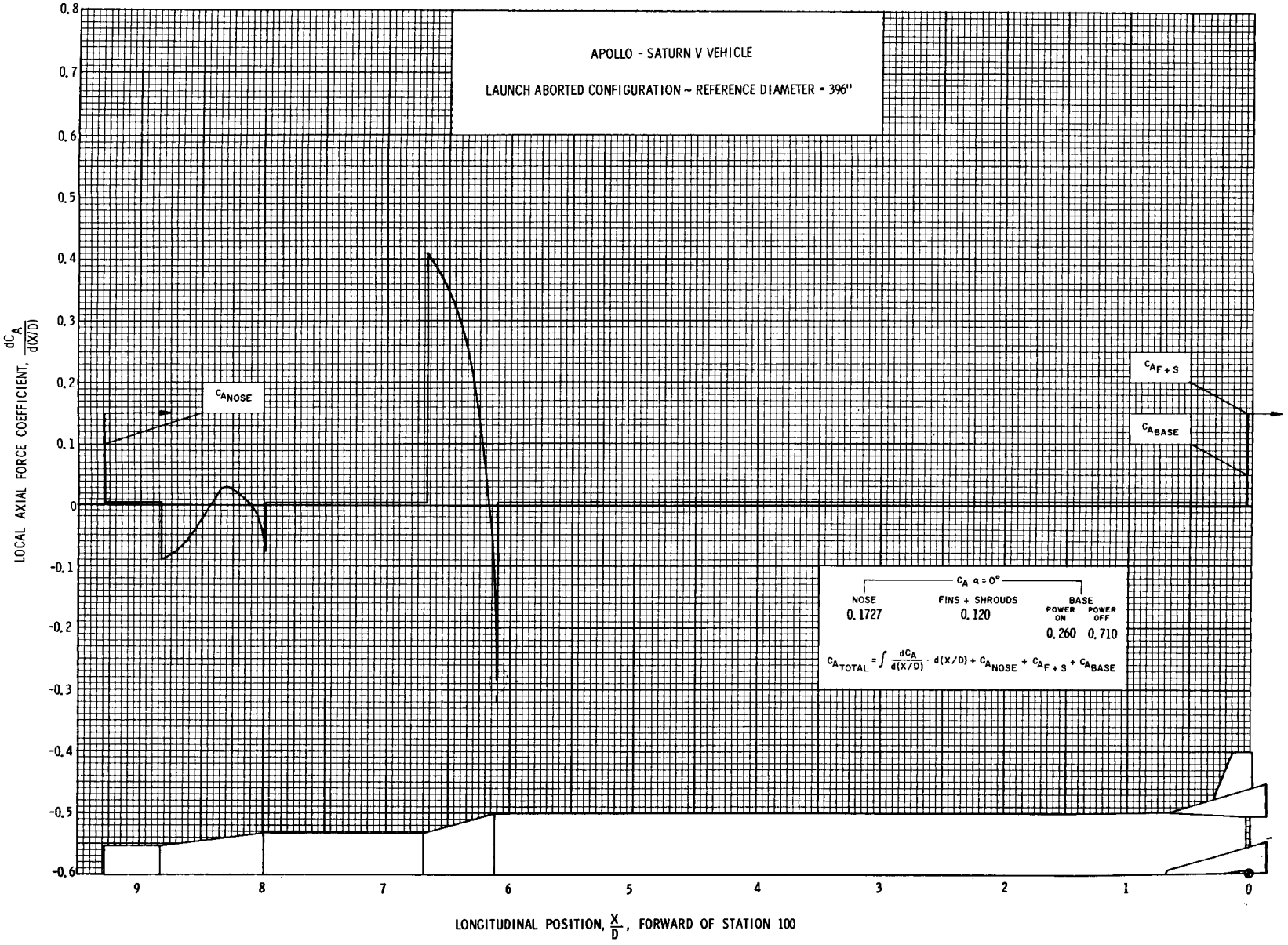

FIGURE 75 DISTRIBUTION OF LOCAL AXIAL FORCE COEFFICIENT, M = 1.00

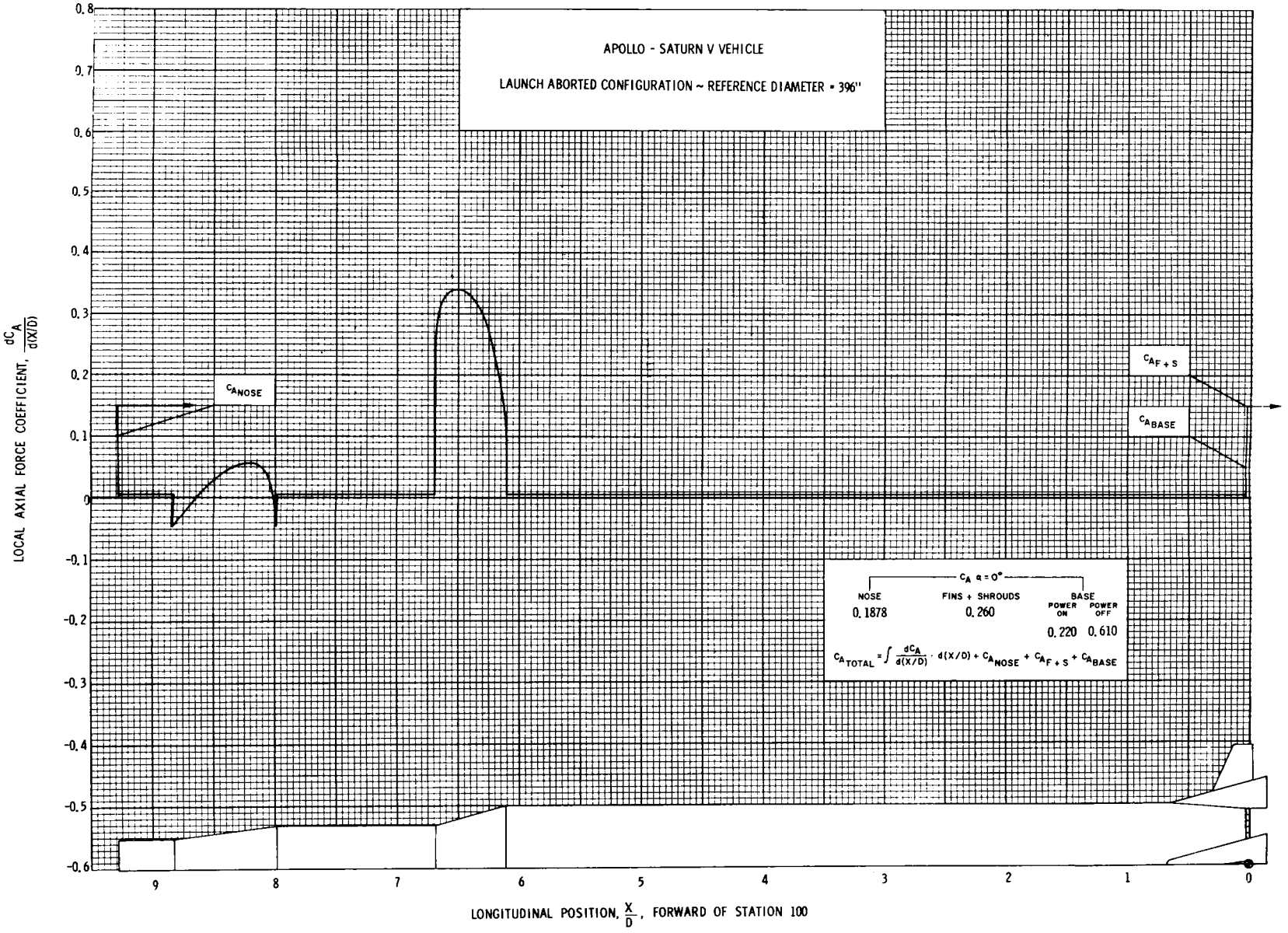

FIGURE 76 DISTRIBUTION OF LOCAL AXIAL FORCE COEFFICIENT, M = 1.20

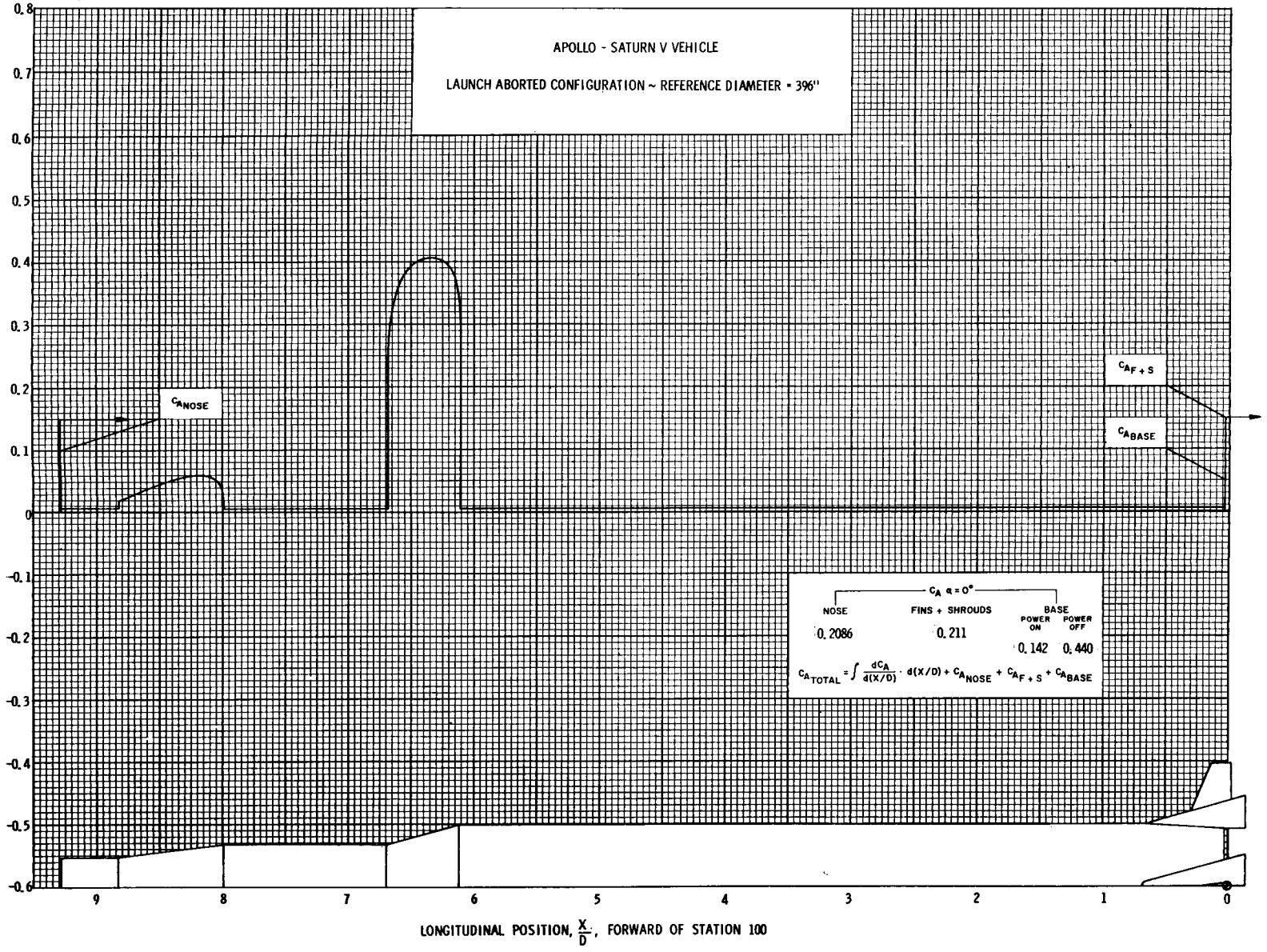

FIGURE 77 DISTRIBUTION OF LOCAL AXIAL FORCE COEFFICIENT, M = 1.50

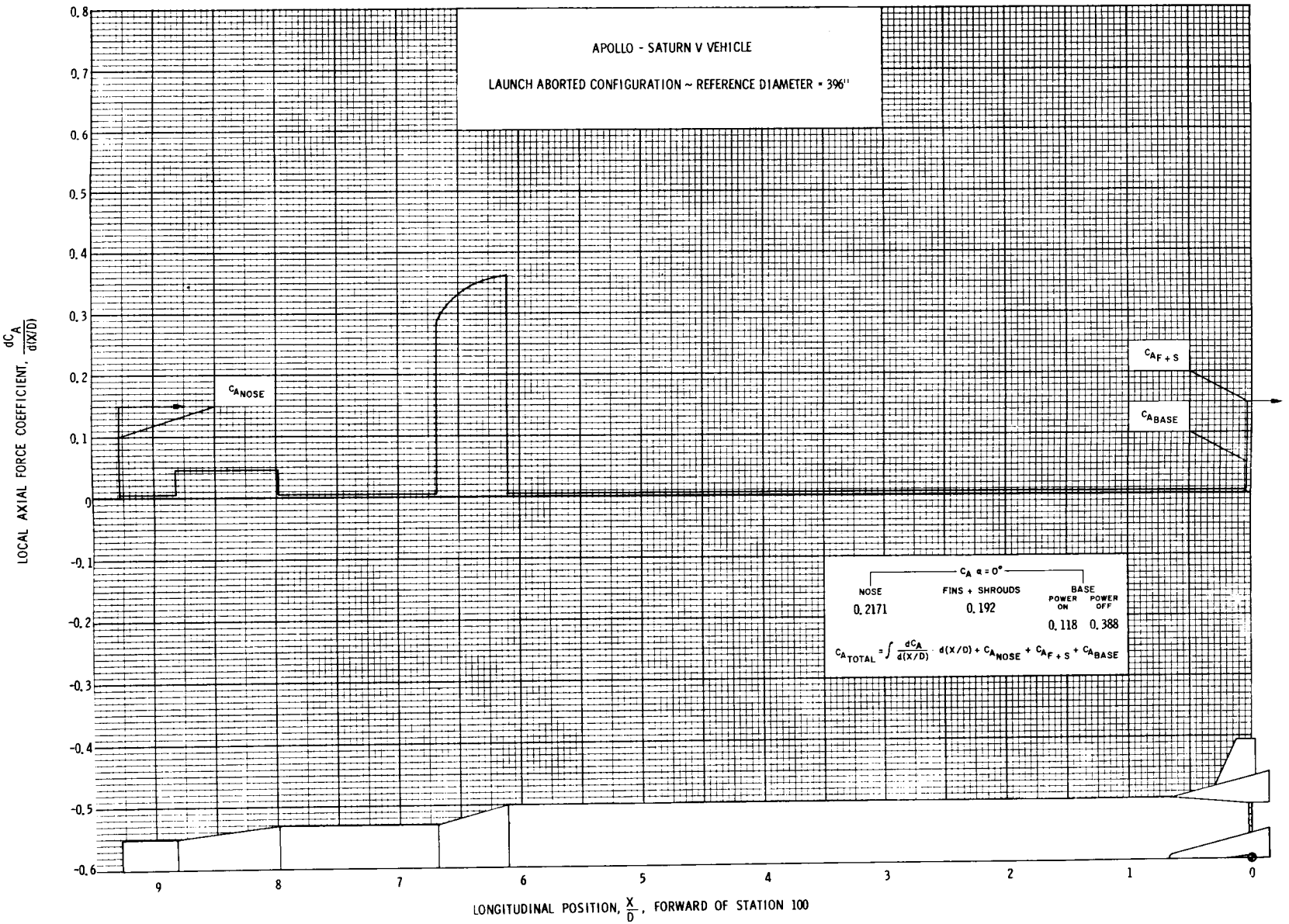

FIGURE 78 DISTRIBUTION OF LOCAL AXIAL FORCE COEFFICIENT, M = 1.70

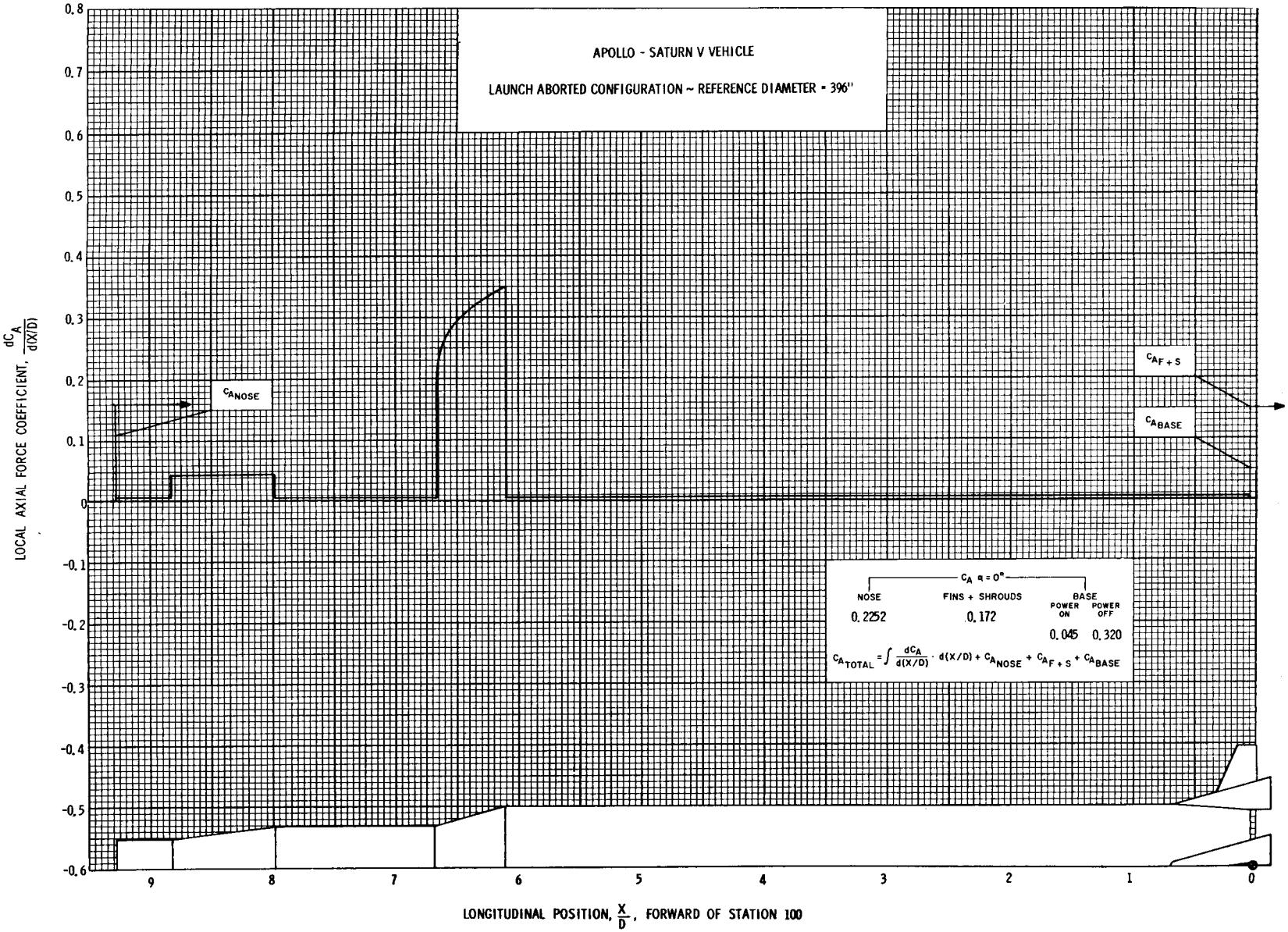

FIGURE 79 DISTRIBUTION OF LOCAL AXIAL FORCE COEFFICIENT, M = 2.00

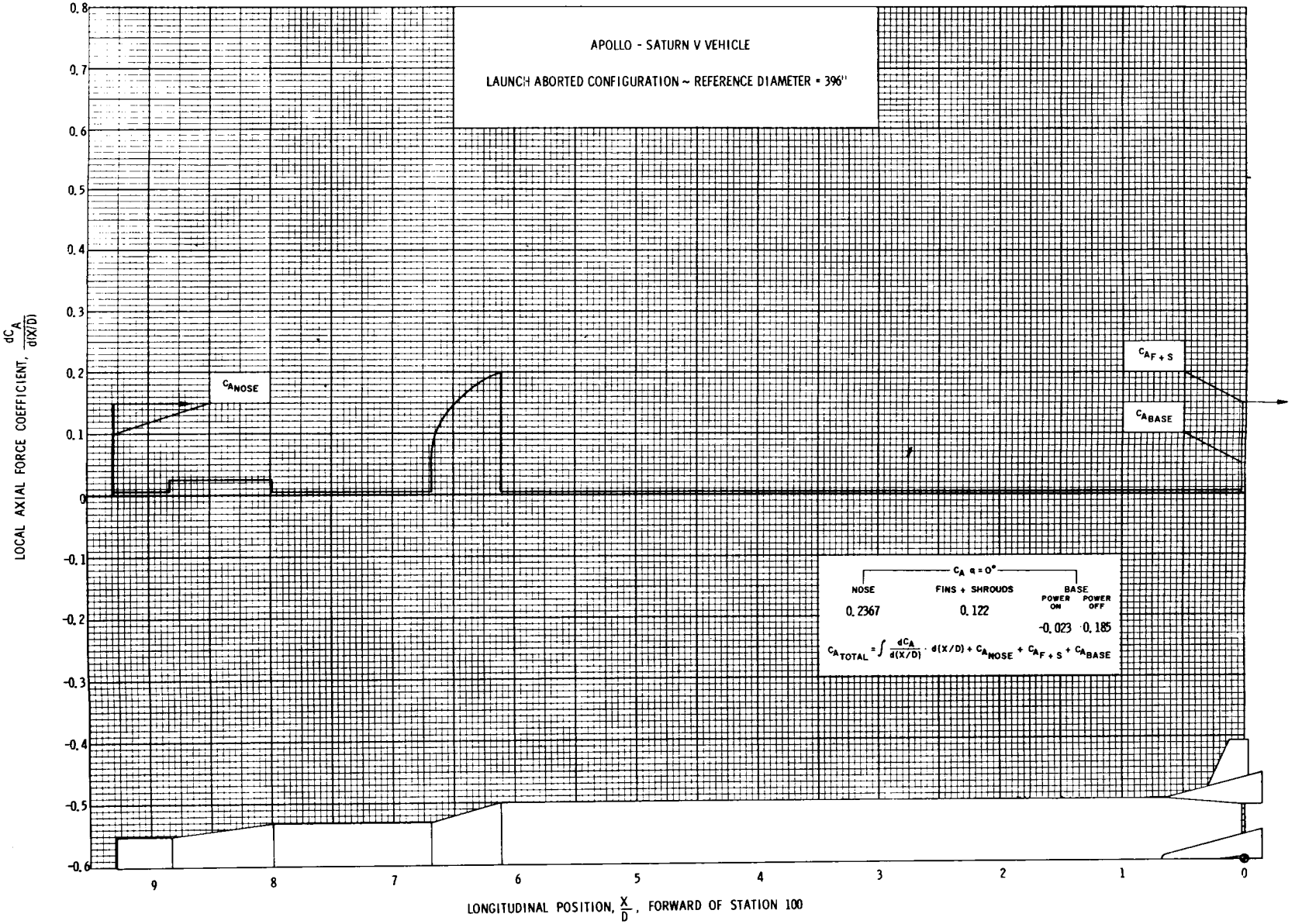

FIGURE 80 DISTRIBUTION OF LOCAL AXIAL FORCE COEFFICIENT, M = 2.75

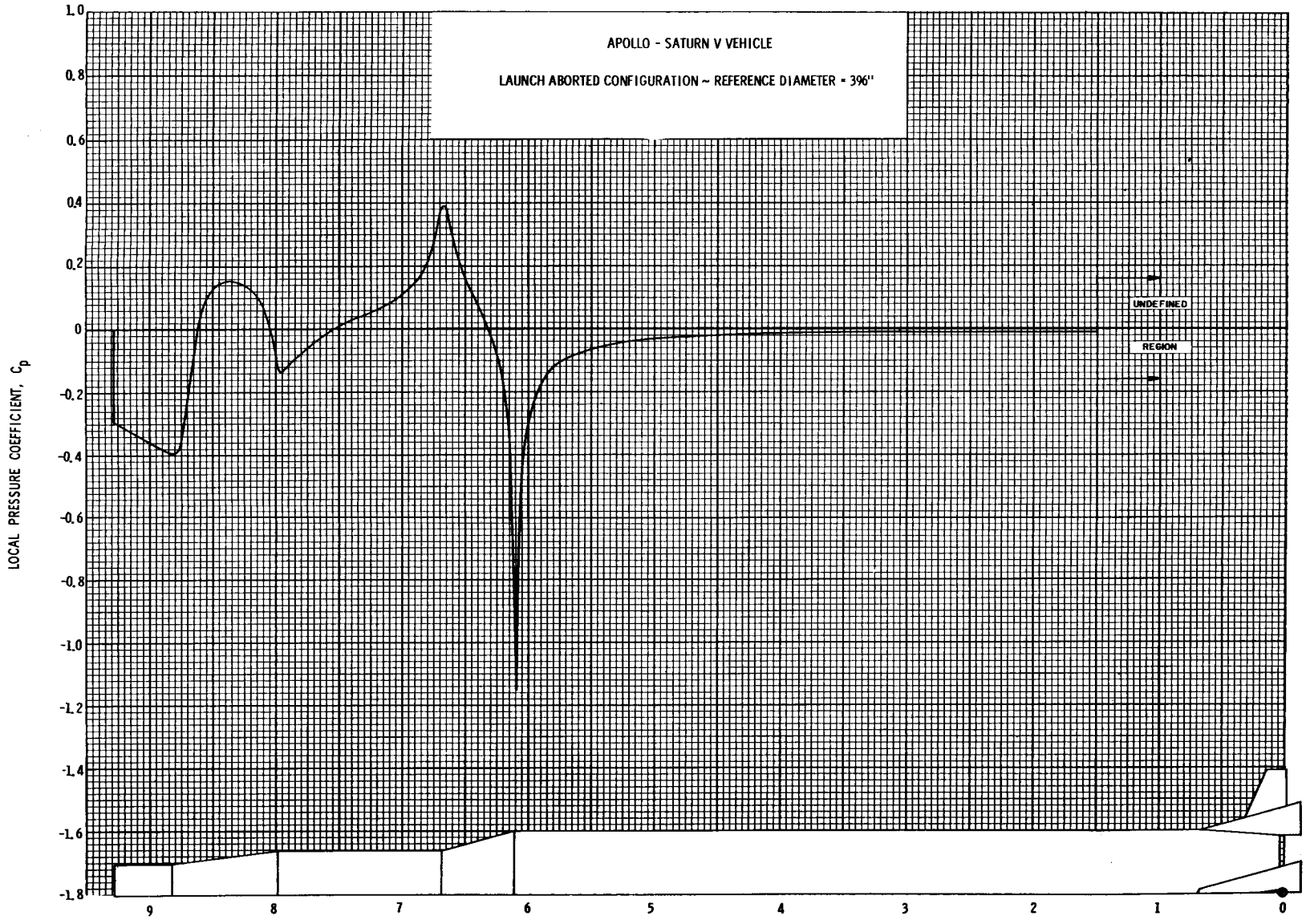

FIGURE 81 DISTRIBUTION OF LOCAL PRESSURE COEFFICIENT AT $\alpha = 0°$; M = 0.60

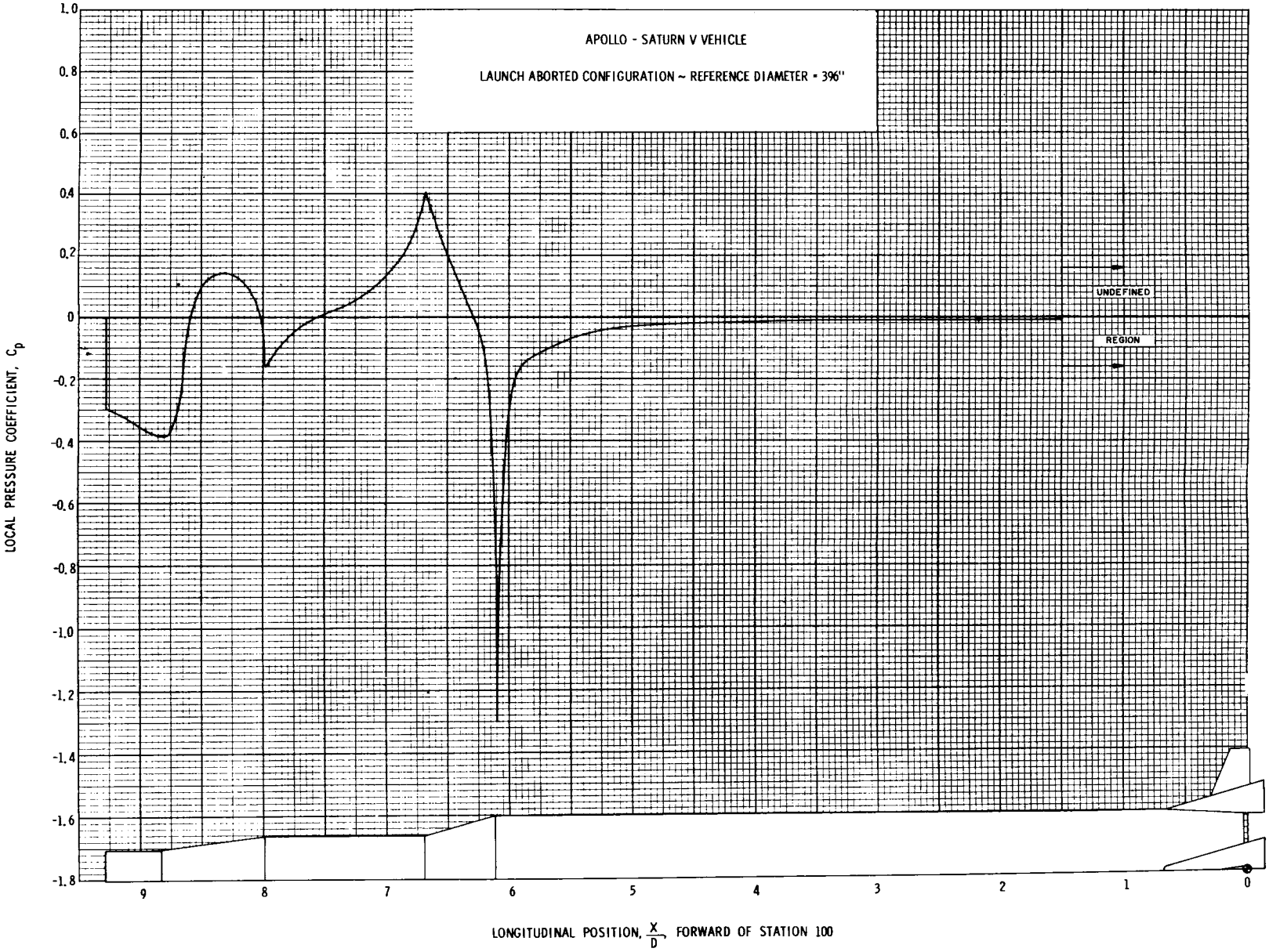

FIGURE 82 DISTRIBUTION OF LOCAL PRESSURE COEFFICIENT AT $\alpha = 0°$; $M = 0.70$

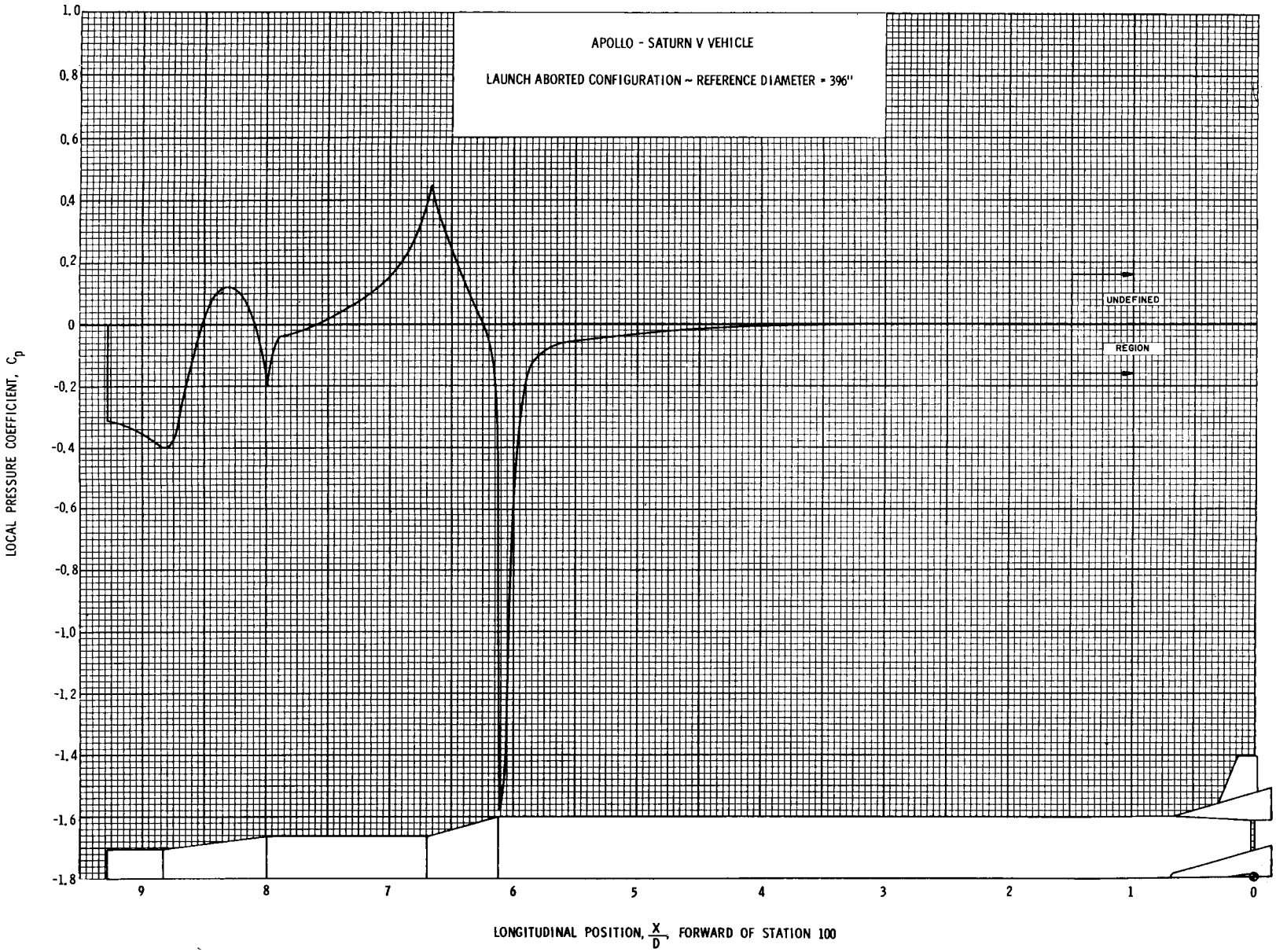

FIGURE 83 DISTRIBUTION OF LOCAL PRESSURE COEFFICIENT AT $\alpha = 0°$; $M = 0.80$

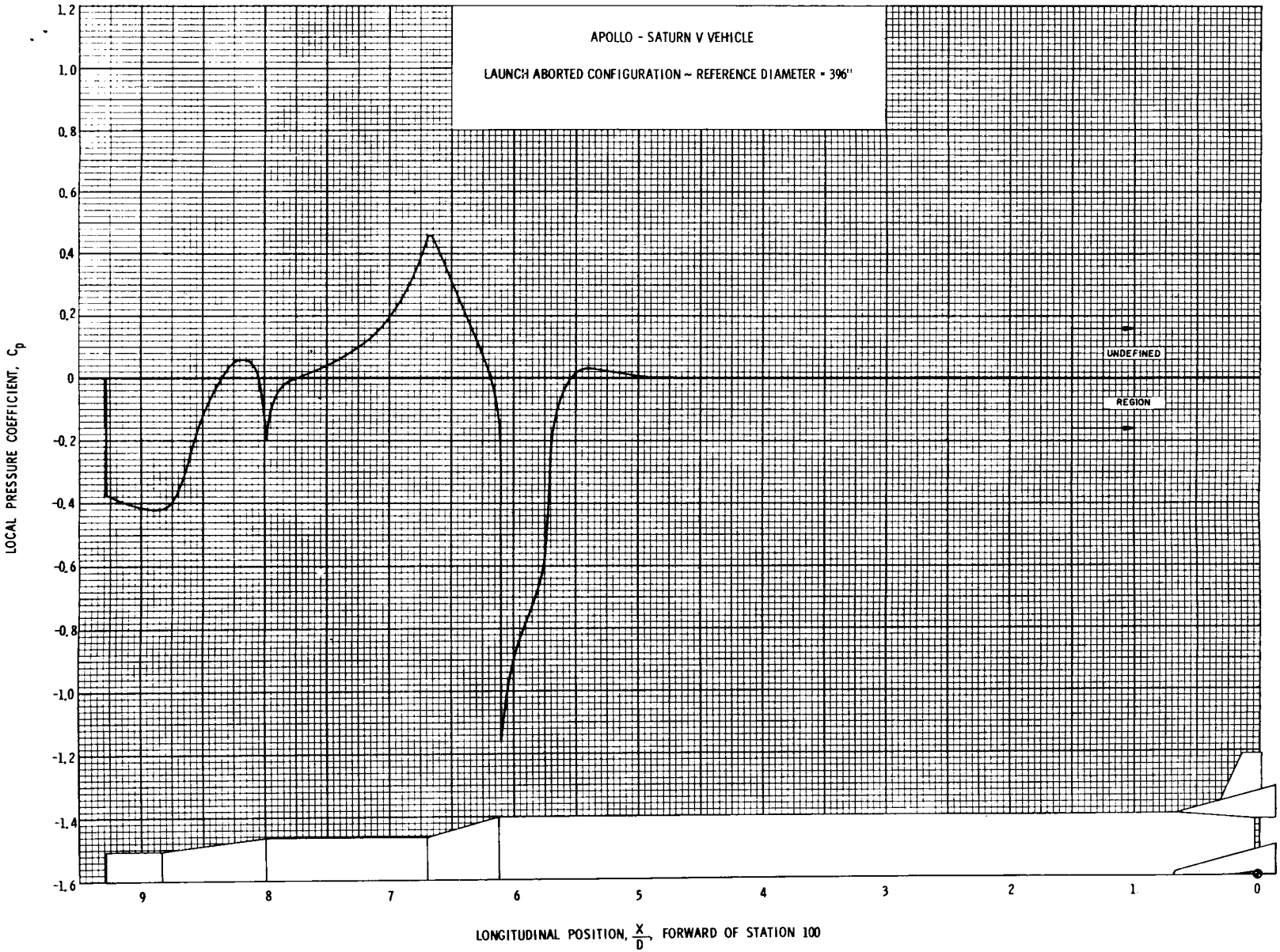

FIGURE 84 DISTRIBUTION OF LOCAL PRESSURE COEFFICIENT AT $\alpha = 0°$; $M = 0.90$

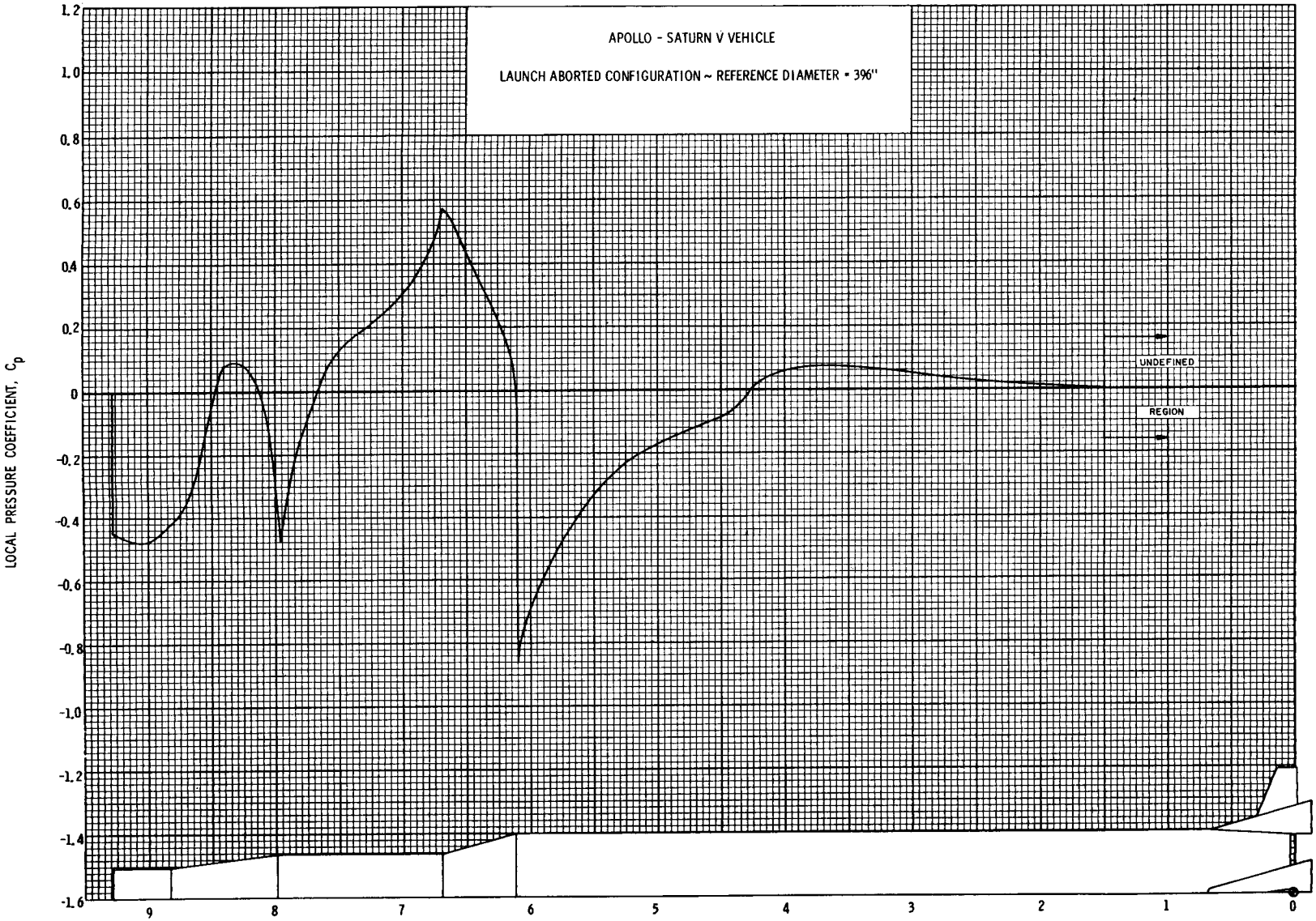

FIGURE 85 DISTRIBUTION OF LOCAL PRESSURE COEFFICIENT AT $\alpha = 0°$; M = 1.00

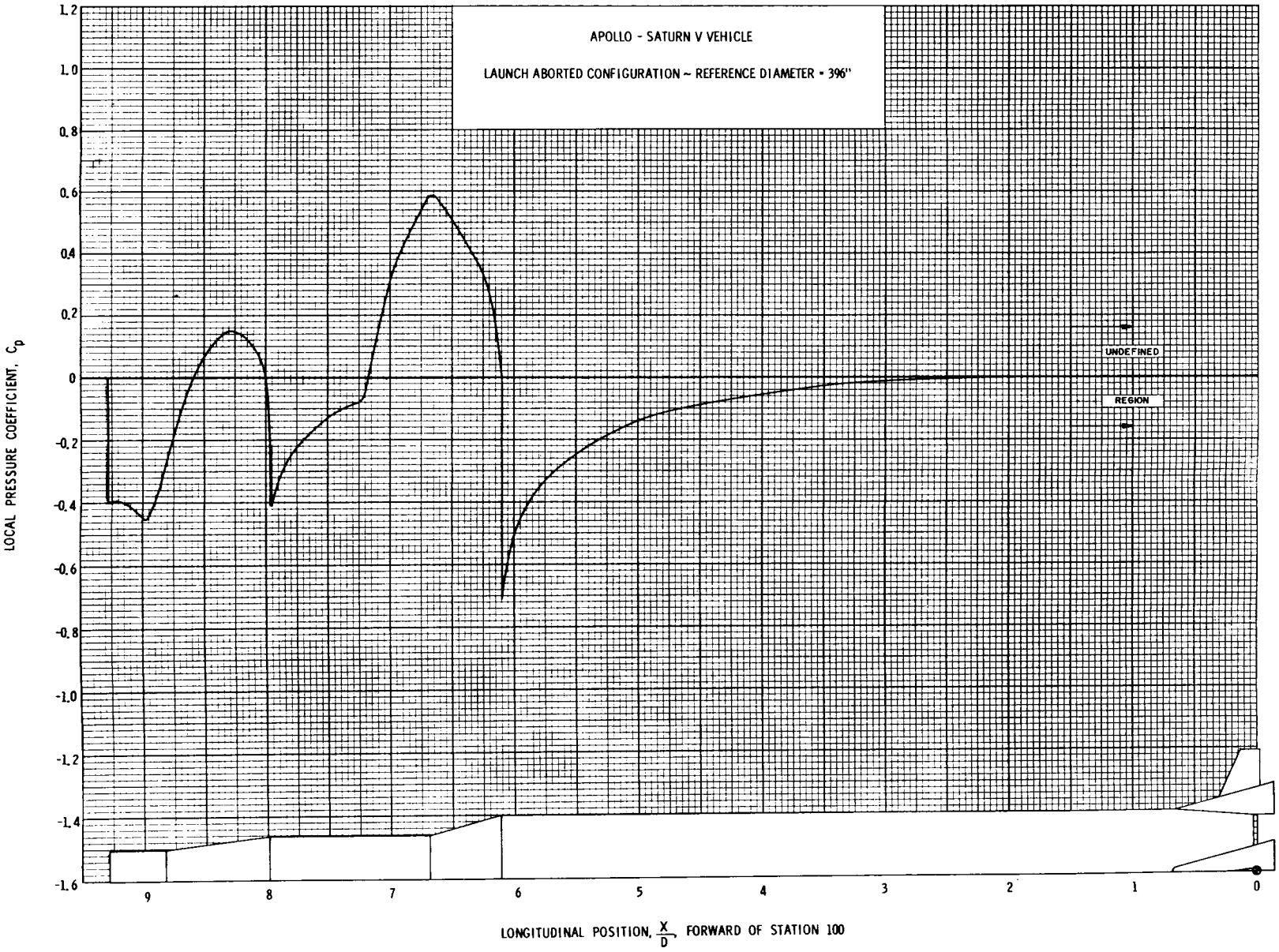

FIGURE 86 DISTRIBUTION OF LOCAL PRESSURE COEFFICIENT AT $\alpha = 0°$; $M = 1.10$

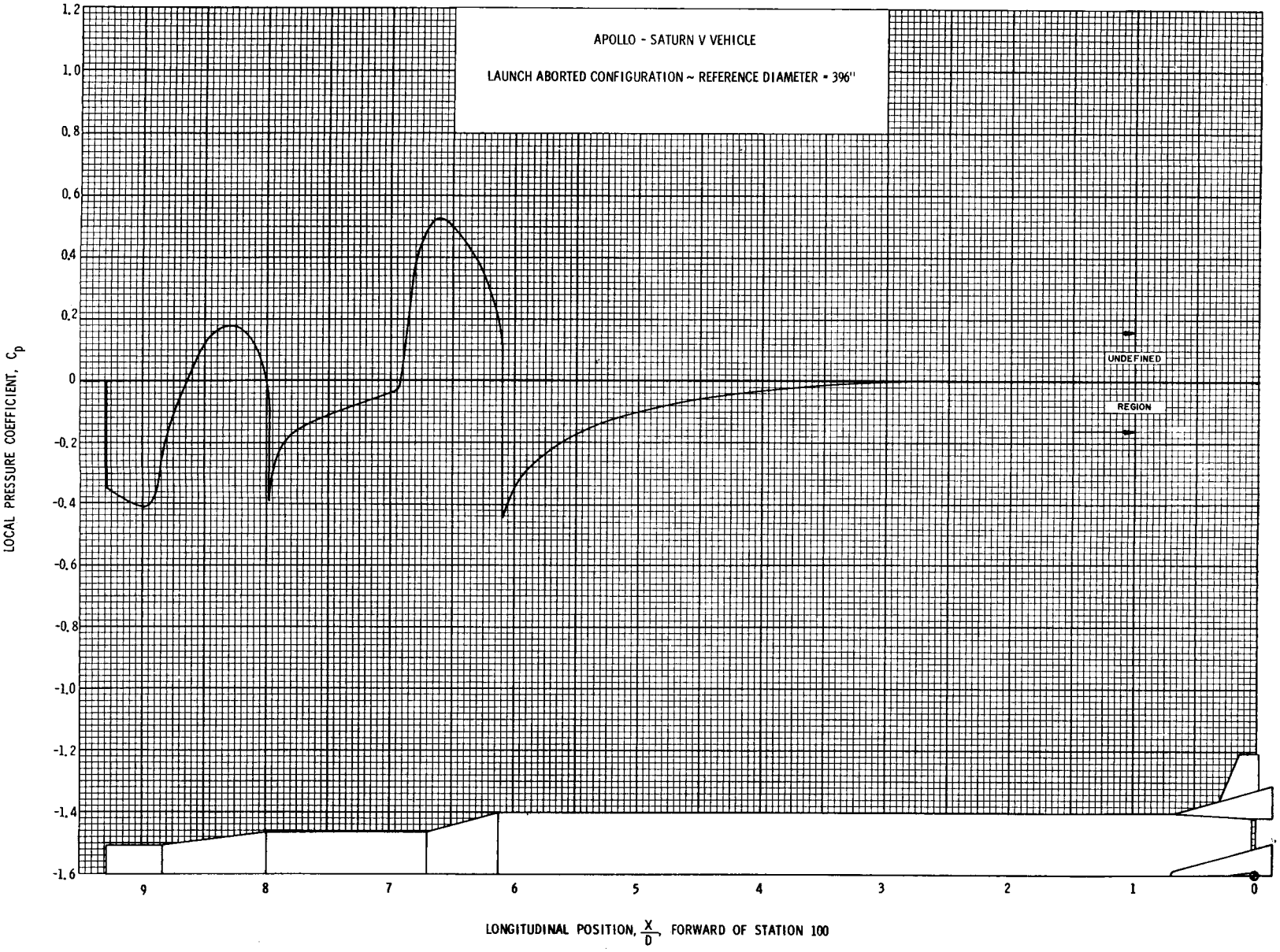

FIGURE 87 DISTRIBUTION OF LOCAL PRESSURE COEFFICIENT AT $\alpha = 0°$; $M = 1.20$

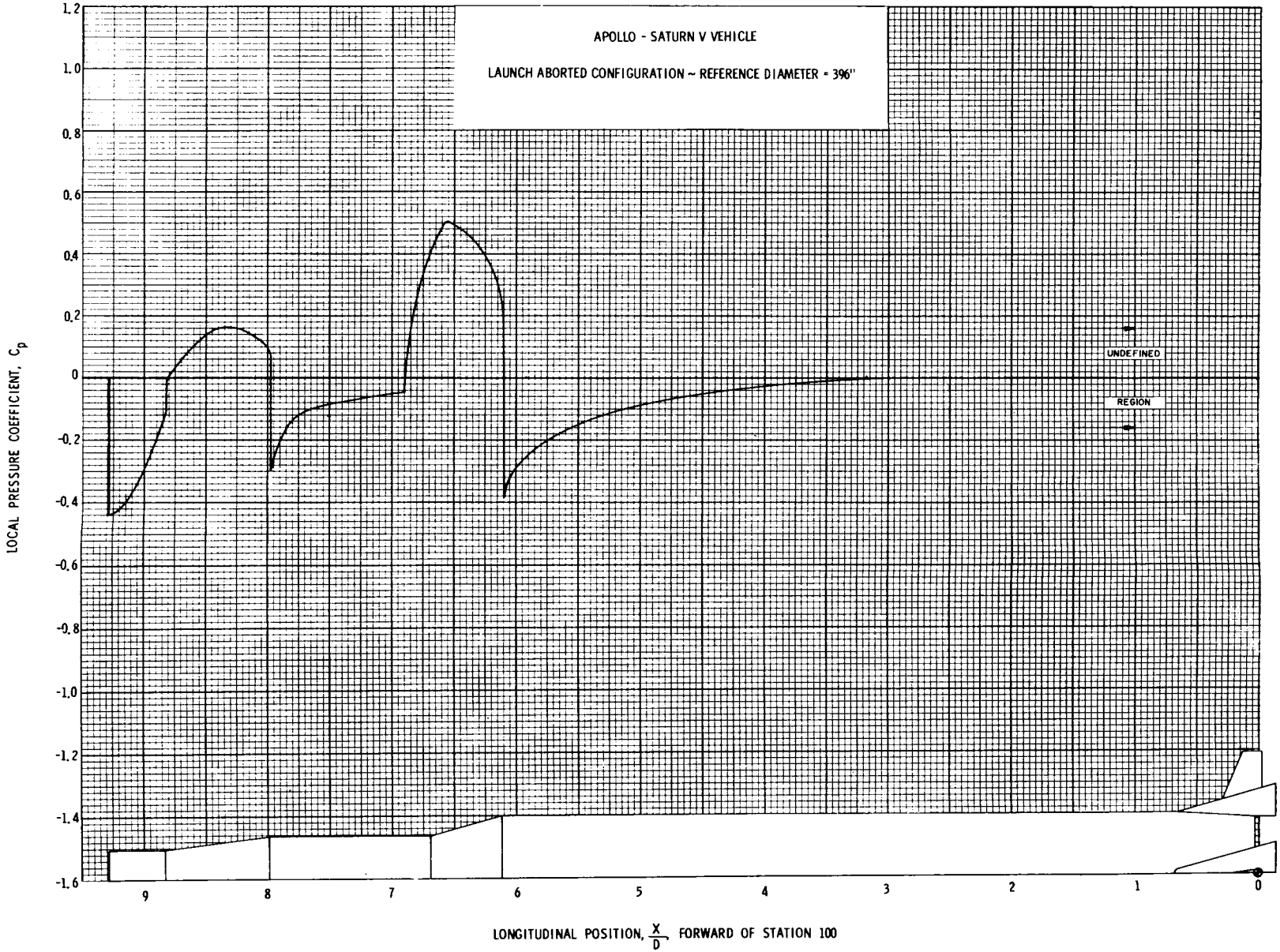

FIGURE 88 DISTRIBUTION OF LOCAL PRESSURE COEFFICIENT AT $\alpha = 0^\circ$; M = 1.30

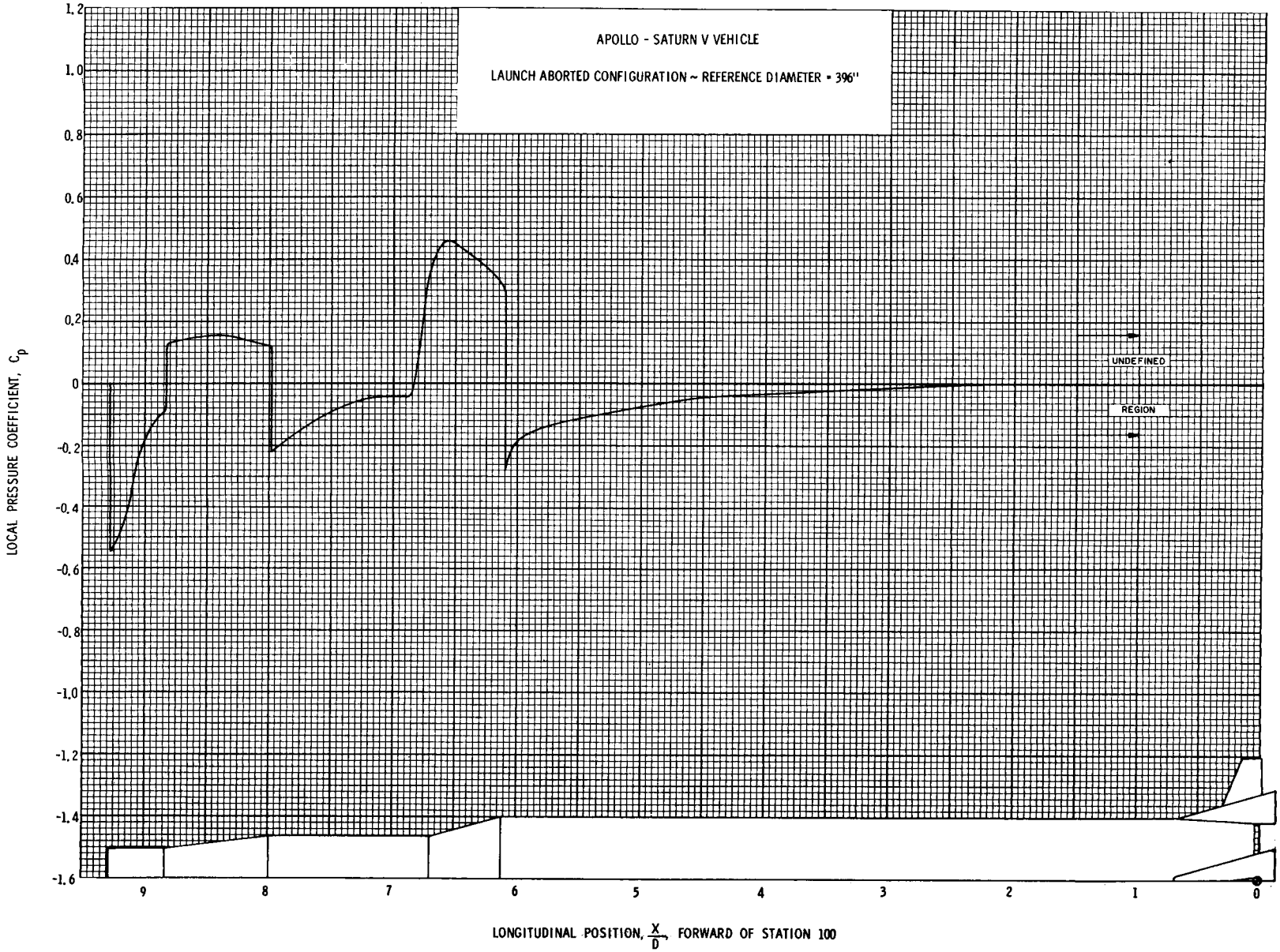

FIGURE 89 DISTRIBUTION OF LOCAL PRESSURE COEFFICIENT AT $\alpha = 0°$; M = 1.50

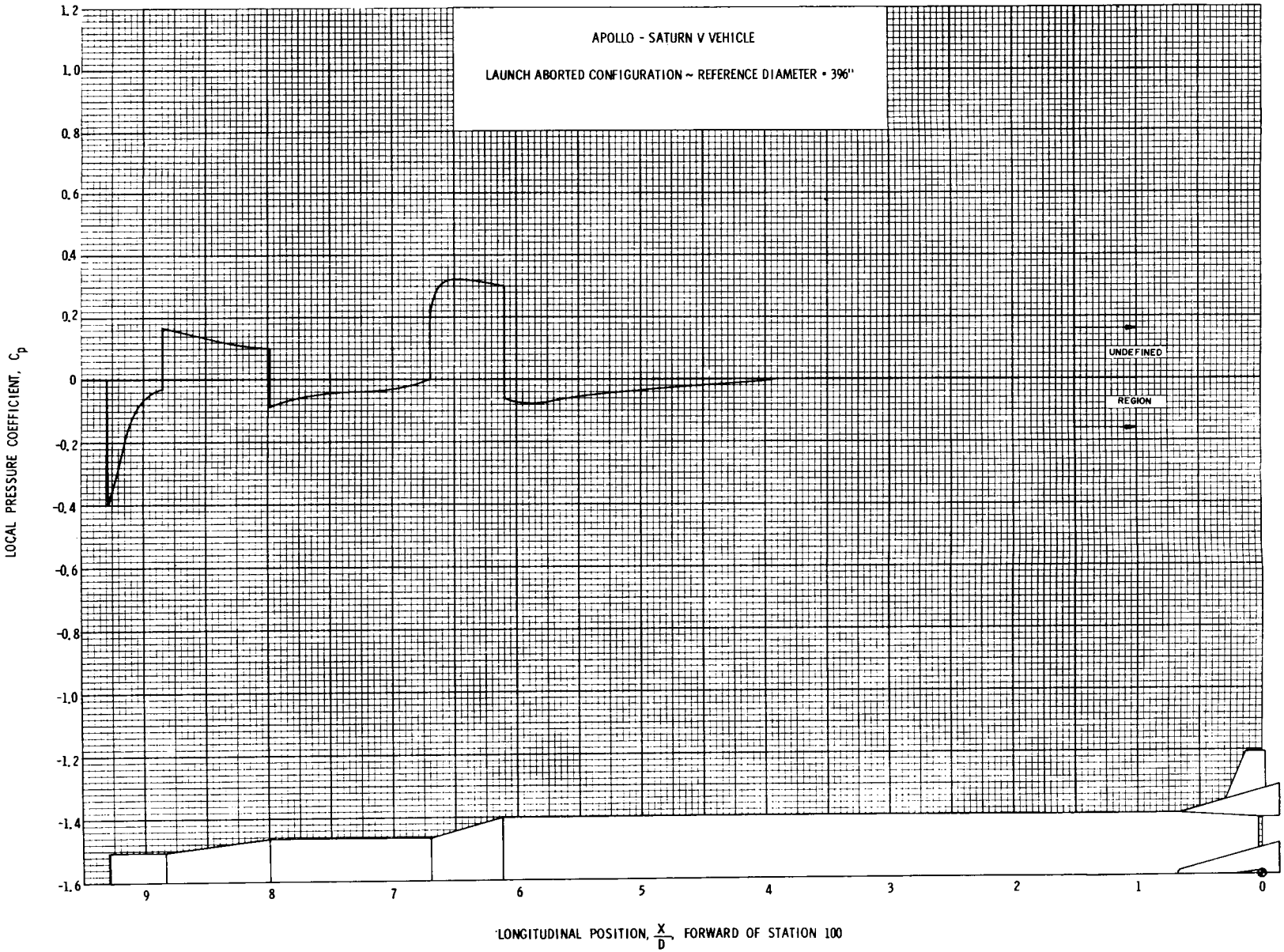

FIGURE 90 DISTRIBUTION OF LOCAL PRESSURE COEFFICIENT AT $\alpha = 0°$; $M = 2.00$

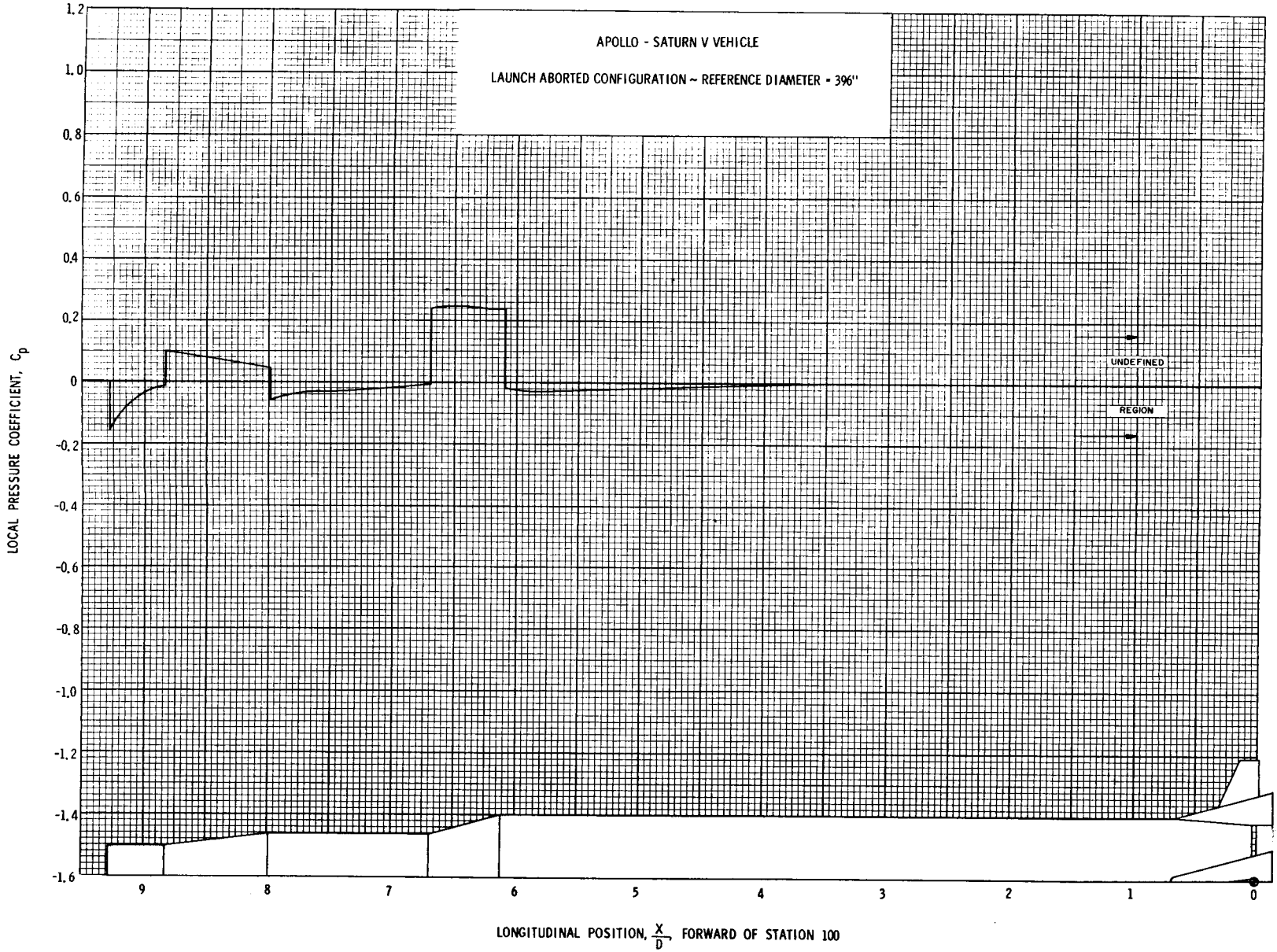

FIGURE 91 DISTRIBUTION OF LOCAL PRESSURE COEFFICIENT AT $\alpha = 0^\circ$; $M = 2.75$

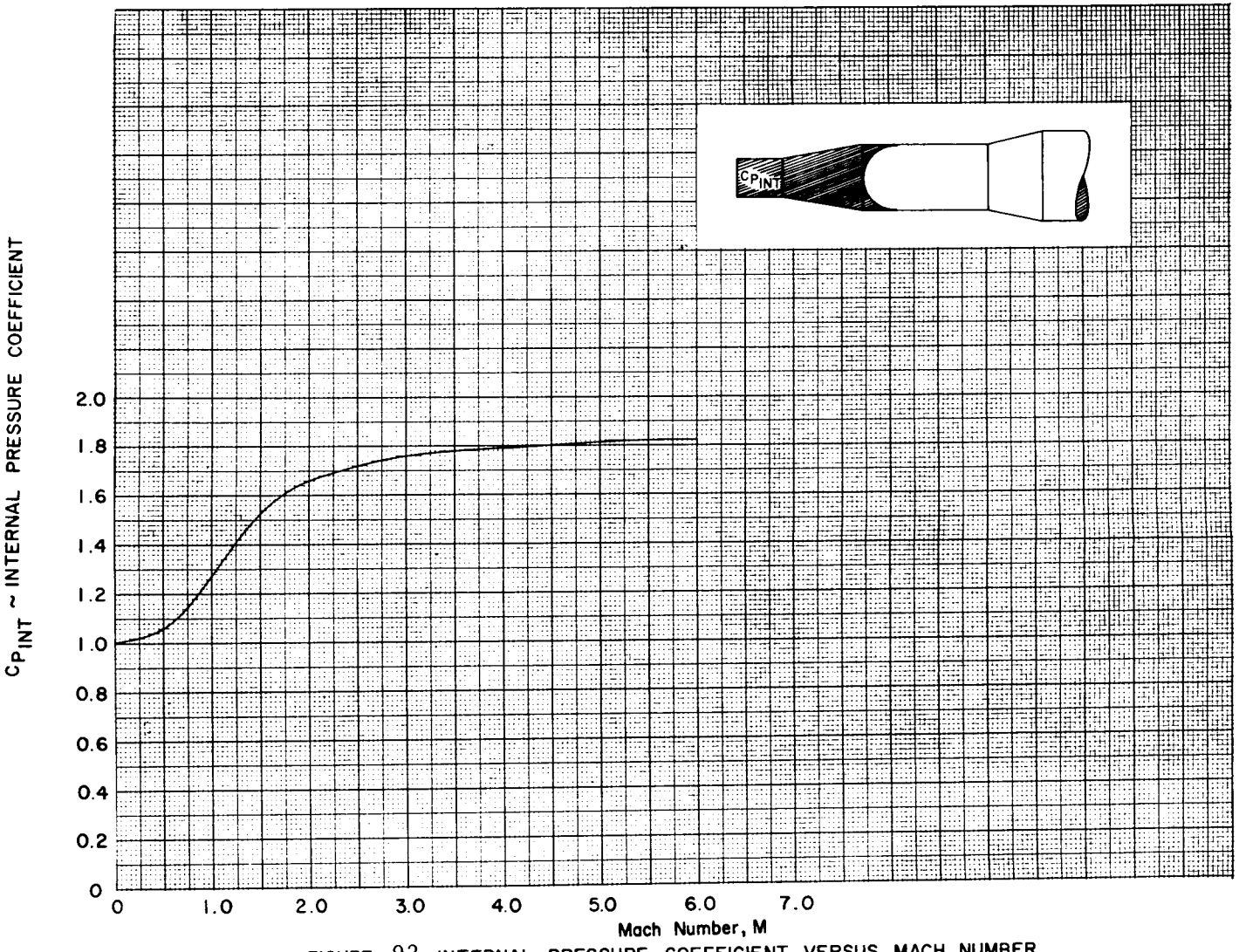

FIGURE 92 INTERNAL PRESSURE COEFFICIENT VERSUS MACH NUMBER

REFERENCES

1. Pitcock, Robert E., "Experimental Static Longitudinal Stability and Axial Force Characteristics of Several Preliminary Saturn V Configurations - Saturn V LOR, Lunar Logistics, Nuclear, and RIFT Vehicles," R-AERO-AD-64-74, July 2, 1964, Unclassified.

2. Pitcock, Robert E., "Experimental Basic Data Results of the Static Transonic Aerodynamic Characteristics of Preliminary Configurations of the Saturn V LOR, Lunar Logistics, Nuclear, and RIFT Vehicles," R-AERO-AD-64-19, February 18, 1964, Unclassified.

3. Fortenberry, Jessie C., "Basic Data Release: Static Longitudinal Stability and Axial Force Characteristics of Saturn V LOR, Lunar Logistics, Nuclear and RIFT Configurations Obtained from Tests Conducted in BRL Supersonic Wind Tunnel (MSFC Project 68)," R-AERO-AD-64-49, May 5, 1964, Unclassified.

4. Henson, Victor K., and Robert M. Glasgow, "Static Aerodynamic Characteristics of the Aborted Apollo-Saturn V Vehicle," NASA TM X-53469, June 3, 1966, Unclassified.

5. Patrick, Donald R., "Saturn V Complex (VLF-39) Model Test Results, Phase 10 - Organization of the S-IC Launch Complex Variables," R-TEST-CV-41, August 31, 1964, Unclassified.

6. Vehicle Aerodynamics Section, "Static Aerodynamic Characteristics of the Apollo-Saturn V Vehicle," NASA TM X-53517, September 16, 1966, Unclassified.

7. Nunley, Billy W., "Static Aerodynamic Characteristics of the Aborted Apollo-Saturn IB Vehicle," NASA TM X-53423, March 30, 1966.

8. Chianese, F., "Static Pressure and Normal Force Coefficient Distributions of the Saturn IB Launch and Aborted Launch Configuration as Determined from Wind Tunnel Tests," CCSD-TN-AE-63-12, December 30, 1963, Unclassified.

9. Henson, Victor K., "Design Criteria: Aerodynamic Loads and Pressure Distributions for the Saturn V, LOR, S-IC Stage 75 Square Foot Fins," MSFC Memo R-AERO-AD-64-68, June 11, 1964, Unclassified.

10. Henson, Victor K., "Aerodynamic Design Criteria for the S-IC Stage Engine Shrouds of the Saturn V, LOR Vehicle, MSFC DWG 10M04106, Rev. G," MSFC Memo R-AERO-AD-64-12, January 29, 1964, Unclassified.

STATIC AERODYNAMIC CHARACTERISTICS OF THE ABORTED APOLLO-SATURN V VEHICLE

by Robert M. Glasgow

The information in this report has been reviewed for security classification. Review of any information concerning Department of Defense or Atomic Energy Commission programs has been made by the MSFC Security Classification Officer. This report, in its entirety, has been determined to be unclassified.

This document has also been reviewed and approved for technical accuracy.

B. G. Dunn
Technical Coordinator

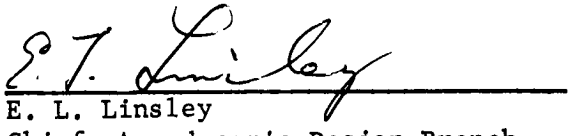

E. L. Linsley
Chief, Aerodynamic Design Branch

Werner K. Dahm
Chief, Aerophysics Division

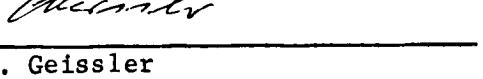

E. D. Geissler
Director, Aero-Astrodynamics Laboratory

DISTRIBUTION

DIR

DEP-T

R-DIR

MS-IPL (8)
MS-IP
MS-H
HME-P
CC-P
MS-T (6)

R-ASTR
Dr. Haeussermann
Mr. Kroeger
Mr. Moore
Mr. Hosenthien
Mr. Blackstone

R-P&VE
Dr. Lucas
Mr. Palaoro
Mr. Aberg
Mr. McCollough
Mr. Goerner
Mr. Kroll
Mr. Furman
Mr. Showers (3)
Mr. Frederick
Mr. Blumrich
Mr. Stevens

R-AERO
Dr. Geissler
Mr. Jean
Mr. McNair
Mr. Thionnet
Mr. Horn
Mr. Ryan
Mr. Rheinfurth
Mr. Hall
Mr. Lindberg
Mr. Lovingood
Mr. Dahm

R-AERO (Cont'd)
Mr. Holderer
Mr. Wilson
Mr. Reed
Mr. Linsely
Mr. Andrews
Mr. Dunn
Mr. Nunley
Mr. Bacchus
Mr. Lowery
Mr. Henson (10)
Dr. H. Krause

Mr. Robert M. Glasgow (10)
Northrop Space Laboratories
6025 Technology Drive
Huntsville, Alabama

Mr. R. L. Hamner
Lockheed Aircraft Corp.
Holiday Office Center
Huntsville, Alabama

The Boeing Co.
Mail Stop AF-75
HIC Building
Huntsville, Alabama
Attn: Mr. W. A. Smith
Mr. W. C. Stain
Mr. K. W. Halvorson

Sci. & Tech. Info. Facility (25)
P. O. Box 5700
Bethesda, Md.
Attn: NASA Rep. (S-AK/RKT)